Pulse-escape fluorescence photoactivation of tau proteins in living neurons at normal and disease-relevant conditions

Dissertation

Zur Erlangung des akademischen Grades eines

Doctor rerum naturalium

(Dr. rer. nat.)

eingereicht am Fachbereich Biologie/Chemie der Universität Osnabrück
von

Carina Weissmann
aus Buenos Aires, Argentinien

Supervisor
Prof. Dr. R. Brandt

Promotionskomission**:**
Erstgutachter: Prof Dr. R. Brandt Zweitgutachter: Prof. Dr. A. Paululat
Prof. Dr. H.J. Steinhoff and Dr. H. P. Schmitz.

Osnabrück, October 2007

"If opportunity doesn´t knock, build a door."
Milton Berle

Table of contents

1. Introduction

1.1 The neuron

There are two main classes of cells in the nervous system: nerve cells (neurons) and glial cells (glia). In contrast to cells from other tissues, neurons are highly polarized. Four different morphological regions can be distinguished in these cells: a cell body, dendrites, an axon and the presynaptic region (**fig. 1.1**). These morphological units have a special role in the generation of signals and the communication of signals between nerve cells (Kandel, Schwartz et al. 2000).

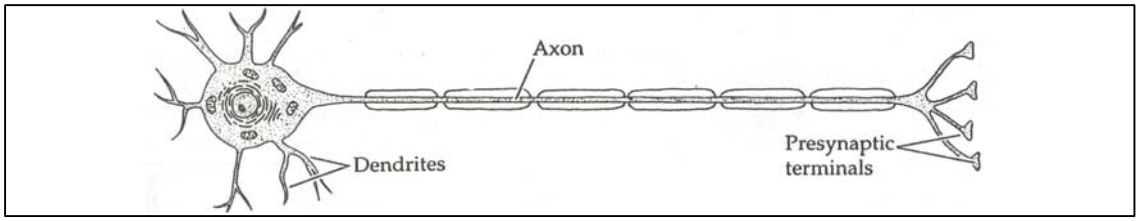

Fig. 1.1 Typical schematic neuron (modified from (Hall 1992).

The cytoskeleton is the major determinant of the shape of a neuron and is responsible for the distribution of the cell organelles. The main filamentous structures that compose it are: microtubules, intermediate filaments and actin microfilaments.

Microtubules form long scaffolds extending the full length of the neuron. They play a role in the development and maintenance of the neuron's dendrites and axons. Microtubule associated proteins (MAPs) regulate this process by promoting the oriented polymerisation and dynamic assembly state of the microtubules. Many MAPs show a polarized distribution in neurons. For example, MAP2 is present in dendrites but absent from axons; whereas tau and MAP3 are enriched in the axon (Kandel *et al.* 2000).

The most abundant of the filament within neurons are neurofilaments, the "bones" of the cytoskeleton. This is the main type of intermediate filament component in the axon.

The third cytoskeletal component, actin, is concentrated at the cell's periphery in the cortical cytoplasm lying just underneath the plasmalemma. Actin filaments are the most prominent element in growth cones, the motile structures at the tips of growing axons and dendrites (Gordon-Weeks 2004).

In addition to providing structure stability, both microtubules and actin filaments act as tracks along which organelles and some proteins are driven by molecular motors.

1.2 Neurodegenerative diseases: Alzheimer's disease and other tauopathies

The dynamic state of the neuronal cytoskeleton may have an important role in neuronal degeneration (Weissmann and Brandt 2007). There are a number of neurodegenerative diseases in which the cytoskeletal tau protein (see **1.3**) is involved in the pathology, and therefore are classified as "tauopathies". Apart from Alzheimer's disease (AD), some other less prevalent diseases belong to this group such as Pick's disease and Frontotemporal dementia and parkinsonism linked to chromosome 17 (FTDP-17).

In AD, tau is redistributed from the axon to the cell body and dendrites. In addition, the normally high soluble tau protein is present in an abnormal filamentous form where it shows a higher degree of phosphorylation and other post-translational modifications (Shahani and Brandt 2002).

Clinically, AD is characterised by a progressive loss of memory and cognitive functions resulting in a severe dementia. Neuropathologically, two type of protein aggregates are the main features found in the disease, the presence of extra cellular amoyloid protein plaques and of intracellular neurofibrillary lesions of abnormally hyperphosphorylated tau proteins (Brandt, Hundelt et al. 2005).

After the first mutation in the *tau* gene was linked to a case of frontotemporal dementia with Parkinsonism, additional mutations were found and all the cases were grouped under the FTDP-17 denomination. A major characteristic of this progressive dementia is the filamentous pathology consisting of aggregated hyperphosphorylated tau proteins. The morphology, isoform composition and distribution of tau filaments and deposits however, vary according to the type of mutation involved (see **1.3**) (Brandt *et al.* 2005).

1.3 Tau proteins

As mentioned before, tau proteins belong to the microtubule-associated proteins (MAP) family and are found in many species such as *Caenorhabditis elegans, Drosophila,* goldfish, rodents, bovines, goat, monkeys and humans. In humans, they are mainly present in neurons (Buée, Bussière et al. 2000). The human *tau* gene is located on the long arm of chromosome 17 and contains 16 exons in the CNS. The different tau isoforms are produced by alternative splicing of exons 2, 3 and 10. Accordingly, the

isoforms range from 352 to 441 amino acids and show apparent molecular weights between 50 kDa and 70 kDa. In addition, a high molecular weight isoform of 120 kDa is only expressed in neurons from the peripheral nervous system (Andreadis 2005).Tau proteins have been described as proteins that bind to microtubules and regulate microtubule assembly and stability.

Structure, functions and intracellular interactions of tau

According to the amino acid composition and sequence, different regions can be distinguished in tau proteins. The N-terminal part of tau contains the projection domain that protrudes from the microtubule surface when tau is bound to microtubules. The C-terminal part encompasses the microtubule binding domain, which contains a repeat-region with three or four repeats (depending on the splicing) and a neighbouring proline-rich region (**fig. 1.2).**

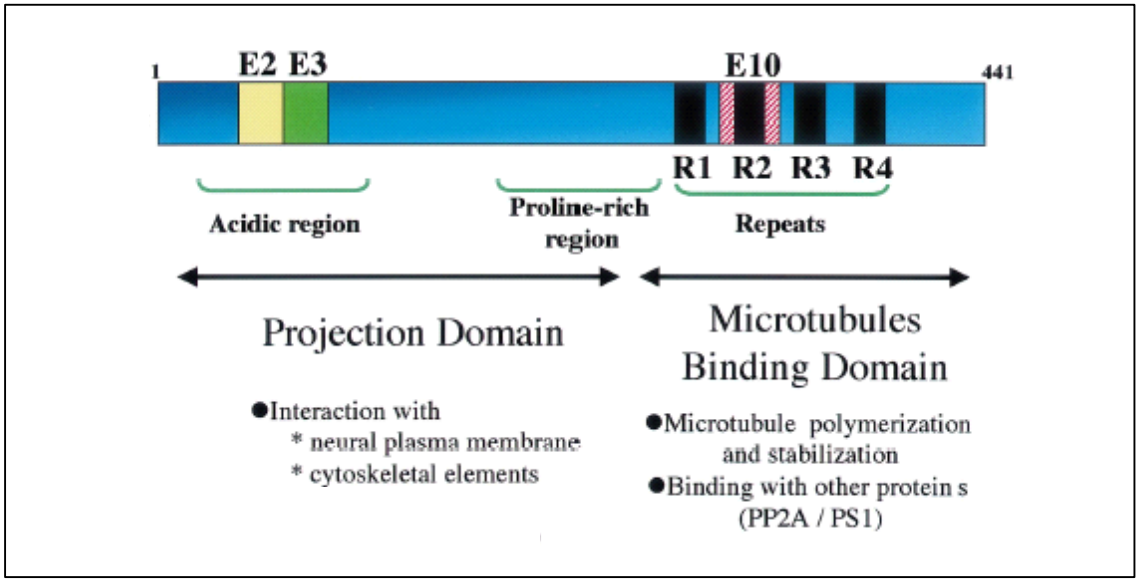

Fig. 1.2 Schematic of regions present in the tau protein and tau interacting partners. Modified from (Buée *et al.* 2000).

The projection domain has been reported to be involved in determining the spacing between microtubules in axons (Brandt and Lee 1993). This domain has also been described to interact with the neural plasma membrane (Brandt, Léger et al. 1995). Thus, tau proteins could act as mediators between microtubules and the plasma membrane.

The repeat region is responsible for the binding of tau to microtubules, and for the regulatory effect on polymerization and stabilization. This region can also interact with other cell components such as microfilaments, mitochondria, and protein phosphatase 2A. This region has also been shown to be important for tau aggregation (Brandt and Leschik 2004). Therefore, all factors that interact with the repeat region are candidates to modulate tau microtubule interaction and tau aggregation during disease processes.

The mentioned interactions could have major consequences in the pathological properties and distribution of tau.

Tau phosphorylation and disease

Tau proteins are substrates for many kinases such as glycogen synthase kinase-3 (GSK3β) and cyclin-dependent kinase 5 (cdk5) (Stoothoff and Johnson 2005)The longest brain tau isoform (441 amino acids) exhibits 79 putative phosphorylation sites (serine or threonine).

Phosphorylation of tau proteins seems to play a key role in tau protein distribution and interaction with cellular structures. Phosphorylation of residues within the repeat region or flanking regions leads to a decrease in the interaction of tau with microtubules.

Furthermore, the phosphorylation state of tau proteins has also an impact on the interaction of tau with the membrane cortex. In general, less phosphorylated tau isoforms appear to have a higher interaction with the membrane cortex as determined by fractionation experiments (Maas, Eidenmüller et al. 2000).

Phosphorylation events are relevant during tau cell sorting. Tau proteins are found in all cell compartments but in different phosphorylation states (Buée *et al.* 2000). A proximal-distal gradient for phosphorylated tau proteins in axons of primary hippocampal neurons and in human NT2N cells, has been reported (Kempf, Albrecht *et al.* 1996; Mandell and Banker 1996; Maas *et al.* 2000).

During development, tau phosphorylation is highly regulated, being high in fetal states and decreasing with age (Kenessey and Yen 1993). In neurite outgrowth, special phosphorylation sites are suggested to be required for the development of cell processes whereas other sites might inhibit the formation of cell extensions (Stoothoff and Johnson 2005).

In both AD and FTDP-17, the degree of tau phosphorylation is highly elevated with

about 6-8 mol phosphate/mol protein higher than normal values of 1.9 mol phosphate/mol protein (Brandt *et al.* 2005). During AD, apart from tau aggregates, extracellular amyloid beta (Aβ) plaques are also a main hallmark of the disease. Interestingly, the Aβ component of the amyloid plaques has been reported to induce tau phosphorylation (Busciglio, Lorenzo et al. 1995; Stoothoff and Johnson 2005).

It is not clear yet however, whether phosphorylation is a cause or consequence of tau protein aggregation into filaments (Buée *et al.* 2000). Consequently, phosphorylation of tau proteins is a key aspect to model in the analysis of neurodegenerative mechanisms underlying tauopathies.

A Model molecule to study tau phosphorylation: PseudoHyperPhosphorylated (PHP) tau.

To determine the effect of disease-relevant tau phosphorylation, a tau mutant was generated by site directed mutagenesis of 10 serine (S) / threonine (T) residues to glutamate (Eidenmüller, Fath *et al.* 2000) to mimic the negative charge of a phosphate group (**fig. 1.3**). The sites mutated were those known to be highly phosphorylated in AD.

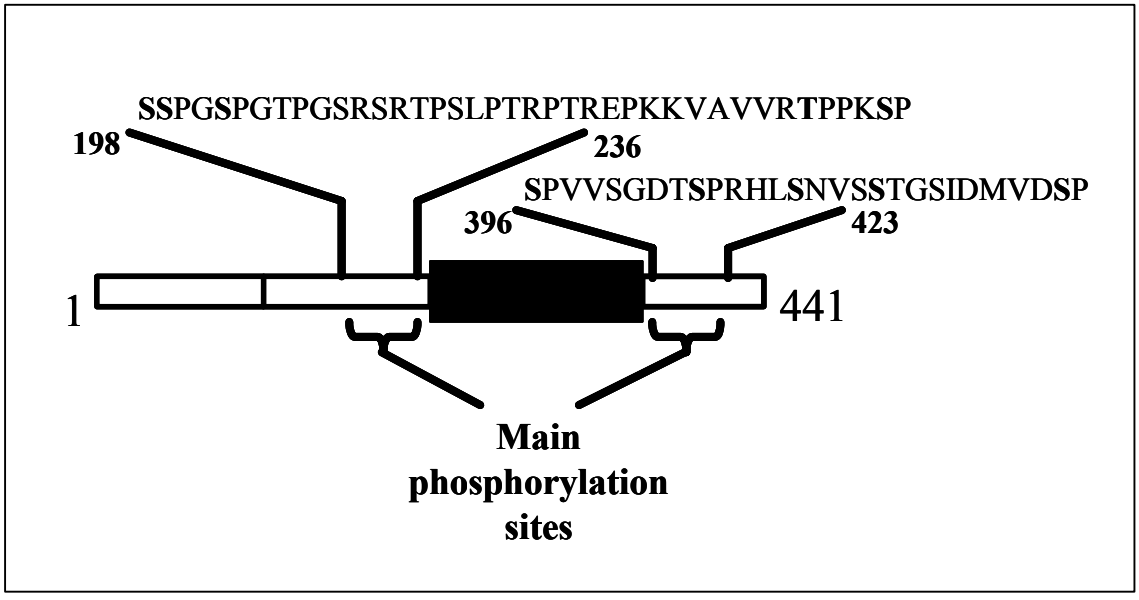

Fig. 1.3 Schematic representation of PHP-tau. S and T residues mutated to E are shown in bold. Modified from (Eidenmüller *et al.* 2000).

The mutant protein showed a deficiency in promoting tau microtubule nucleation in cell free assays, a loss of interaction with PP2A, and a reduced level of tau filament

assembly in conjunction with specific conformational changes in the protein similar to those found in hyperphosphorylated tau protein from AD patients (Eidenmüller *et al.* 2000). Thus, the data indicated that this mutant, which was termed "PseudoHyperPhosphorylated" (PHP) tau could be useful as a model to analyse the effect of tau hyperphosphorylation in cells.

PHP tau showed a loss of interaction with the neural membrane cortex (Brandt *et al.* 1995), and cytotoxicity in differentiated PC12 (rat Pheochromocytoma Cells) and NT2N (NTera2) neurons (Fath, Eidenmüller et al. 2002). In mouse hippocampal slices and primary cortical culture, the expression of PHP tau was associated with the development of a ballooned phenotype as a mechanism associated to cell death (Shahani, S.Subramaniam et al. 2006) (Leschik, Welzel et al. 2007). The data indicates that PHP tau simulates functional effects of disease-like modified tau protein and provides a model to analyse AD-relevant changes in cell and animal models in more detail.

Tau mutations in FTDP-17

Comparative analysis revealed over 25 mutations in the *tau* gene that are correlated with the FTDP-17 disease. The different mutations in *tau* can have different effects according to whether they affect the splicing of exon 10 or whether they are missense mutations located inside or outside of exon 10. Missense mutations lead to a change in the protein conformation that may determine a reduced ability of tau proteins to interact with microtubules. In the case of mutations whose primary effect is at the RNA level however, the net effect of the mutation is an overproduction of a tau isoform in detriment of another. Generally, the isoform with higher microtubule affinity is over-expressed. As a result, in the disease, microtubules become less dynamic. For this reason, a certain ratio between the different isoforms has been suggested to be essential for the normal function of tau in human brain.(Goedert and Jakes 2005). It remains to be clarified, the specific role played by the different mutations in the disease.

The R406W mutation

One of the mutations present in FTDP-17 cases is the R406W mutation in which the codon for arginine at position 406 is replaced by tryptophan (W) and is located on exon 13 at the 3´-end of the tau gene (Brandt *et al.* 2005).

In tau deposits from FTDP-17 cases with this mutation, the level of phosphorylation on mutant tau is higher than normal leading to a decrease in its microtubule-binding capacity. In contrast, different cell models have indicated that the protein is phosphorylated to a lesser extent (Pérez, Lim et al. 2000; Zhang, Higuchi et al. 2004). In this case, the effect of the mutant was a slight increase in microtubule stability. The fraction of the mutant which was found phosphorylated however, was unable to bind to microtubules, suggesting that this pool might then accumulate in the cytoplasm (Pérez *et al.* 2000).

On the other hand, a neuronal cortical cell model showed that the mutant tau protein was phosphorylated to a higher extent and bound less to microtubules, suggesting that an increased cytosolic free tau would be available for aggregation (Krishnamurthy and Johnson 2004). In addition, Miyasaka *et al* found that the mutant tau incorporated into aggregates was aberrantly phosphorylated similar to aggregated wild type, but the mutant from the soluble fraction was present in a hypophosphorylated state (Miyasaka, Morishima-Kawashima et al. 2001). Thus, the data on the effect of this mutation remains controversial and requires further analysis.

1.4 Cell models

Tau interactions with cell structures and regulation of these have been analyzed in several *in vitro* studies, as previously mentioned. It seems important to determine whether these interactions occur *in vivo* and to determine the contribution to tau distribution and disease-related misdistribution. To this effect, different cell models that simulate a neuronal context can be used.

The PC12 pheochromocytoma is a clone of chromaffin-like cells derived from a transplantable rat adrenal medullar tumour. When these cells are cultured in a monolayer and exposed to nerve growth factor (NGF), they exhibit several neuron-like characteristics: outgrowth of long neuritic processes, formation of small synaptic-like vesicles, and increased synthesis and storage of acetylcholine (Tischler, Grene et al. 1983). NGF treatment has been used to study neurite behaviour. In many aspects, the neurites of NGF-differentiated PC12 cells resemble the axon or dendrite precursors called “minor neurites”.

A more complex model is that of primary neuron cultures. In this case, a fully differentiated neuronal phenotype is acquired. This is important for the specific analysis of tau developmental sorting in axons and dendrites (Garth and Yao 2005).

Primary hippocampal and cortical neurons develop differentiated and functional axons and dendrites which form functional synapses, and they reproduce many aspects of neuritogenesis (Dehmelt and Halpain 2003).

Both cell models could be useful to analyse tau proteins in a more physiological context.

1.5 Protein dynamics in living cells

Tau proteins in tauopathies are localized in the somato-dendritic compartment instead of its normal distribution in axons. It seems therefore relevant to investigate the dynamics of tau proteins in living cells at normal and disease-like conditions to understand the distribution and sorting, as well as the misdistribution found in the disease.

The mechanism of protein distribution should explain the way in which these molecules which are synthesised at the cell body and proximal dendrites reach axonal terminals in neurons. Diffusion and transport of proteins are general mechanisms underlying protein mobility.

Diffusion of proteins

All proteins undergo diffusive movement if they are not immobilized or actively transported. A parameter to quantify this behaviour is the measurement of its diffusion constant (D). D reflects the mean squared displacement that a protein explores through a random walk over time (Lippincott-Schwartz, Snapp et al. 2001). This is a consequence of the random migration of molecules or small particles due to thermal energy (Berg 1993). According to the Stokes-Einstein formula, D depends on the temperature, the viscosity of the solution where the movement occurs, and the radius of the particle in motion.

Other factors that influence diffusion in living cells are protein-protein interactions, binding to a matrix, or collisions to other molecules all of which hinder free diffusion.

Diffusion has been studied in neurons. Fluorescent macromolecules (albumin, and dextrans conjugated to a fluorescent label) were tracked down on *Xenopus laevis* neurons, and this movement could be modelled as a diffusion process (Popov and Poo 1992). Interestingly, diffusion measured in the neurite cytoplasm was found to be 5

times lower than that measured in aqueous solution; this effect was attributed to the presence of a cytoskeletal meshwork.

Directed transport

In 1948, Weiss visualized the movement of the axoplasm by tiding off a sciatic nerve and checking on the accumulation of material at the ligature. The term used to describe this movement was "axoplasmic flux" (Kandel *et al.* 2000). It was proposed as a mechanism that would deliver cell components to the distal part of the axon (anterograde direction), since diffusion from the cell body becomes limiting for long axons (Brown 2003).

Distinct components of this type of transport have been described, i.e., a fast and a slow one which differ in their cargoes and the speed. Membranous organelles move most rapidly (50-400 mm/day) in the fast component of axonal transport, whereas cytoskeleton polymers and cytosolic protein complexes move more slowly (0.2-8 mm/day) in the slow components (Baas 2000). Fast axonal transport was demonstrated to be carried out by different motor proteins such as kinesins for the anterograde direction, and dyneins for retrograde transport on microtubule tracks. The chemical energy is converted into mechanical energy through the hydrolysis of ATP, causing a small conformational change in a motor domain that is translated into movement.

The inability to observe slow axonal transport determined that the mechanism underlying it remained a mystery for a long time. More recently, new methods gave strong indication that all transport is carried out by fast motors and that the difference between the transport speeds is determined by the time of paucity between phases of active motion (Brown 2003).

1.6 Methods to study protein dynamics within cells

The dynamics and distribution of proteins expressed in living cells can be studied by different approaches that use fluorescent molecules.

Fluorescent proteins and Photoactivatable Green Fluorescent Protein (PA-GFP)

Fluorescent molecules are nowadays extensively used for tagging proteins. The most common tags used for this purpose are different variants of GFP. GFP was originally obtained from the jellyfish *Aequorea victoria* and is about 27 kDa in size (Tsien 1998).

It shows 2 absorption peaks at 397nm and a minor 475 nm peak as a consequence of its state as a mixed population of 2 species, a neutral phenol and anionic phenolate. A variant of GFP that shows increase absorption of the molecule at 475 nm, "enhanced GFP" (eGFP) was afterwards generated. More recently, a photoactivatable variant (PA-GFP) was produced. The mutations on eGFP to produce the PA-GFP molecule were described by Lippincott-Schwartz *et al* in 2003 and included 4 different mutations. Two mutations (L64F, T65S) recover the wild type absorbance properties of GFP; a third mutation (V163A) improves folding at 37°C, and a fourth mutation (T203H) reduces the minor peak while retaining the major peak at 400 nm (Patterson and Lippincott-Schwartz 2002). PA-GFP which shows only weak fluorescence when illuminated by a 488 nm laser can be activated with near U.V. irradiation and increases its fluorescence up to 100 fold after 488 nm illumination (**fig. 1.4**).

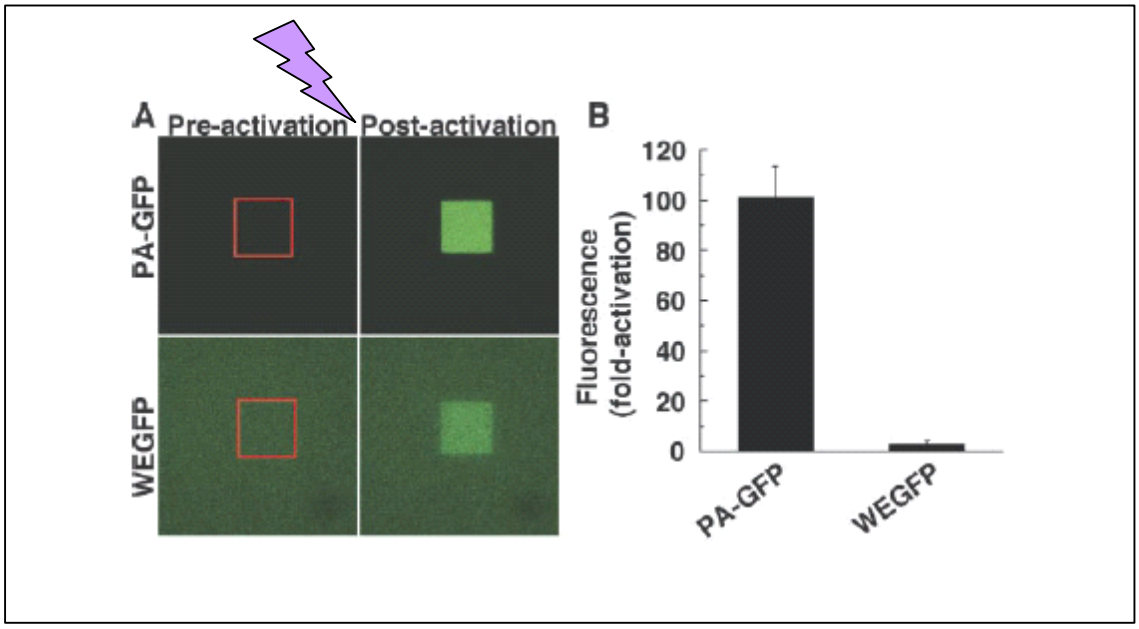

Fig. 1.4 Photoactivation of wt-GFP and PA-GFP. In (A) embedded PA-GFP and WEGFP in polyacrilamide were imaged with a 488 nm laser before and after the irradiation of the square region (in red) with a 400 nm light. In (B) the fold of fluorescence after photoactivation is shown. Modified from (Patterson and Lippincott-Schwartz 2002).

PA-GFP used as a protein tag shows advantages in comparison with other photoactivatable molecules available. For example, Kaede and kindling fluorescent protein 1 (KFP1), show a self association property into tetrameric forms limiting its use as tag to study localization and trafficking of proteins. In contrast, PA-GFP self associates only to a small extent (Lippincott-Schwartz, Altan-Bonnet et al. 2003). In this respect, the diffusion properties of GFP-tagged versus mGFP-tagged (a monomer

form of GFP) trans-membrane and GPI-anchored proteins were found to be similar (Goodwin and Kenworthy 2005).

These fluorescent or photoactivatable molecules fused to proteins, in combination with special equipment, allow the measurement of protein dynamics**.**

Techniques

Fluorescent molecules within cells can be analysed with different approaches. Time-lapse fluorescence microscopy enables the localization and distribution of fluorescently-tagged proteins in time. Fluorescent recovery after photobleaching (FRAP) experiments, and photoactivation (PA) experiments select a subpopulation of tagged proteins to study their distribution and equilibration in time (**fig. 1.5**).

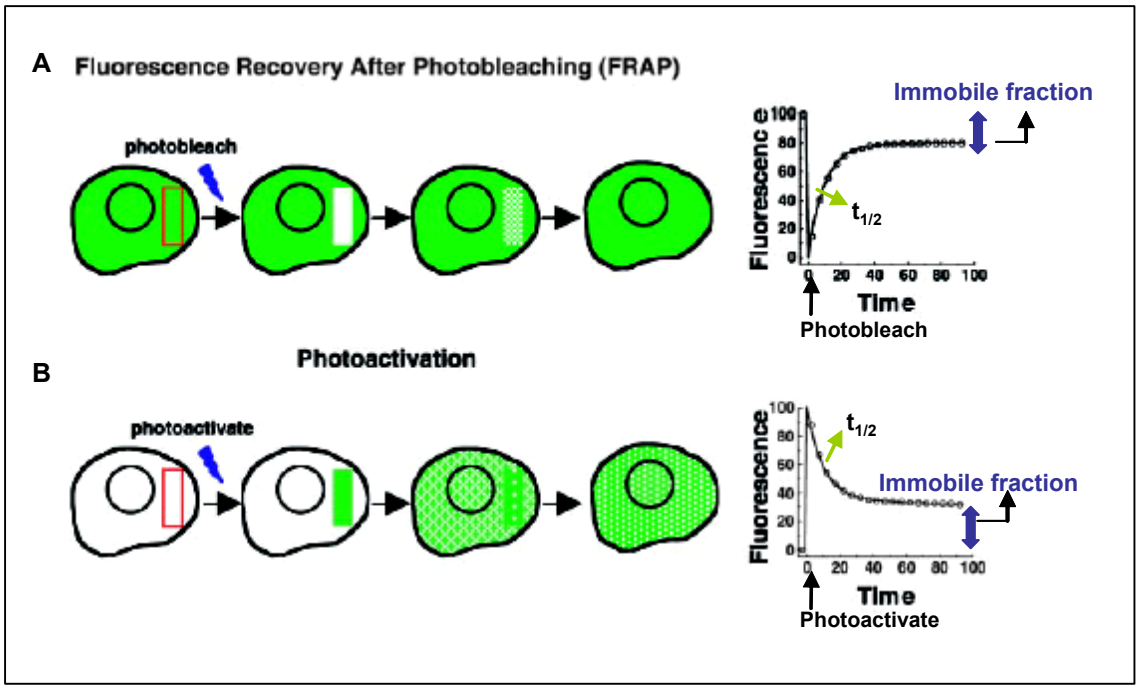

Fig. 1.5 Fluorescence techniques to measure protein dynamics within living cells, modified from (Lippincott-Schwartz and Patterson 2003).

Native photoactivatable molecules display little initial fluorescence at the imaging wavelength but increase their fluorescence after activation (**fig. 1.5, B**). This allows the direct labelling of a pool of molecules (the photoactivated molecules) in a cell to follow their mobility in time. This is the inverse to a FRAP experiments: while FRAP switch a subpopulation of molecules "off" by photobleaching (**fig. 1.5 A**), photoactivation experiments switch them "on".

FRAP and photoactivation techniques can provide an estimation of the effective diffusion coefficient, mobile fraction, and half time of decay ($t_{1/2}$), the time required for the intensity to reach 50% of the initial value (**fig 1.5**). These parameters are affected by molecule interactions. For example, the incorporation of the protein into an aggregate or a large complex determines a lower mobility. Inversely, a faster mobility constant could be a consequence of the protein being actively transported by motor proteins (Lippincott-Schwartz *et al.* 2003).

Photoactivation experiments were performed to study movement of neurofilaments along axons, and the experiments using it were named as "pulse-escape fluorescence photoactivation techniques" (Trivedi, Jung et al. 2007). This method shows several advantages to photobleaching approaches (Lippincott-Schwartz *et al.* 2003) allowing to follow the labelled proteins in time.

1.7 Studies on tau distribution and mobility in cells

Tau proteins in nerve cells show a polarized distribution: they are enriched in the axon. Several mechanisms have been proposed for this polarity: the selective transport of tau mRNA to the proximal axon in cultured neurons (Litman, Barg et al. 1993); a differential stability of tau against proteolytic degradation in the axon (Hirokawa, Funakoshi et al. 1996); a locally regulated microtubule binding in the appropriate compartment (Hirokawa *et al.* 1996); and a specific binding of tau to an axonal plasma membrane component (Brandt 1996). Phosphorylation could play a regulatory role in tau distribution since a proximal-distal axonal gradient of phosphorylated tau has been reported (Kempf *et al.* 1996; Maas *et al.* 2000). Phosphorylation could act in two ways: it could influence microtubule affinity thereby affecting its mobility, or it could regulate tau degradation, since phosphorylated forms are less prone to proteolytic cleavage. All these mechanisms could act in concert to determine the segregation of tau to the axonal compartment of neurons (Hirokawa *et al.* 1996). Initial studies on the mechanisms responsible for this distribution identified tau proteins as components of the slow axonal transport (Tashiro, Sun et al. 1996). Experiments using fluorescently-tagged tau proteins supported the slow axonal transport rate of tau for different isoforms and mutants (Utton, Connell et al. 2002). Studies using a radiolabel mark determined a retarded axonal transport of the R406W mutant tau in transgenic mice with a tauopathy as compared to wild type tau mice (Zhang *et al.* 2004).

Tau-microtubule interactions were analysed by different approaches. Data showing the movement of tau ahead of labelled tubulin implied that interactions of tau with microtubules were highly dynamic with a cycling of tau on and off microtubules during axonal transport (Mercken, Fischer et al. 1995). In agreement, photobleaching experiments performed on eGFP-tau proteins indicated that the interaction of tau with microtubules was very dynamic (Samsonov, Yu et al. 2004).

Fluorescent tracking methods in rat cortical cells were recently used to study tau mobility (Utton, Noble et al. 2005). Tau was described as being present in **particulate structures** in low fluorescent axons and moving in the same fashion as neurofilaments: through fast axonal transport in combination with pauses and associated to kinesin-1 motors. However, no other reports have described tau as present in such particles.

Additionally, tau dynamics investigated quite recently by FRAP analysis in neuron cells described tau proteins as diffusing along short processes (Konzack, Thies et al. 2007). Understanding tau distribution and mobility could shed light on mechanisms underlying tau pathology, and using the proper technique seems of main importance to give accurate results to this aim.

1.8 Aim of the project

Tau proteins are MAPs which are normally enriched in the axons of neurons. In a number of diseases (tauopathies), tau is found in a modified form and aggregated in the somato-dendritic compartment.

The aim of this work was to establish a system to study tau dynamics in living neuronal cells. Using this system, the mobility and distribution of tau at normal and disease related conditions should be analysed. This would help to clarify mechanisms that account for the normal tau distribution and the misdistribution during the disease.
For this purpose, several steps had to be undertaken:

(1) A system had to be developed to perform photoactivation experiments using photoactivatable-tau expressing cells.
(2) A quantitative parameter for different tau proteins (wild type, mutants, deletions, and controls proteins) had to be measured.
(3) Interactions with cellular components had to be tested and confirmed by disrupting cytoskeletal structures with the use of drugs.
(4) Disease-relevant conditions had to be modelled.

2. Materials and methods

2.1 Materials

2.1.1 Chemicals

All chemicals used were purchased from Chemicon (Hofheim), Merck (Darmstadt), Carl Roth GmbG & Co. KG (Karlsruhe), Serva Feinbiochemica GmbH (Heidelberg), Sigma-Aldrich Chemicals GmbH (Deishofen) and Riedelde Haen AG (Seelze) unless otherwise stated. Cell culture products were obtained from GIBCO BRL Life Technologies GmbH (Karlsruhe). Double distilled water (ddH_2O) was obtained with a Milli-Q Plus Ultra-Pure Water System from the Company MILLIPORE GmbH (Eschborn), 18.2 MegaOhm. Liquid nitrogen was obtained from the Physics Institute form the University of Osnabrück.

2.1.2 Materials molecular biology

Available Plasmids

Kan^R: Kanamycin resistance Neo^R Neomyicin resistance Amp^R Ampicilline resistance

Name	**Selection marker/**	**From**
peGFP-C1	Kan^R Neo^R	Clontech
pCMV-eGFP-tau wt	Kan^R Neo^R	Jochen Eidenmüller
pRC/CMV-flag-tau wt	Amp^R Neo^R	Jochen Eidenmüller
pRC/CMV-flag-tau delta	Amp^R Neo^R	Jochen Eidenmüller
pRC/CMV-flag-tau mut	Amp^R Neo^R	Tarja Lappeteläinen
pRC/CMV-flag-tau PHP	Amp^R Neo^R	Jochen Eidenmüller
pCMV-eGFP-tau PHP	Kan^R Neo^R	Jochen Eidenmüller
pCMV-eGFP-tau PHP	Kan^R Neo^R	Jochen Eidenmüller

Constructed plasmid

Vector	**Insert**	**Enzymes (vector)**	**Enzymes (insert)**	**Resulting plasmid**	**Comment**
peGFP-C1	pCMV-PA-GFP-tauwt	*Bgl*II, *Nhe*I	*Bgl*II, *Nhe*I	**PA-GFPx1**	
pCMV-PA-GFP-tau wt	Amplified PA-GFP-C1 fragment; primers**	*Bgl*II, *Bam*HI	*Bgl*II	**PA-GFPx2**	Orientation checked with *Bpu*I10
PA-GFPx2	Amplified PA-GFP-C1 fragment; primers**	*Bgl*II, CIAP	*Bgl*II	**PA-GFPx3**	Orientation tested with *Bpu*I10 and finally western blot.
pCMV-eGFP-tau wt	PA-GFP-tau-wt after site-directed mutagenesis on eGFP-tau-wt primers*	*Bgl*II, *Eco47*III	*Bgl*II, *Eco47*III	**PA-GFP-tau wt**	*Bfi*I to check for absence of a band in PA-GFP constructs as opposed to eGFP constructs.
pRC/CMV-flag-tau mut	PA-GFP-tau	*Sac*I, *Nde*I	*Sac*I, *Nde*I	**PA-GFP-tau mut**	Presence of *Bgl*II site used as indicator of positive clones.
pRC/CMV-flag-tau PHP	PA-GFP-tau	*Sac*I, *Nde*I	*Sac*I, *Nde*I	**PA-GFP-tau PHP**	Presence of *Bgl*II site used as indicator of positive clones.
pRC/CMV-flag-tau delta	PA-GFP-tau	*Sac*I, *Nde*I	*Sac*I, *Nde*I	**PA-GFP-tau delta**	*Bgl*II site used as indicator of positive clones.

Primers

F: Forward R: Reverse

Name	Sequence
"L64F-T65S"(*)	5 ´- CCC TCG TGA CCA CCT TCA GCT ACG GCG TGC AG -3´ **F** 5´-CTG CAC GCC GTA CGT GAA GGT GGT CAC GAG GG -3´ **R**
"V163A" (*)	5´-GCA GAA GAA CGG CAT CAA GGC GAA CTT CAA GAT CCG CCA C-3´ **F** 5´-GTG GCG GAT CTT GAA GTT CGC CTT GAT GCC GTT CTT CTG C-3´ **R**
"T203H" (*)	5´- CGA CAA CCA CTA CCT GAG CCA CCA GTC CGC CCT GAG CAA AG -3´ **F** 5´ -CTT TGC TCA GGG CGG ACT GGT GGC TCA GGT AGT GGT TGT CG -3´ **R**
"Tandem " (**)	5´ -CCG GTC **AGA TCT** ATG GTG AGC AA -3´ **F** 5´-GCG GTA CCG TCG ACT GCA GAA TT- 3´ **R**
eGFP	(Clontech)

All primers used were purchased from biomers and were dissolved in ddH_2O to a final concentration of 100 pmol/µl

Bacteria strain

E. coli DH5α — supE44 ΔlacU169 (j180 lacZΔM15) hsdR17 recA1 endA1 GyrA96 thi-1 relA1, from Dr. Gerdes (Heidelberg)

Bacteria culture conditions

LB-Agar — Autoclaved LB-Medium with 15g/l Bacto-Agar
After cooling the media to about 37°C the required antibiotic was added.

LB-Media — 10g/l Bacto-Trypton (Gibco), 5 g/l yeast extract (Gibco), 10g/l NaCl, with 1 M NaOH to pH 7.5 (autoclaved)

Ψ-Media — LB-Media with 5g/l $MgSO_4$

TfbI: — 30 mM potassium acetate, 100 mM RbCl, 10 mM

	$CaCl_2$, 15% Glycerine, set with 0.2 M acetic acid to pH 6. 0.99 g $MnCl_2$ set to pH 5.8 and sterile filtered.
TfbII	10 mM MOPS, 75 mM CaCl2, 10 mM RbCl, 15% glycerol, set pH with KOH to 6.5 and sterile filtered.

Antibiotics

Ampicillin stock solution	100 mg/ml in ddH_2O, sterile (storage at -20°C) (Sigma).
Kanamycin stock solution	100 mg/ml in sterile ddH_2O (stored at -20°C), (Sigma).

Enzymes and size markers

All enzymes unless otherwise stated, were purchased from MBI Fermentas (St. Leon Roth).

The DNA-marker used was geneRuler^{TM} 1 kb DNA Ladder 0.5 µg DNA/µl (Fermentas). Enzymes used for molecular cloning are listed in **2.1.2.6**.

*Xho*I, *Mlu*I, *Xba*I were used to linearize plasmids for the generation of stable lines.

2.1.3 Material cell biology

Cell lines

PC12 cells were obtained from Dr. Wagner (Boston).

Animals

Mice	*Mus musculus* C57BL/6 NCrl (Charles River) Jico (Harlan Winkelmann)

Cell media

All culture media was sterile-filtered before use and stored at 4°C. The media was

pre-warmed at 37°C prior to use. Heat-inactivation of fetal calf serum and horse serum was achieved at 56°C for 1 hour.

Culture media

PC12 cells:

DMEM	Dulbecco´s Modified Eagle Medium (high gluocose), Gibco^{BRL} Life Technologies.
DMEM-Ser(um)	DMEM with 10% (v/v) FCS (Fetal Calf serum heat-inactivated), 5% (v/v) HS (Horse serum heat inactivated) 2 mM glutamine, 1% Penicillin/Streptomycin. 500 µg/ml of Geneticin (Gibco) were added for stable line production and 250ug/ml for maintenance of stable lines.
Imaging medium	Dulbecco´s modified eagle medium (high glucose) without Phenol red (Gibco).
Differentiation medium	DMEM or imaging media with 1% serum (0.67% FCS and 0.33 % HS) with 100 ng/ml 7S mouse NGF (Alomone Labs, Jerusalem, Israel). Stored in aliquots at 100 µg/ml in PBS at -80°C.

Mice primary cortical culture:

NB/B27	Neurobasal medium with 2% (v/v) B27-supplement, 2 mM NB/B27 glutamine, 1% FCS heat- inactivated 1% HS heat- inactivated, 25µM β-mercapthoethanol 100µg/ml Primocin^{TM}(InvivoGEn).
Dissection medium	Hanks´ balanced salts solution (HBSS) without

	calcium and magnesium (Life Technologies Bethesda; MD).
Dissociation media (PAA Laboratories)	Earle´s Minimum essential medium (1 x MEM) with Na- Bicarbonate, without L-glutamine.
Transfection media	
PC12	OPTIMEM- Media, Gibco^{BRL} Life Technologies, with 5% FCS, 2mM glutamine, 50 U/ml penicillin and 50 µg/ml streptomycin
PC12 stable lines	DMEM
Primary cortical culture	MEM 1% serum
Transfection agents	Lipofectamine^{TM} 2000 (Invitrogen)

Drug treatments

Compound	**Concentration**	**Incubation time**	**Source**	**Reference**	**Effect**
Colchicine	0.1 µM	30 min	Sigma	(Kempf *et al.* 1996)	Microtubule disruption
Taxol (Paclitaxel)	1 µM	1 hour	Sigma	(Pisano, Pratesi *et al.* 2003; Samsonov *et al.* 2004)	Microtubule stabilization
Cytochalasin	20 µM	30 min	Fluka	(Léger, Brandt et al. 1994)	Actin filaments disruption
Okadaic acid	10 nM	30 min	Sigma	(Brandt *et al.* 1995)	Phosphatases inhibition
Iodoacetic acid	0.5 mM	30 min	Sigma	(Toll and Howard 1979)	Glucolytic enzyme inhibition
Aβ (1-42)	1 µM	15 min	Bachem	Used according to (King, Kan *et al.* 2006; Leschik *et al.* 2007)	To determine

2.1.4 Material biochemistry

Primary antibodies

IFl: immunofluorescence WB: Western blot

Designation	Antigen	Type/species of origin	Dilution (application)	Source
Anti-GFP	GFP	Polyclonal/rabbit	1:100 (IFl) 1:5000 (WB)	MoBiTec
Anti-MAP2	MAP2 a and b	Monoclonal/mouse	1:200 (IFl)	Chemicon international
DM1A	α-tubulin	Monoclonal/rabbit	1:5000 (WB)	Sigma
Acetylated tubulin	Acetylated tubulin	Monoclonal/mouse	1:2000 (WB)	Sigma
Tau-5	All tau isoforms	Monoclonal/mouse	1:5000 (WB)	Neomarker

Secondary antibodies

Conjugated fluorophor or enzyme	Antigen/species of origin	Dilution (application)	Source
Cy3™ (Indocarbocyanine)	Mouse IgG (H+L)/Donkey	1:250 (IFl)	Jackson ImmunoResearch Laboratories Inc.
FITC (Fluorescein-5-isothiocyanate)	Rabbit IgG (H+L)/ Donkey	1:250 (IFl)	Jackson ImmunoReserach Laboratories Inc.
HPR (horse radish peroxidase)	Mouse IgG/ Goat	1:20000 (WB)	Dianova
HPR (horse radish peroxidase)	Rabbit IgG (H+L)/Goat	1:25000 (WB)	Jackson ImmunoReserach Laboratories Inc.

Fluorescent stains

Compound	Target structure	Dilution	Source
DAPI (4´-6-diamidino-2-phenylindole)	Double-stranded DNA (nucleus)	1:1000 (IFl)	Sigma
Rhodamine-Phalloidin	Actin	1:50 (IFl)	Invitrogen

2.1.5 Buffers and stock solutions

Molecular biology

1% Agarose solution	1% (w/v) in 1x TBE
TBE (5x)	TE pH 8.0, 0.45 M boric acid, 1 mM EDTA, 10 mM Tris/HCl, pH 7.4.
TE buffer	10mM Tris/HCl, pH 8.5; 1 mM EDTA.
Ethidiumbromid- stock solution	25 mg/ml in ddH_2O Applichem GmbH, Darmstadt.
Loading buffer (6x)	6x loading dye solution (MBI Fermentas)
1 x Ligation buffer	50 mM Tris-HCl, 10 mM MgCl2, 1mM ATP, 10 mM dithiothreitol, 25 µg/ml BSA, pH 7.5 at 25°C.
Site directed mutagenesis	Quick Change® Site-Directed Mutagenesis kit (Stratagene).
DNA kits:	Qiagen ®DNA-Extraction kit (plasmid preparation) mini and Maxi Promega Pure Yield^{TM} Plasmid Midi Prep System Qiagen PCR purification kit Qiagen gel extraction kit

Cell biology

Fixation reagents

DAPI stock solution	1 mg/ml 4´, 6´-diamidino-2-phenylindol in DMSO
Extraction solution	0.5% (v/v) Triton X-100 in PBS

Glycine solution	0.1M glycine in PBS
Anti-fade solution	Confocal matrix® Micro-tech-lab
Triton solution	0.5% (v/v) of triton x-100 (t-octyl-phenoxypolyehoxyethanol) in PBS prepared from 10% (w/v) triton-stock
Paraformaldehyde- Fixation solution	4% (w/v) paraformaldehyde added to 70°C-heated PBS, 1M NaOH drops are added until the solution is clear; once cool, 4% sacharose is provided.
NP-40 fixation-buffer	80 mM Pipes/KOH pH6.8, 5 mM EGTA, 1 mM $MgCl_2$, 0.5% (v/v) NP-40; 0.3% (v/v) glutaraldehyde (added before use).
PBS (1x)	8g NaCl, 0.2 g KCl, 0.2 g KH_2PO_4, 1.15g Na_2HPO_4 Ad 1l with ddH_2O, pH 7.4
PBS/BSA-buffer	1% (w/v) BSA in PBS
PBS/BSA/Tween buffer	1% (w/v) BSA in PBS, 0.1% (v/v) Tween 20, 0.02% (w/v) Sodiumazid
PBS/BSA/Tween buffer	1% (w/v) BSA in PBS, 0.1% (v/v) Tween 20, 0.02% (w/v) Sodiumazid
Collagen solution	50 µg/ml collagen in 0.02 N acetic acid (sterile filtered)
Poly-L-lysine solution	100 mg/ml poly-L-lysine in borate buffer.

Laminin solution	4 µg/ml laminin (Chemicon) in carbonate buffer.
Trypan blue solution	0.4% (v/v) Trypan blue (Sigma) in ddH_2O.
Borate buffer	1.24 g borate, 1.9 g borax (Na-Tetraborate) filled to 400 ml ddH_2O, pH 8.5
Carbonate buffer	0.05 M Na_2CO_3 in ddH_2O, pH 9.6

Immunoblot analysis

Lysates

Lysis buffer (with proteinase and phosphatase inhibitors)	RIPA buffer supplemented with 2% (v/v) Na-orthovanadate (100 mM), 2% (v/v) Na-pyrophosphate (100 mM), 2% (v/v) NaF (2 M), 2% (v/v) pepstatin, 1% (v/v) leupeptin, 1% (v/v) PMSF (in ethanol) ad 1ml with ddH_2O
RIPA buffer (2x)	ddH_2O supplemented with 100mM Tris-HCl (pH 7.5), 300 mM NaCl, 2 mM EDTA; 2% (v/v) NP-40, 1% (v/v) DOC, 0.2% (w/v) SDS

Agarose gel electrophoresis

Sample loading buffer (5x Laemmli)	300 mM Tris/HCl pH 6.8, 10% (w/V) SDS, 50% (v/v) glycerol, 0.005% bromopnenol blue, 6.25% (v/v) β–mercaptoethanol; aliquots stored at -20°C.
Acylamide/Bisacrylamide	Rotiphorese® Gel 30 (Roth)
APS solution in ddH_2O.	10% (w/v) ammonium Peroxydisulfate (Roth)

TEMED	N, N, N, N´-tetramethylethylenediamine (Aplichem)
Electrophoresis buffer (10x) 57.6g glycine, 4g SDS	400ml ddH_2O supplemented with 12 g tris-base,
Lower Tris (4x)	1.5M Tris/HCl, 0.4% (w/v) SDS; adjusted to pH 8.8
Upper Tris (4x)	0.5M Tris/HCl, 0.4% (w/v) SDS; adjusted to pH 6.8
SDS gel electrophoresis	300mM Tris/HCl pH 6.8, 10% (w/v) SDS;
Sample-loading buffer (5x)	50% (v/v) glycerol, 0.005% (w/v) bromophenol blue, 6.25% (v/v) β–mercapthoethanol; aliquots stored at -20°C
TBE electrophoresis buffer (5x) Tris/HCl pH 7.4	TE pH 8.0, 0.45 M boric acid, 1mM EDTA, 10 mM
TBS (10x) with HCl.	90g/l NaCl, 12.1g/l tris-base, adjusted to pH 7.4
Transfer buffer	0.2M glycine, 250mm Tris, 20% (v/v) methanol
TBS-Tween	1x TBS solution supplemented with 0.05% Tween (polyethylenesorbitan monolaurate)
Blocking solution milk powder.	TBS-Tween supplemented with 5% (w/v) non-fat
ECL detection reagent	50% (v/v) Luminol/Enhancer solution, 50% (v/v) peroxidase buffer (Pierce), prepared fresh before use.

PVDF transfer membranes	Immobilion-PVDF- 0.45 µm Polyvinylidenfluorid-Membrane: Transfer membrane Immobilion-P™ (Millipore GmbH, Eschborn)
Stripping solution	0.2% (v/v) SDS in 20 mM tris (2-carboxyethyl) phosphine hydrochloride (TCEP) in ddH_2O prepared fresh before use.

2.1.6 Equipment and others

Confocal microscope	Eclipse TE 2000-U (Nikon) equipped with T-RCP Remote Control Pad (Nikon), CO_2 enrichment accessory (Solent Scientific Ltd.) ConfocalC1 scan and detector unit (Nikon).
Fluorescence microscope	Eclipse TE 2000-U (Nikon Gmbh, Düsseldorf).
Light-optical microscope	Leitz Labovert (Leica Microsystems AG; Wetzlar).
Objectives	
Nikon Plan Apo Fluor air/oil immersion objectives	100x oil/1.3; 40x oil/1.3;40x/0.75; 60x oil/1.4 (VC)

Lasers

A 405 nm blue-diode laser (JDS Uniphase), a 488 nm argon-laser (Spectra-Physics Lasers) and a 543 nm Helium/Neon-Laser (Coherent) were used with the cLSM.

Incubation system

The cLSM was equipped with a 37°C incubator chamber for Nikon TE 2000 microscopes (Solent Scientific Ltd.).

Common equipment

Centrifuges	Megafuge 10R (Heraus) Biofuge fresco table top centrifuge (Heraueus).
Molecular Biology	
Agarose gel chamber	Custom manufactured (University of Osnabrück)
Gel imaging accessories	Gel Jet Imager (Intas), UV-chamber and optics (Intas)
Thermal cycler (PCR)	Eppendorf Mastercycler gradient (Eppendorf).
Cell biology	
Clean bench	HeraSafe (Heraeus).
Hemocytometer	Neubauer-type (Hecht), Volume 0.0025 mm^2, depth 0.1 mm.
Glass bottom culture dishes	P35G-1.0-14-C MatTek Corporation, Ashland, USA
Biochemistry	
ECL camera	Chemocam (Intas Science Imaging Instruments GmbH, Göttingen).
ECL chamber	EpiChemi II Darkroom (Intas).

Software

Molecular cloning	pDRAW32

Agarose gel-Documentation	Intas GDS imaging software
ECL documentation	Image Pro ® Plus, Version 4.5.1.2.7 (Media Cybernetics).Gel-Pro™ Analyser (Media Cybernetics).
Confocal microscope	EZ-C1 3.00 (Nikon)
Fluorescence microscope	Lucia GF 4.80 (Nikon)
Image editing	Adobe Photoshop 7.0 Adobe Illustrator 7.0 Scion image Version Beta 4.0.2
Data analysis	Microcal Origin 7.0, Statview™SE+graphics Matlab version 7.0

2.2 Methods

2.2.1 Molecular biology methods

Preparation of competent cells

To prepare cells for transformation, 5 ml LB- media were inoculated with a small aliquot of competent cells from a previous preparation and incubated overnight at 37°C. 100 ml of pre-warmed medium were inoculated with the overnight culture and agitated at 37°C for approximately 2 h until an optical density of about 0.5 at a wavelength of 600 nm was reached. The cultures were incubated for 2 min on ice and centrifuged at 5000 X g for 2 min at 4°C. The pellet was resuspended in 40 ml of ice-cooled TbfI solution, further incubated on ice 5 min and centrifuged for 2 min at the same conditions. The pellet was resuspended in 4 ml of ice-cooled TbfII solution and incubated for 15 min on ice. The suspension was frozen liquid nitrogen and stored as 100 µl aliquots at -80°C.

Transformation of competent cells

One µl of DNA was added to a 100 µl of competent cells and incubated for 30 min followed by a heat shock at 42°C for 1.5 min. After a further incubation on ice for two min, the volume was filled to 1 ml with LB-media and incubated at 37°C for an hour. Cells were pelleted at 5000 X g for 2 min, and the pellet resuspended in 100 µl. This suspension was plated on agar plates containing the antibiotic encoded in the incorporated plasmid. Cells were grown at 37°C overnight until colonies appear (12-15 hours).

Analysis of DNA

Plasmid DNA preparation (maxi, midi and mini preparation)

Plamids DNA from E. coli was isolated using different Qiaquick extraction kits.
5 ml LB-medium containing the antibiotic was inoculated with a colony or a small amount of a glycerol stock (see below) and cultured overnight. A glycerol stock of the bacteria containing the plasmid was prepared by loading 150 µl of glycerol and 850 µl of the overnight culture in a 1.5 ml cup. The suspension was shocked frozen in liquid nitrogen and stored at -80°C. The rest of the culture was used for a mini-prep preparation or further incubated to a larger volume for a midi (50 ml) or maxi (500 ml) preparation. Then the cells were harvested by centrifugation and the plasmid DNA was extracted according to the manufacturer's instructions.

Determination of DNA concentration

The DNA concentration was determined via photometric measurement at 260 nm. To determine the purity of the DNA, the 260/280 nm (DNA/protein) ratio was assessed. The DNA used for transfection had a DNA/protein ratio between 1.7 and 2. For the measurements, the DNA was diluted 1/70 with ddH_2O and the mixture was placed in a quartz cuvette.

Analysis of plasmids by restriction analysis

An analytic restriction analysis was used to identify plasmids according to a profile

of DNA bands obtained after digesting with a particular restriction enzyme. The restriction enzymes used were selected according to the pDRAW32 cloning program. For this, 0.2- 0.5 µg DNA was used for analytic digestion in a total volume of 10 µl. This was adjusted with ddH_2O. The restriction enzyme was added in a 1/10 dilution from a 10-fold stock. The mix was incubated at 37°C for an hour unless otherwise indicated for a particular enzyme in the product information. The samples were then analyzed via electrophoretical separation on an agarose gel.

Agarose gel electrophoresis of DNA

After analytic restriction, the digest was subjected to electrophoresis to separate the bands. The samples were loaded onto a 1% agarose gel supplemented with ethidium bromide. Before loading, samples were adjusted with the appropriate volume of 3x loading buffer. 2 µl were loaded per lane (samples and DNA marker).Gels were run for about an hour at approximately 70V. DNA bands were visualized and photographed under the UV-chamber using the INTAS imaging software.

Manipulation of DNA

Site directed mutagenesis

Mutations on eGFP to obtain the PA-GFP plasmid were performed using the Qiagen Quickchange® mutagenesis kit according to manufacturer's instruction. The primers used were "L64F-T65S", "V163" and "T203H" (**section 2.1.2)**.The Cycler program used to perform the mutations was the same one described in **section 2.2.1,** but in this case, the Ta used to perform the first mutation of eGFP was 63.2°C and for the second and third 61.8°C. PCR products were cleaned with the PCR clean kit from Qiagen. For sequencing, the DNA was eluted in ddH_2O.

Addition of restriction sites by PCR

To generate the PA-GFPx3 molecule (**section 2.1.2**; **fig. 3.6**), a new *Bgl*II site was added in the PA-GFPx1 plasmid by PCR:

- **AGA TCT** which was recognized by the *Bgl*II enzyme.

The primers used are listed in **section 2.1.2** and the PCR reation was performed using the *Pfu*Turbo® DNA Polymerase from the Stratagene kit with the volumes and steps as described in the following tables:

Substance	**Volume (µl)**
Reaction buffer	5
DNA template	(5-50) ng
Primers (10 pmol/µl) (for R and F)	1.25
dNTP	1
ddH2O	Ad 40

Ta: annealing temperature

Segment	**Cycles**	**Temperature (°C)**	**Time (sec)**
1	1	95	300
2	18	95	30
2		55 (**Ta**)	30
2		72	30
3		72	300

The PCR products were purified from the mix with the PCR purification kit from Qiagen.

Generation of new plasmids

PA-GFP fusion proteins were prepared from plasmids available at the laboratory as described in **section 2.1.2.**

Vector and insert were prepared in large amount by maxi preparation (Qiagen). 5 µg vector and 15 µg insert were digested with enzymes at concentration 3 times higher (for vector) and 7.5 times higher (for insert) than what was used for an analytical restriction. Digestion volumes were adjusted to a total of 30 µl (insert) and 15 µl (vector).

The samples were incubated 2 to 3 hours and then loaded onto 1% agarose gels. A DNA marker was loaded as a size reference. After the gel was run, the bands with the expected size were excised with a scalpel. The DNA was separated from the agar with the gel extraction kit from Qiagen®.

Vector and insert DNA were incubated at 65°C for 5 min and a ligation mix was prepared and incubated at 16°C overnight. The mix used for the reaction was:

Reagent	Volume (µl)
10 x T4 DNA ligation buffer	1
Digested vector	X
Digested insert	Y
H_2O	Ad 10
Ligase	1

5 µl of the solution was then transformed in competent cells for plasmid amplification. The colonies obtained on selective agar plates were analysed by extraction of the DNA, restriction, and identification of separated DNA bands after electrophoresis.

Sequencing the DNA

To verify that the DNA sequence obtained was correct, plasmids were sequenced. This was performed at the Sequencing facility of the University of Osnabrück. Alternatively, it was sent to sequencing companies.

2.2.2 Cell culture

Cell culture work was carried out according to biological safety regulations in clean benches. Glassware was autoclaved prior to use and solutions sterile filtered. Incubators were adjusted to 37°C and 10% CO_2 (PC12 cells) and 5% CO_2 (primary cortical cultures).

Culture of PC12 cells

PC12 cells are derived from a rat adrenal pheochromocytoma (Tischler *et al.* 1983).

PC12 cells were cultured on collagen-coated culture dishes and splitted to new dishes when confluence was reached (every 2 to 3 days). The cell media used was DMEM-serum and was exchanged every 2 to 3 days. For splitting, the cells were rinsed off the dishes by pipeting the media up and down along the dishes. The cultures were incubated at 37°C and 10% CO_2 in a humidified atmosphere.

Preparation and culture of mouse primary cortical cultures

Primary cortical cultures were prepared from E15-17 (embryonic, day 15-17) mouse

cerebral cortex tissue as described by Leschik *et al*, 2007.

Viable cells were counted and plated in 35 mm pre-coated glass bottom dishes with NB/NB27 culture medium. Cultures were maintained at 37°C and 5% CO_2 in a humidified atmosphere prior to transfection.

Transfection

In this work the transfection method used was the liposome-mediated gene transfer with lipofectamine reagent (Invitrogen).

Transient transfection

PC12 cells

One day prior to transfection, PC12 cells were plated out in 35 mm glass bottom dish (1.5 ml medium) at a density of $1x10^4$cell/dish or in 4-well dishes to achieve a confluency of 70-80 % after 24 h incubation at 37°C and 10% CO_2. The transfection reagents were prepared in different tubes:

Tube 1: DNA 0.5 µg (4-well dish)/ 2.5 µg (35 mm dish) + 20 µl (4-well dish)/100 µl(35 mm dish) transfection media.

Tube 2: Lipofectamine 4 µl (4-well dish)/ 10 µl (35 mm dish) + 20 µl/100 µl transfection media.

The tubes were incubated at RT for 5 min and then the content of tube 1 was added to tube 2 drop wise. The mixture was incubated for 15 min or 45 min (stable lines) at RT, transfection media was added to pour the content drop wise to the culture dish. Cells were kept for 5 hours in the incubator and then DMEM-serum was added to the dish. After an ON incubation, the media was changed. The volumes used were:

Volume added to transfection mix: 200 µl (4-well dish)/ 500 µl (35 mm dish).

Volume added to cells after 5h incubation: 260 µl (4-well dish)/ 650 µl (35 mm dish).

Volume exchanged for: 500 µl (4-well dish)/ 2 ml (35 mm dish) DMEM-serum.

Transfection medium: OPTIMEM (for transfection of wild type cels); DMEM (for transfections of stable lines).

Primary cortical cultures

Primary cortical cultures were plated on PLL and laminin coated (**section 2.2.3**) 35 mm culture dishes at a density of $4x10^5$cells/chamber and incubated for 8 days at 37°C, 5% CO_2 with NB27 medium before transfection. The transfection mix was prepared by preparing the DNA (1-2 µg) in a total of 100 µl 10% MEM (tube 1), and a second tube with 7 µl Lipofectamine 2000 in 100 µl of 10% MEM (tube 2). Tube 2 was added to tube 1, mixed and incubated for 30 min at RT. The transfection mix was filled to 1 ml with 10% MEM and mixed. The medium from the dishes containing the cells was removed, and immediately the transfection mix added drop wise. The cells were incubated for 2.5 h at 37°C, 5% CO_2 and after this period, the medium was exchanged for fresh 10% MEM. Cells were further incubated until imaging on the next day.

Stable transfection

The generation of stable lines is schematized in **fig. 2.1**. PC12 cells were cultured to reach a 70-80% confluent 10 cm dish. For transfection, the following reaction mix were prepared:

Tube 1: 14.6 µg DNA + 584 µl pre warmed (37°C) OPTIMEM
Tube 2: 116.8 µl Lipofectamine + 584 µl pre warmed (37°C) OPTIMEM

Tube 1 was added drop wise into tube 2 and incubated for 15-20 min at RT. 5.84 ml OPTIMEM was added. The cell dish was washed twice with OPTIMEM to remove serum. With the addition of 7ml OPTIMEM, the transfection mix was loaded.
The dish was kept for 5 h in the incubator and then 7.6 ml DMEM-serum was added. On the next day, the media was changed with DMEM-serum. To increase the efficiency of plasmid integration into the cell genome, the plasmids used included also a sequence coding for the resistance to neomycin (G418). After 2 days, the medium was replaced with DMEM-serum containing 500 µg/ml G418 to start selection of transfected cells.
The medium was replaced every 2-3 days for 14 days. From then onwards, the medium was exchanged with DMEM-serum containing 250 µg/ml G418 until colonies could be detected with the naked eye. Colonies were picked under the dissection microscope and transferred to a collagen-coated 96-well plate containing 150 µl of 250 µg/ml G418 in DMEM-serum. Confluent culture dishes were divided onto collagen coated 24-well

plates in duplicates. One plate was used to check for the presence of the protein by western blots.

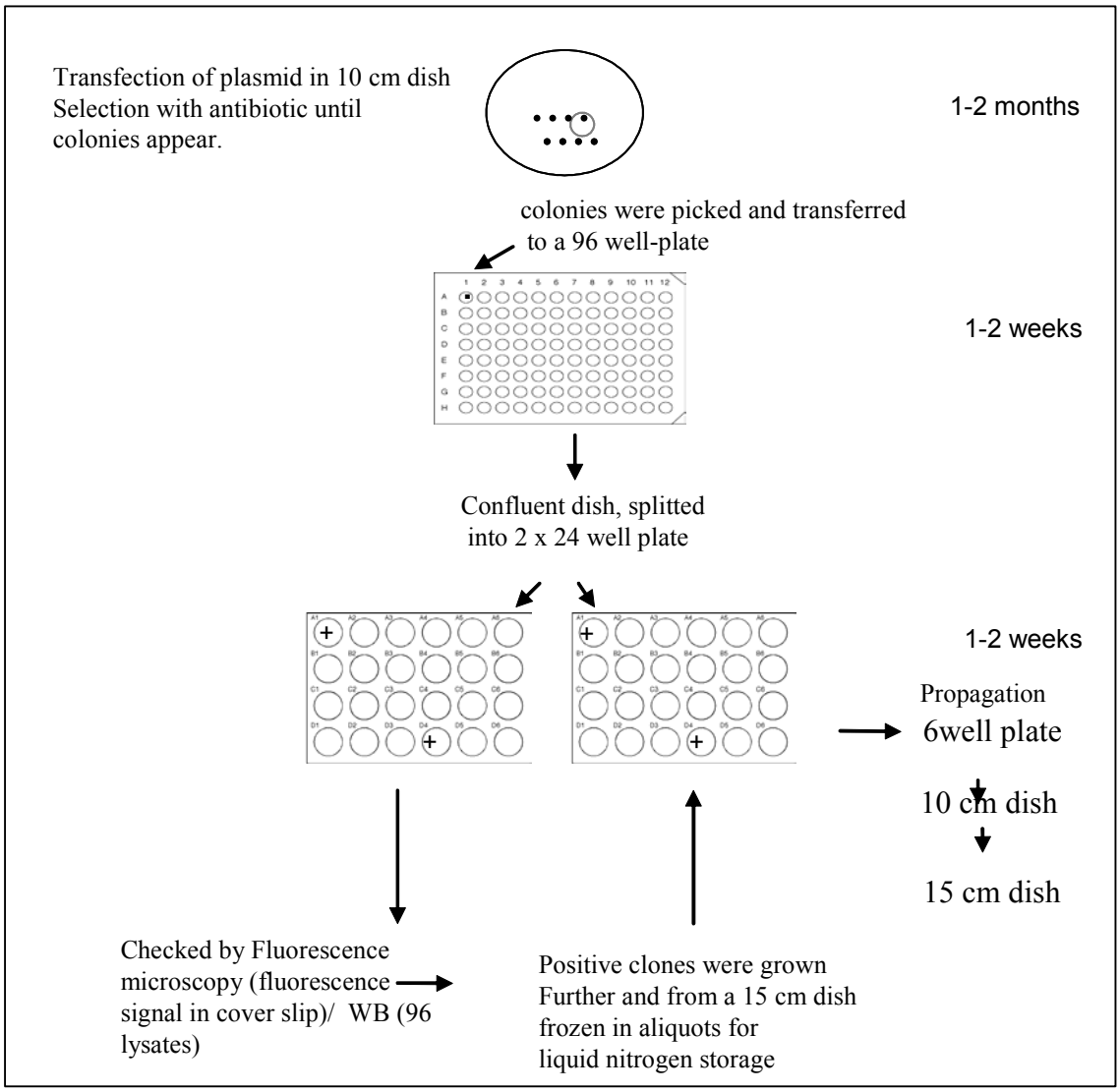

Fig. 2.1 Schematical preparation and time scale of the generation of stable lines.

The other dish was further incubated until confluent. Positive clones were transferred to a 6-well plate, later on to a 10 cm dish to a final 15 cm culture dish from which aliquots were prepared to store in liquid nitrogen.

Aliquot from positive clones were stored in liquid nitrogen with the addition of DMSO in a 1/10 dilution. These aliquots were re cultured and used for a maximum of 3 weeks.

NGF differentiation of PC12 cells

PC12 cells develop neurites in response to Nerve Growth Factor (NGF) treatment

(Tischler *et al.* 1983). Stable lines were seaded at a density of $1x10^4$ cells/chamber in DMEM-serum and incubated at 37°C, 10% CO_2. The following day the media was exchanged with differentiation media consisting of DMEM-1% serum instead of the normal 15% serum to decrease proliferation, and containing 100 ng/ml NGF for differentiation. For transient transfections, the transfected cells were subjected to NGF treatment two days after transfections.The media were changed every 2-3 days. Cells were analysed up to 6 days after NGF treatment.

Drug treatment of PC12 cells

PC12 stable lines cultured on 35 mm glass bottom dishes were differentiated for 6 days with NGF and different drugs were tested. The incubation media was exchanged with DMEM-1% serum without phenol red and containing the drug. Drug concentration and incubation times were those described in **section 2.1.3**.

2.2.3 Immunocytochemistry

To visualize proteins within cells, cells were grown on attaching surfaces, fixed and treated with antibodies and dyes against target structures. The fluorescent antibodies and dyes were visualized by microscopy.

Coating of coverslips and chambers

For culturing PC12 cells, glass-bottom culture dishes or coverslips were coated with PLL solution (100 mg/ml in borate buffer) to improve the attachment of the cells to the surface and incubated over night at 37°C. The following day the PLL solution was removed and the dishes were washed twice for 1 hour with ddH_2O. Then a collagen solution (50 µg/ml) was applied to the dish and further incubated for 1 h at 37°C. The collagen solution was then removed from the dish, and washed with PBS**.**

For primary cortical cultures, bottom-glass dishes PLL coating was followed by laminin coating. The laminin solution (4µg/ml) was incubated for 5 hours and washed twice in ddH_2O before use.

Fixation and staining of cells

Paraformaldehyde (PFA) fixation

Fixation of cells grown on coverslips or glass bottom dishes was performed according to Leschik et al, 2007. For immune staining, coverslips were incubated with antibodies or dyes in the concentration and time indicated in **sections 2.1.4**; **2.1.4** and **2.1.4**.

NP40 extraction/fixation

To remove soluble cytosolic proteins and visualize cytoskeletal and cytoskeletal-associated proteins, an NP40 extraction/fixation protocol was used as described by Léger *et al*, 1994. The coverslip could be used for subsequent immunostaining as indicated for PFA fixation.

2.2.4 Immunoblot analysis

Immunoblot analysis was performed as described by Fath *et al*, 2002. Lysates were prepared from confluent cell cultures, either from 4-well dishes (from transient transfections or stable line screening), 10 cm dishes or 15 cm dishes (analysis of stable lines). The volumes of the reagents were rescaled in each case according to the growth area of each culture dish. Electrophoretic separation was done on a discontinuous system of 3.5% (stacking) and 10% (resolving) SDS polyacrilamide gels. Gels were run at 100 V until the bromophenol blue dye-front entered the separation gel, and then the voltage was increased to 150 V. The blots were stained with the antibodies described in **sections 2.1.4 and 2.1.4.**

To quantify the proteins within the samples, protein standards of known concentration were run on the gel together with the samples. The quantification analysis of the recorded images was performed with Gel-Pro^{TM}Analyser.

In order to perform different immunodetection analysis on the same membranes, these were stripped off their bound antibodies. PVDF membranes were washed 3 times for 10 min in ddH_2O, and incubated with stripping solution for 1h at 37°C. After the incubation, the membrane was washed 3 times for 10 min with ddH_2O and was ready to be incubated with new antibodies.

2.2.5 Microscopy

Bright field microscopy

Inverted bright field microscopes was used for daily checking of cells, to determine confluency, and, with the help of a contrasting dye (trypan blue), to determine cell density in a Neubauer counting chamber as described by Fath *et al*, 2000.

Conventional fluorescence microscopy

For the imaging of fixed samples, the Nikon ECLIPSE TE2002-U inverted fluorescence microscope equipped with a high-pressure mercury lamp as a light source and a panel of monochromatic filters allowing excitation of specific fluorophores was used. The samples were imaged with 100x and 40x objectives and the images acquired with a cooled-CCD-camera. The software used was Lucia GF (Nikon).

Confocal Laser Scanning Microscopy (cLSM)

For photoactivation experiments of living cells, a cLSM was used. Confocal microscopy allows the suppression of out of focus information at the level of image acquisition. The light source used in this case is typically a laser that produces high-intensity, and coherent light of a defined wavelength. The spatial selectivity is especially useful for thick specimens where light emitted from different layers can distort the final image. This selectivity in z-direction (perpendicular to the specimen plane) or axial selectivity is strongly influenced by the so called “pinhole”, an adjustable iris in the detection beam path. Closed pinhole leads to high z-resolution whereas open pinhole allows the detection of the light emitted from the whole thickness of the sample. This is an important point for the present examination. In this work, the set-up of the cLSM was used to perform photoactivation experiments of single cells or regions of the cell with the possibility of using lasers for activating (400 nm blue diode laser), and acquiring (488 nm laser) images of cells at conditions which were optimized in the system. During the experiments cells were kept at 37°C and 5% CO_2 by means of an incubation chamber attached to the cLSM.

Microscope set-up and systematic automatization of PA experiments

The major components of the confocal microscope used on this study (**fig. 2.2**):

1 Inverted microscope with a x-y and z axis controller.

2 Light source power: laser lines.

3 Scan head: scanning mirrors filter wheels, shutters, and confocal aperture.

4 Detector (photomultiplier).

5 Computer with scan controller.

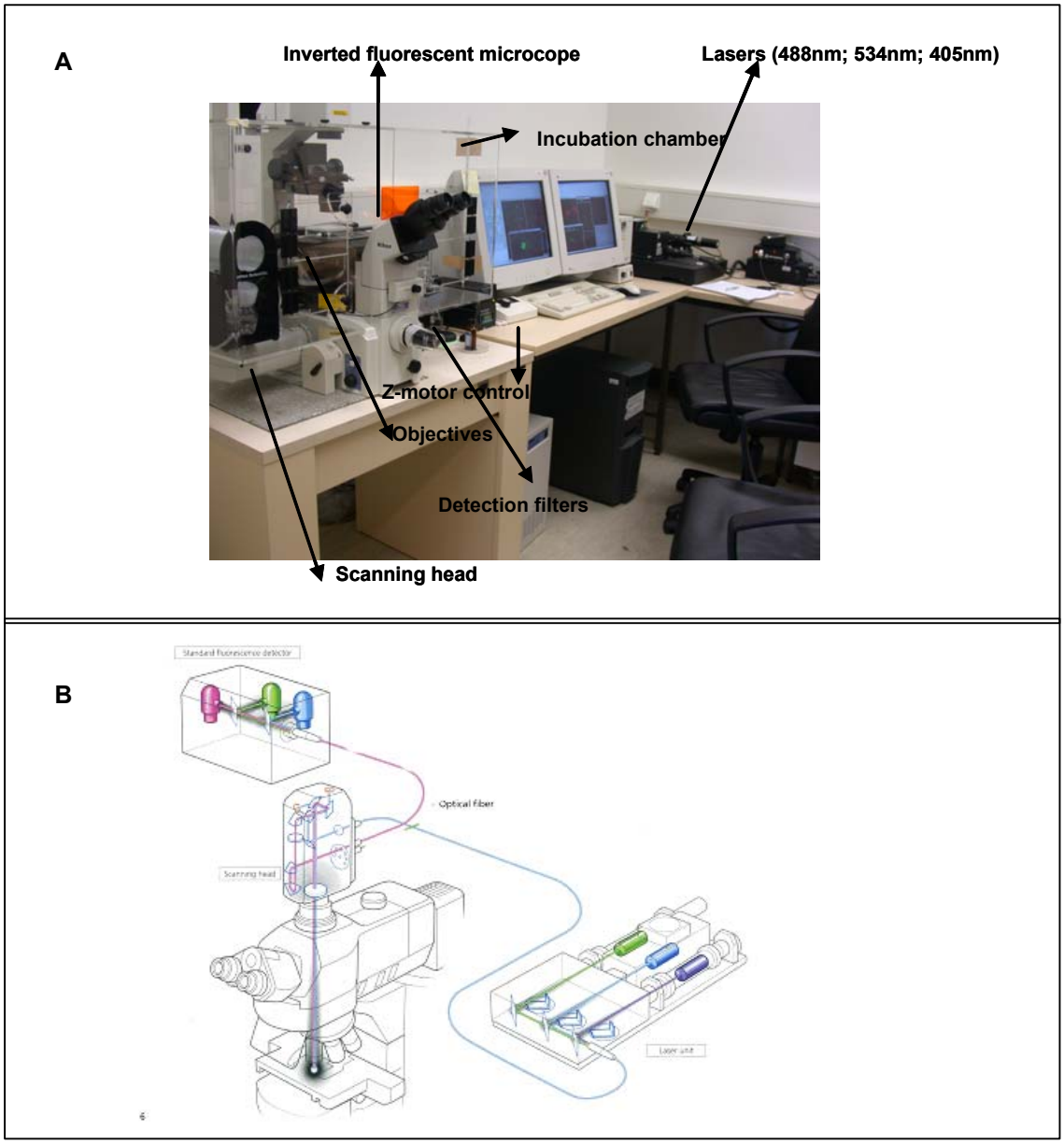

Fig. 2.2 A) View of the set up present at the laboratory showing the inverted microscope and additional parts.B) Simplified scheme showing the scanning head with the galvanometric mirrors, the detection set-up, and the lasers, except that an upright fluorescence microscope, thus scanning head position differs (Nikon brochure on EZC1).

Several parameters were adjusted to perform photoactivation experiments.These included laser filters, objective, pinhole, pixel dwell time, resolution, number of scans, field of view and time interval. The selection of the optimal settings is explained in **section 3.1.3**.

Optimized conditions (see below) were incorporated in a macro created in collaboration with Nikon-Amsterdam by Kees van der Oord, Dr.Robert Stad, and Dr. Maarten Balzar in visual basic system within the EZ-C1 microscope software.

The set up used is described in the following tables.

Optimized Parameters for photoactivation of living (A) and fixed (B) cells

A) For living specimens

Parameters	**Settings**
Objective	Nikon Plan Apo oil immersion VC 60x/1.4
Laser for image acquisition	Argon ion 488-nm. Neutral density filter 8
Laser for photoactivation	Blue diode 405 nm. No neutral density filter
Scans for photoactivation	2
Pinhole	Open
PMT gain	Varying according to probe (70-130)
Resolution	256x256 pixel
Field of view	(100x100-212x212) μm^2 according to cell size.
Pixel Dwell time	4.08 μs/pixel
Time delay	1s
Number of frames measured	50 or 112

B) For fixed specimens (PFA fixation):

Parameters	**Settings**
Objective	Nikon Plan Apo oil immersion VC 60x/ 1.4
Laser for image acquisition	Argon ion 488-nm. Neutral density filters 8.
Laser for photoactivation	Blue diode 405 nm. **Neutral density filter 8**.
Scans for photoactivation	2
Pinhole	Open
PMT gain	Varying according to probe (70-130)
Resolution	256x256 pixel
Field of view	(100x100-212x212) μm^2 according to cell size.
Pixel Dwell time	**3.06** μs/pixel
Time delay	1s
Number of frames measured	50 or 112

The parameters as visualized on the microscope software are shown in **fig. 2.3**. They were used in consecutive steps to perform PA experiments. These include:

1) Scanning of the sample with the microscope at high gain with the 488nm laser in the live mode.

Positive cells to be imaged were placed at a position that allows the whole cell and its processes to be included in the field of view. A typical scan size was 100x 100 µm.

2) The detector gain used for the 488nm laser was decreased so that no signal is detected. An initial "pre activation" image was saved.

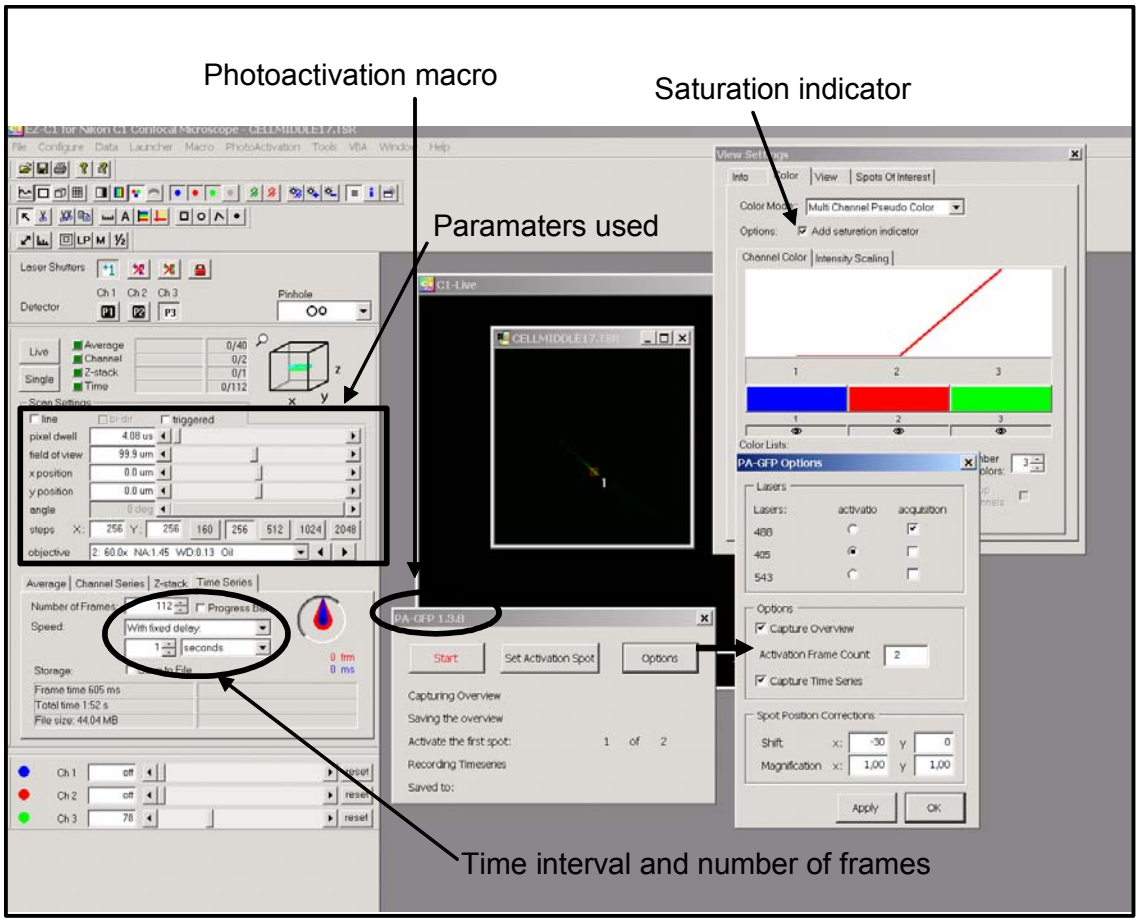

Fig. 2.3 Screen shot showing the different options and tools used from the EZ-C1 Nikon software for the photoactivation experiments.

3) The scan window was reduced to the smallest possible size described as 0 µm by the software in a region of the cell ("activation spot"). The true size of the activation spot was determined to be 5 µm in diameter as determined from the activation of fixed samples.

4) Irradiation of the "activation spot" with the 405nm laser.

5) The window was zoomed out to the initial size. Scanning with the 488nm laser over the whole region after activation was performed as described in step 1 and images (frames) were acquired every second for up to 2 minutes.
6) Provided that no pixels in the initial frames were saturated (checked by saturation detector, see **fig. 2.3**), a movie was recorded consisting of the pre activation frame and all frames after activation in "ids" format.
All steps (except step 1) were incorporated in the "PA-GFP" macro and were performed in an automatic way by clicking the PA-GFP macro (**fig. 2.3**) after localizing a positive cell and placing a photoactivation tool spot at the region to be activated.

Pixel analysis of photoactivation experiments

To analyse the images, the "ids" files obtained were converted to "RAW tiff" files (12-bit intensity resolution per colour channel). The converted images were then analysed with the program "IntMotion" in Matlab 7.0. This program, which was developed by Dr. Reyher (Physics Department) in a collaborative approach, processes the images in the following way:
1) The raw data were smoothed by a Gaussian 2D-filter in a frame by frame mode. The filtered data were kept in files in the working directory.
2) The initial frame (pre activation frame) was used to subtract its intensity from all subsequent frames pixel wise ("Dark frame correction"). This correction eliminates residual stray light which was at very low level.
3) An optional step allows for defining a reference area on a nearby cell where no activation has been performed (**fig. 2.5 A, arrow**). From this area, a mean intensity per pixel was calculated and stored for each frame. This averaged reference intensity which was calculated for every frame can be used to correct for drifts of photo multiplier supply voltage, laser intensity and other slowly drifting experimental parameters that influence the sensitivity ("drift correction").
4) The cell under investigation or part of the cell were defined as a "Region Of Interest" (ROI) by a mask technique, (i.e., pixels outside the ROI were masked off) and a filled contour plot of the cell in the ROI was obtained (**fig. 2.5 A, B**). A contour line corresponds to adjacent pixels with constant light intensity. The edge of the cell was defined by an intensity threshold just above zero. This was possible since any background intensity had been subtracted in step 2.

5) The ROI was kept for all frames. If applicable, the pixel intensities of each frame were corrected using the "drift correction (see step 3). The "centre of intensity" (CI) was calculated analogous to the way in which a centre of gravity would be computed with respect to a coordinate system situated at the CI, the momentum of intensity tensor (IT) was calculated analogous to the momentum of inertia. Then, the IT tensor was diagonalized what yielded the so called main axes system of the momentum of intensity. For a two dimensional system, these axes describe the axis of

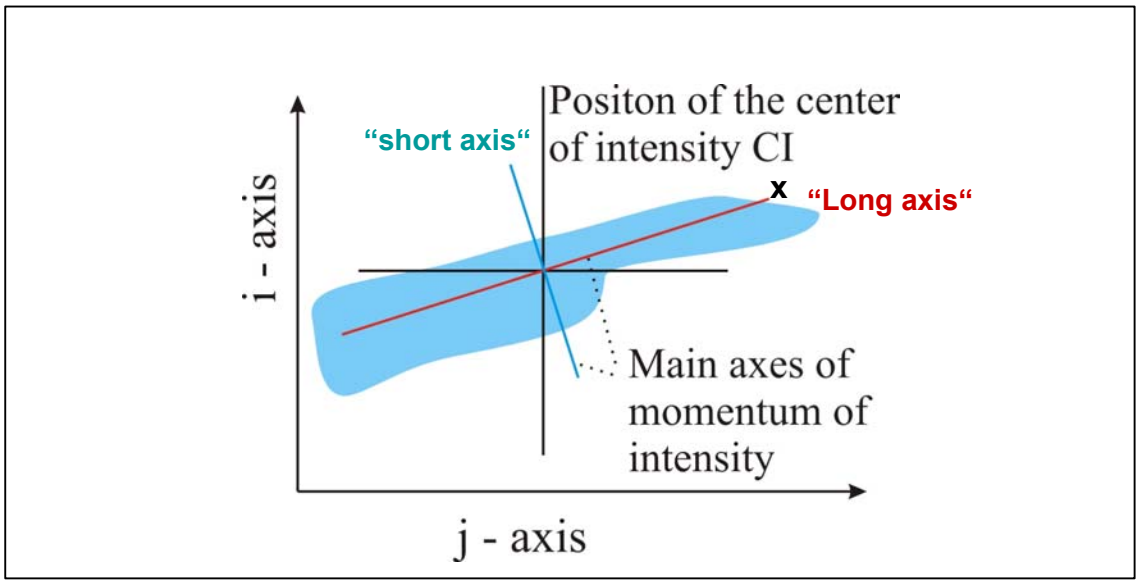

Fig. 2.4 Calculation of the main axes of momentum of intensity determined on the region of the cell analysed. Grey area illustrates the cell contour region to be analysed. "Long" and "short" lines show axes with lowest and largest quadratic intensity spread respectively (diagram by Dr. Rehyer).

lowest quadratic intensity spread ("long axis"), and of maximum spread ("short axis"). The main axes system of IT was plotted at the position of the CI (**fig. 2.4**).

6) The axis of lowest intensity spread, i.e. the long axis, was then divided into 100 channels of equal width (W). Geometrically, a channel corresponds to a rectangular strip of width w perpendicular to the long axis. The intensity of each pixel falling into a channel was summed up. This sum was then divided by the number of contributing pixels. Hence, each channel contains the mean intensity per pixel in that channel. This calculation was done frame by frame, but the main axis system of the first frame was kept throughout since the main axes system move very little during the whole frame set because the cell edge is defined by an intensity threshold.

By this method, an averaged intensity distribution projected on the long axis was obtained for all frames. Thus the distribution was reduced to one dimension.

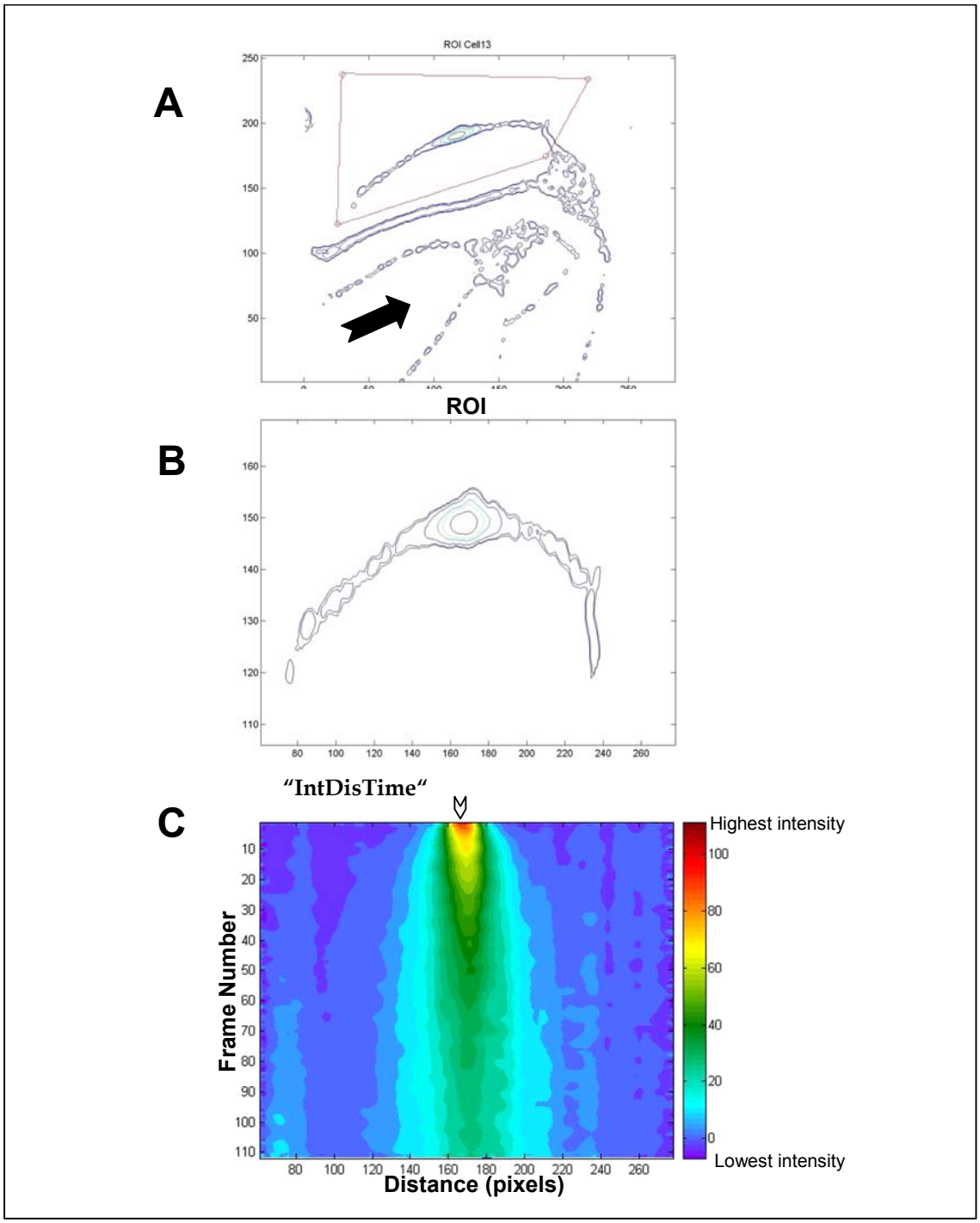

Fig. 2.5 Example of a cell analysed by "IntMotion". A) The contour of the cell is recognized and a ROI is selected (red rectangle); B) The ROI is rotated so that the long axis of the momentum of intensity tensor (IT) is parallel to the abscissa. Both axes are still in pixels. C) The result is the "IntDisTime" plot with the averaged intensity distribution I(x,t) throughout time and distance. White arrowhead indicates the site of photoactivation.

This seems to be adequate in view of the shape of the processes. A similar approach could be done with the short axis to study the intensity distribution in the lateral process

direction. This has not been undertaken yet. A 2D-function I (P, F) was finally plotted as a colour coded filled contour plot (for the averaged intensity, **fig. 2.5 C**).

The mean intensity per pixel in a channel at position x (in pixels, which can be re scaled to µm with the known magnification) on the long axis, I(x), is stored for each frame.

Since each frame corresponds to a specific time point t, a 2D-function I(x,t) could be defined. This function I(x,t) can be plotted as colour coded contour plot ("IntDisTime") as shown in **fig. 2.5.C**. The vertical axis corresponds to the frame number, the horizontal axis to position x on the long axis. Since, there are only 112 times points and 100 discrete intensities in fig. **2.5.C,** the plot interpolated between the data points.

The way in which the intensity was mapped in colour can be seen from the colour bar to the right of the contour plot. Red represented maximum and violet, minimum intensity in the data set I(x,t).

The plots allowed an immediate overview of development of temporal changes in the intensity distribution along the long axis. In the example, the intensity hump at the activation spot (x ≈ 170 pixels) decreases with frame numbers without appreciable shift to the sides. At x ≈ 70 pixels (corresponding to the process tip) some intensity is accumulating with time.

Immobile Fraction (IF) and Flux analysis

To analyse I(x,t) in a quantitative manner, the program "IntFlux" developed by Dr. Reyher was used (**fig. 2.6**).

This program, loads the information I(x,t) already processed by "IntMotion". Information on the pixel size of the original image and the size of field of view (µm per pixel) and time between frames has to be entered**.** With this information x and t were rescaled to µm and seconds respectively.

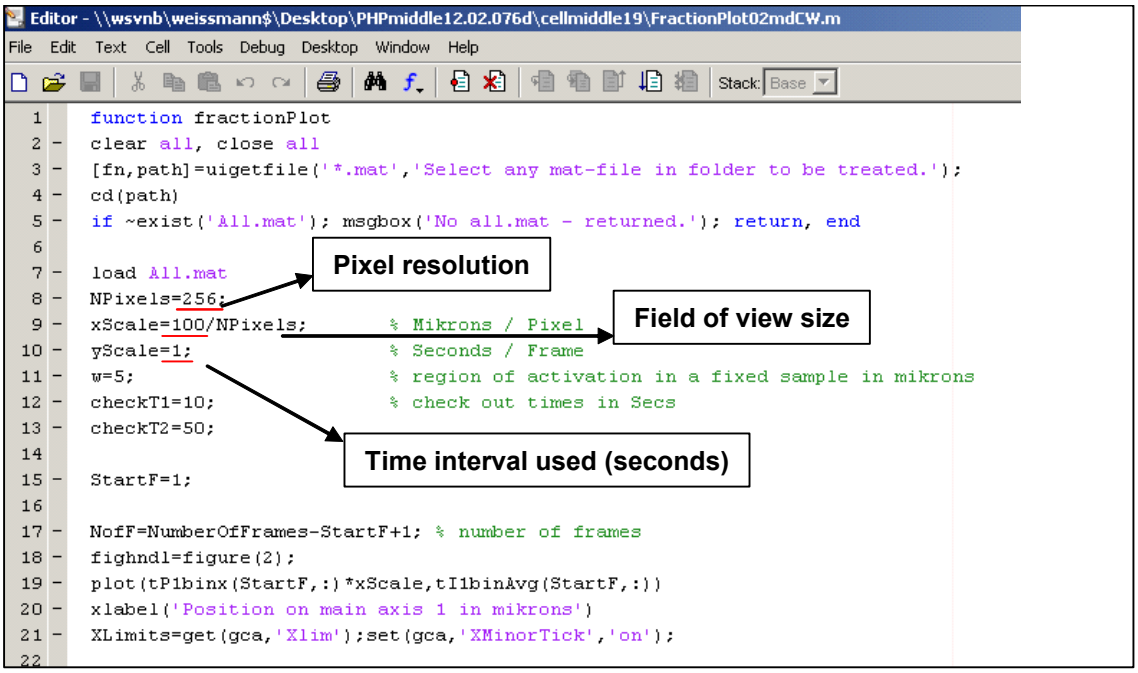

Fig. 2.6 Screenshot of the "IntFlux" program run in Matlab showing parameters which can be modified according to variables used for the photoactivation experiment.

Subsequently, a window where the contour of the cell part in the ROI is shown and a matching window where the projected mean intensity I(x) is plotted against x (which is the distance on the long axis for the first frame) is loaded (**fig. 2.7**). The intensity is plotted in arbitrary units, and the distance in micrometers according to the rescaling.

The cell fragment selected as ROI is rotated to have the long axis as abscissa (**fig. 2.7**). It is then possible to select regions on the long axis x, e.g. a centre region (C), where the photoactivation occurred, a region to the left (L) and to the right (R). The regions are selected manually by mouse clicking at the centre of the regions. From the spots selected, a distance of 2.5 µm to left and right is determined and intensities in these 5µm regions I_C, I_L, I_R are calculated for each frame. In addition, the total intensity I_0, detected for the first frame in the ROI is calculated, I_0 corresponds to the area centre I (x,t=0) (bottom plot in **fig. 2.7)**.

The data output can be depicted in a plot like the one shown in **fig. 2.8**. Here, the intensity I_t, for t=C,L,R, divided by the total intensity I_0 is shown as function of time (i.e., for all frames). This analysis is referred to as "flux analysis" since it shows the flux of fluorescence intensity from the centre to close-by regions.

The partial intensities I_C are divided by I_0 because, from microscopic data, one has to assume that the activation of PA-GFP (at t=-1s) occurs in a region which is much narrower than the selected central region C of 5 µm width. Consequently, during the

delay between activation and acquisition of the first frame (1s), some intensity has already migrated outside region C, as I(x,t=0) in **fig 2.7** shows. The proper reference intensity I_0 corresponds therefore to the whole area under I(x, t=0) rather than to I_C (t=0) and yields the "Immobile Fraction" (IF).

I_R and I_L are divided by I_C to obtain the fraction of the central region appearing to either side, distal (towards the tip) or proximal (towards the soma).

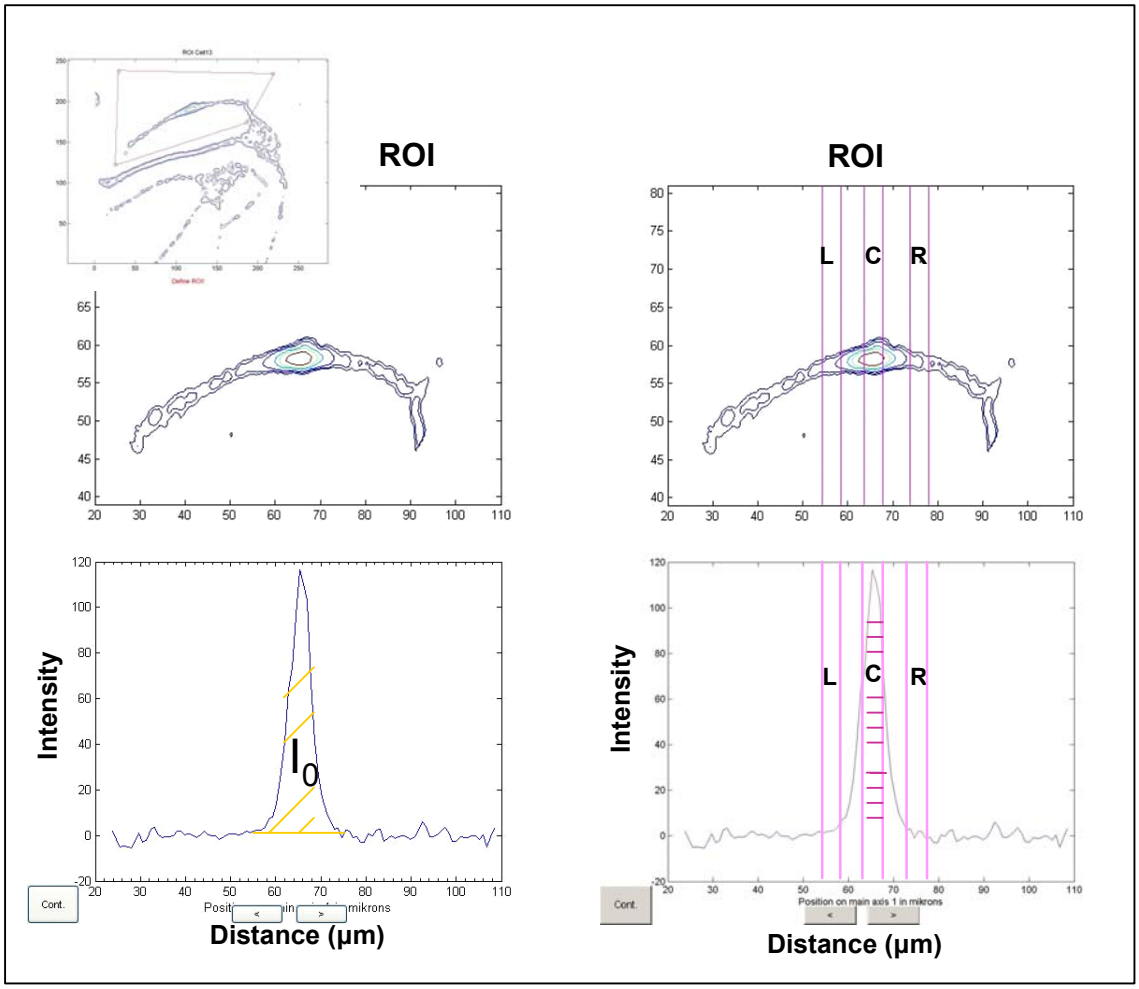

Fig. 2.7 Selection of regions to be analysed by "IntFlux" program. The cell analysed is shown in an inset at the top left with the ROI selected in red. The program loads windows showing the selected cell fragment in the main axis system of the IT, i.e. rotated (contour plots on top). Both axis are shown in µm. Below is shown the projected mean intensity I(x,t=0), i.e. for the first frame. The program allows the manual selection of a central region (C) and regions to the left (L) and right (R) which are 5 µm wide (pink lines on the contour plot and red lines on the curve I(x,t=0), right side)

The curve I_C/I_0 shall be used for further modelling. This curve reflects the decay of the relative intensity at the activation spot (projected on the long axis and summed over 5 µm).

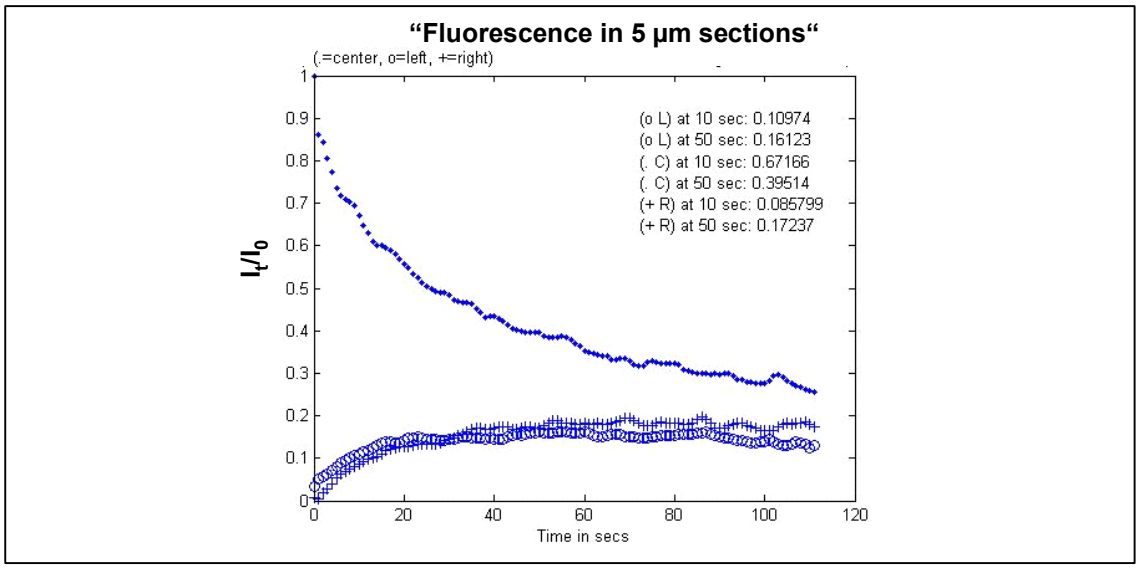

Fig. 2.8 Plot for "flux analysis". The figure shows the decay of fluorescence in the photoactivated region and the fractions that appear left and right. The inset shows the values at 10 and 50 s. Regions L-C-R with a distance of 10 µm have been selected as shown in fig 2.7.

Modelling of intensity decay curves

The correct interpretation of the decay curve shall give information on the mechanism responsible for protein mobility. A typical curve in conjunction with a fit curve is shown in **fig. 2.9**. The fit is based on a diffusion model which is still further modified.

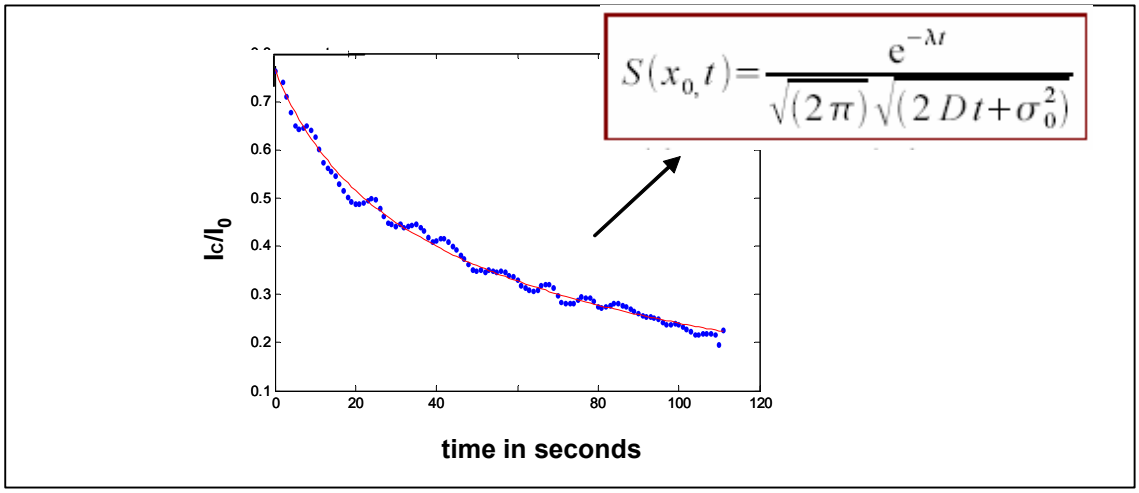

Fig. 2.9 Curve fitting performed with a "Diffusion" program. The equation shown in the figure was used to fit (continuous curve) the experimental data (dotted curve). The diffusion coefficient can be obtained directly with the program.

3. Results

3.1 Development of a system to study tau protein dynamics in living cells

The aim of this study was to analyse dynamic properties of normal and disease-related tau proteins in living cells. For this purpose, different tau proteins and fragments of these were fused to a photoactivatable molecule and a system was devised to record and analyse protein mobility after near UV-photoactivation.

The system was applied to 3 different contexts:

I a "normal scenario" where a fetal tau isoform, a fragment of it and an unrelated control were analysed to study the cellular distribution of the constructs, and factors that affect it (**section 3.2**);

II a FTDP-17 disease-related situation where a mutant tau protein present in some cases of FTDP-17 was analysed (**section 3.3**);

III a hyperphosphorylation scenario where the increased phosphorylation state of tau in AD was tested (**section 3.4**).

3.1.1 Generation of the photoactivatable-tau molecules

To study the kinetic properties of tau proteins in living cells, a wild type fetal tau isoform, 352 amino acids long (wt tau), a smaller fragment, 223 amino acids long (delta tau), a protein mimicking the high phosphorylation state of tau (PHP tau), and a tau protein including a mutation present in cases of FTDP-17 (mut tau) were fused to the photoactivatable GFP molecule (PA-GFP); as a control, a protein made up of three PA-GFP molecules in tandem (PA-GFPx3) was also prepared (**Fig. 3.1)**. PA-GFP is a variant of the GFP molecule that exhibits dim fluorescence in the native state when excited with a 488 nm excitation beam, but increases its fluorescence up to a 100 fold if previous near UV irradiation (photoactivation) is performed (**section 1.6.1**). This property was used throughout this work to study PA-GFP-tagged protein mobility in living cells.

To obtain the PA-GFP-tau proteins, different plasmids encoding eGFP- and flag-epitope-tagged tau available in the laboratory (**section 2.1.2**) were used. As a first step, a pRC/CMV-eGFP-tau wt plasmid was used to obtain PA-GFP in exchange for the eGFP sequence (Patterson and Lippincott-Schwartz 2002).

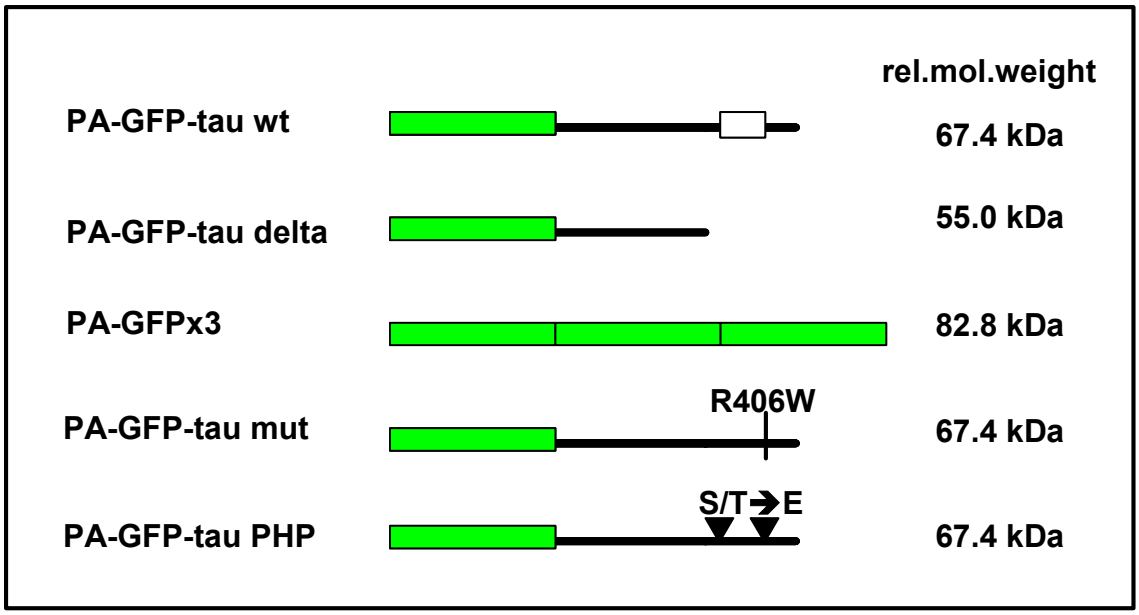

Fig. 3.1: Schematic representation of the different constructs used. The PA-GFP sequence was fused to: the full length (wt) and a fragment (delta) of fetal tau, or other PA-GFP molecules (PA-GFP-x3), a tau protein with the R406W mutation (mut), or to the pseudohyperphosphorylated tau (PHP) where 10 S or T residues were mutated to E. Grey boxes represent the PA-GFP sequence; white box shows the microtubule binding domain sequence only present in the wt tau protein;

For that, 3 rounds of consecutive PCR-site directed mutagenesis (**section 2.2.1**) were carried out using primers "L64F-T65S";"V163A"; "T203H" (**fig. 3.2** and **section 2.1.2**).

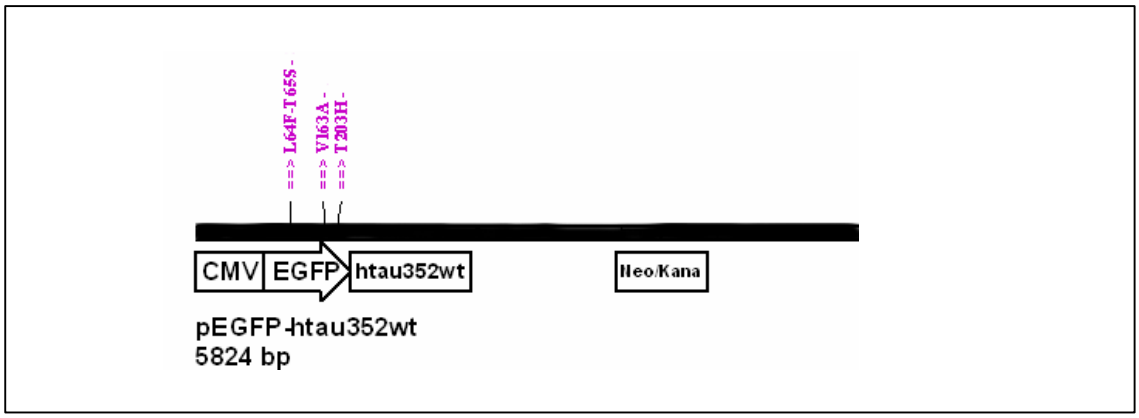

Fig. 3.2 Schematic representation of the eGFP-tau molecule used to produce the PA-GFP-tau molecule. The main features of the plasmid are represented (CMV promoter, eGFP-tau encoded protein, and a Neomycin/Kanamycin resistance) with the mutations performed at the respective position. The PA-GFP fragment was sequenced and to avoid the presence of mutations in other parts of the vector, the PA-GFP sequence was recloned into the initial vector in exchange for the eGFP fragment.

Several of the PCR products were transiently transfected in PC12 cells to test their functionality. The construct with the right sequence that showed photoactivation properties after irradiation under the microscope with a mercury lamp with a UV filter was chosen as "starting plasmid".

The PA-GFP-tau wt, "starting plasmid", was used in subsequent cloning schemes to produce all other PA-GFP fusion plasmids.

The cloning of PA-GFP-tau delta, PHP, and mut was performed by exchanging the tag (eGFP or flag) from the plasmids (**section 2.1.2**) for the PA-GFP sequence (**section 2.2.1**). As an example, the cloning steps to obtain PA-GFP-tau delta are shown in **fig. 3.3**.

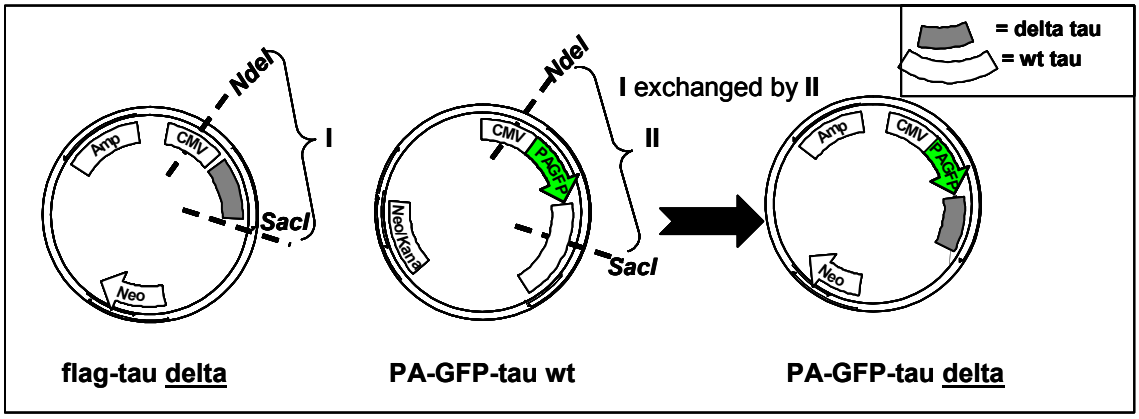

Fig. 3.3 Schematic representation of the cloning steps performed to obtain the PA-GFP-delta tau. Starting from a vector encoding flag-delta tau, the indicated portion was exchanged for the PA-GFP portion of a plasmid encoding the wt-tau sequence with the indicated restriction enzymes.

To generate a control vector encoding an unrelated protein of similar size to the wt tau, a construct made up of three PA-GFP molecules arranged in tandem "PA-GFPx3" was prepared (**fig. 3.1**). To obtain this molecule, the cloning was performed in a number of steps to add the PA-GFP sequence one at a time. Thus, first a PA-GFPx1 encoding plasmid was generated by exchanging the eGFP sequence of a peGFP-C1 vector for a PA-GFP sequence. A new restriction site was added on PA-GFPx1 by PCR using "tandem" primers (**section 2.2.1**). This amplified fragment was inserted to obtain the PA-GFPx2. Subsequently, the same insert was added in PA-GFPx2 and the PA-GFP-x3 was generated (**fig. 3.4**).

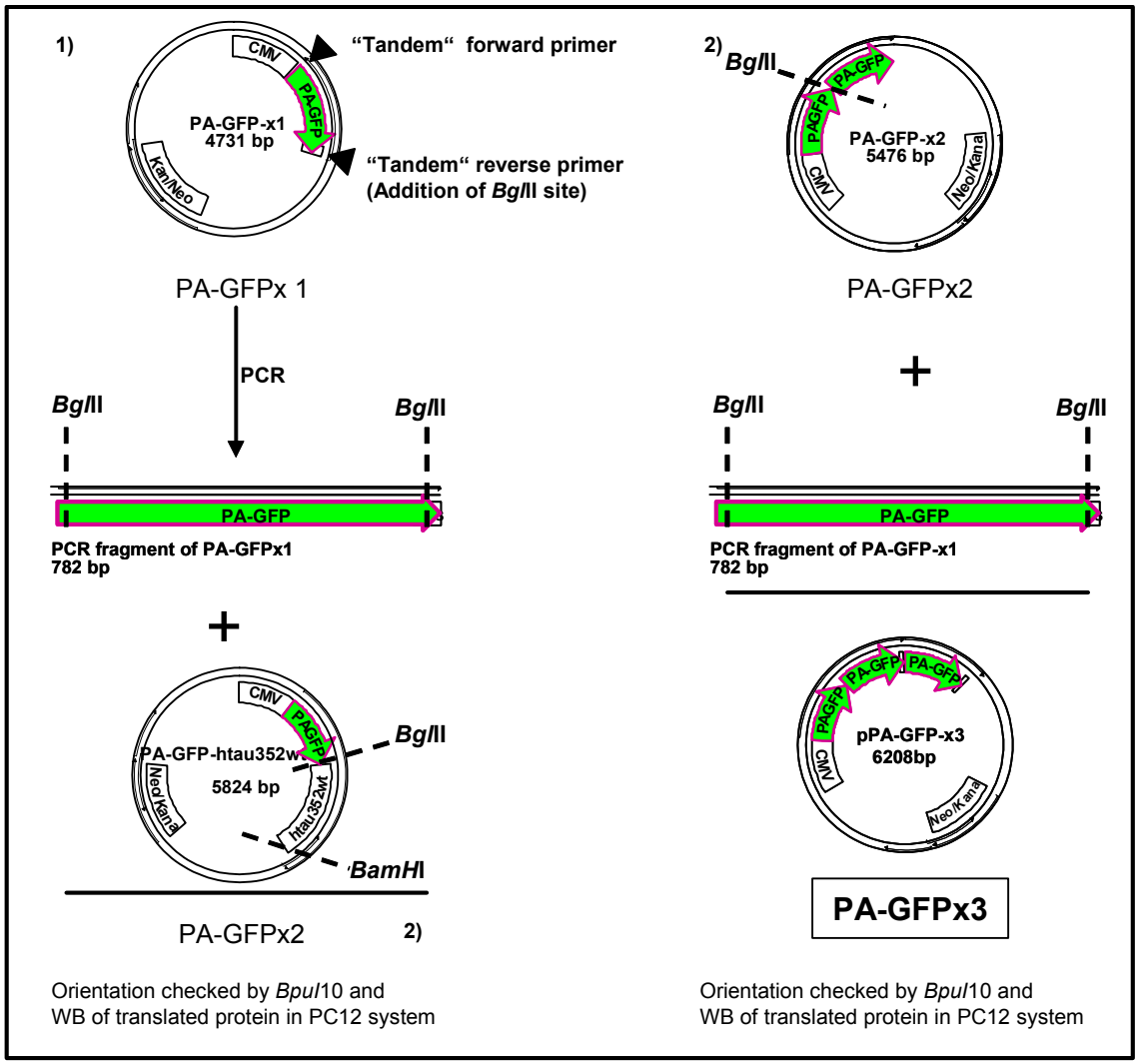

Fig. 3.4 Schematic representation of the cloning steps to obtain PA-GFPx3. The cloning started from a PA-GFPx1 plasmid. A second *Bgl*II site was included by PCR, and the PCR product was added first to a PA-GFP-tau plasmid, and then on the resulting PA-GFPx2 vector to obtain the PA-GFPx3. The proper orientation of the insert was checked as indicated. The plasmid coding regions for PA-GFP tau molecule and the antibiotic resistance (Kan/Neo for Kanamycin, Neomycin) are given. Discontinued lines represent digestion by the indicated restriction enzymes.

3.1.2 PA-GFP-fusion proteins expressed in living cells

PC12 cells were chosen to study the PA-GFP fusion proteins in a neuronal cell model. These cells develop neurites after NGF treatment making them a useful model to study axon-like processes. In addition, PC12 cells are easy to transfect by liposome-mediated methods. To obtain a homogeneous cell population expressing the desired protein at a constant level, stable lines were generated by stable transfection of the different PA-GFP-tau and control plasmids (**fig. 2.1**; **section 2.2.3**). To increase the

efficiency of plasmid incorporation into the genome of the cell, the plasmids were linearized before transfection, with a single cutting enzyme (**section 2.1.2**), which did not cut in regions required for the expression of the protein or the selection marker.

Screening for positive clones was performed either by immunocytochemistry (**section 2.2.3**) using an antibody against GFP which also recognized the PA-GFP variant, or by checking whether the protein could be photoactivated under the microscope. As a further parameter, the absence of fluorescent signal from the nucleus was checked since the size of the protein should be large enough to exclude it from the nucleus. Different percentages of positive clones were obtained for the different constructs (**table 3.1**).

Table 3.1

Protein expressed	% positive clones (fluorescence microscopy)
PA-GFP-tau wt	14
PA-GFP-tau delta	6

Lysates from positive clones were prepared and analysed by western blots (**section 2.2.4**). Many of the selected clones did not express the complete protein, as could be determined by the presence of bands of lower molecular weight as expected (**fig. 3.5**).

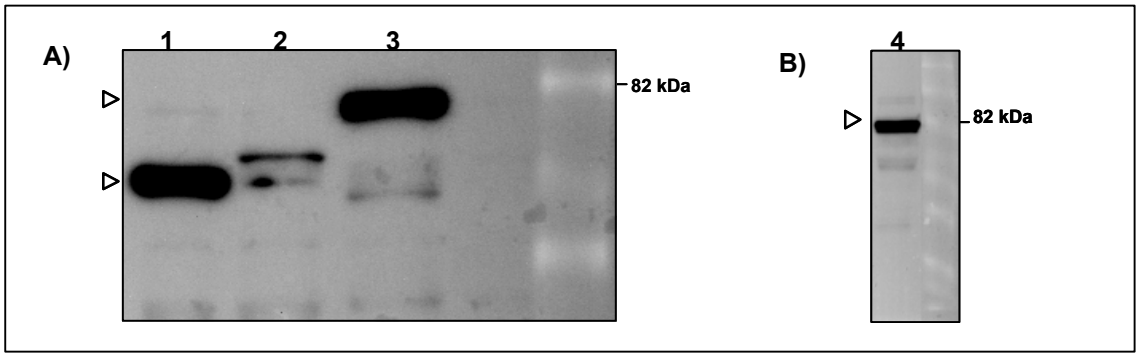

Fig. 3.5 Western blots of clone lysates to show different proteins expressed after A) transfection of a linearized plasmid (clones 1,2,3) and B), transfection of a circular plasmid (clone 4). Note bands of lower (A) and the approximate (B) 82 kDa expected size. Arrowhead points at the position where the bands were obtained. A polyclonal rabbit against GFP was used to detect the bands.

Because the plasmids had been linearized before the transfection, it is possible that the linearization led to plasmid DNA fragmentation before its incorporationto to the genome. Thus, in a second set of experiments, circular plasmids were used to generate stable lines. In fact, these lysates showed a higher percentage of selected clones with the expected bands after western blotting (**table 3.2**). For this reason, all subsequent stable

lines were produced by transfecting non-linearized plasmids and performing the screening by western blots.

Table 3.2

Protein expressed	% of positive clones (western blots)
PA-GFP-tau wt	53
PA-GFP-tau mutant	45
PA-GFP-tau PHP	58
PA-GFPx 3	8

The clones used for experiments were those expressing the protein to a high level (**fig. 3.6**).

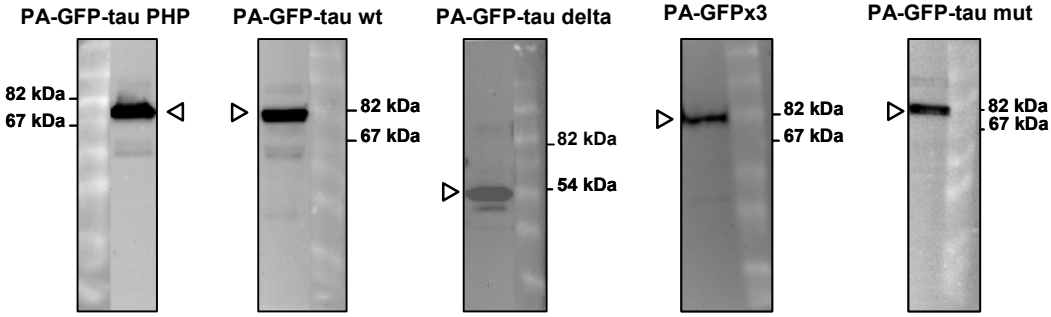

Fig. 3.6 Western blots of stable lines showing examples of the positive clones used in photoactivation experiments. The arrowhead shows the band recognized by a polyclonal rabbit anti GFP antibody. Note the similar band size for all proteins except for the smaller delta fragment. For each experiment cells from a confluent 24 well-dish were used for lysate preparation.

The amount of protein expressed for the different constructs ranged from 11 to 36 pmol protein per 10^6 cells as determined by immunoblot of cell lysates. In comparison, the amount of endogenous tau protein present in undifferentiated PC12 cells was calculated as 7.1 pmol per 10^6 cells (Brandt *et al.* 1995; Fath *et al.* 2002). After NGF treatment, however, tau expression levels increases about 5 times the initial undifferentiated levels (Drubin, Feinstein et al. 1985);(Babak, McCarty et al. 1994). Thus, the lines express the exogenous proteins near to endogenous tau NGF-induced levels.

In addition, the tau wt fusion protein showed a filamentous distribution in cells (**fig. 3.7 A**) suggesting its interaction with microtubules. This was confirmed by photoactivation experiments where co localization of microtubules with the photoactivated tau was visualized after an NP40 extraction-fixation protocol (**section**

2.2.3) that retains only cytoskeletal associated proteins (**Fig. 3.7 C**). In contrast, PA-GFP-tau delta proteins lacking the MBR expressed in cells did not show such a filamentous pattern (**fig. 3.7 B**).This indicated that the tau fusion protein was functional.

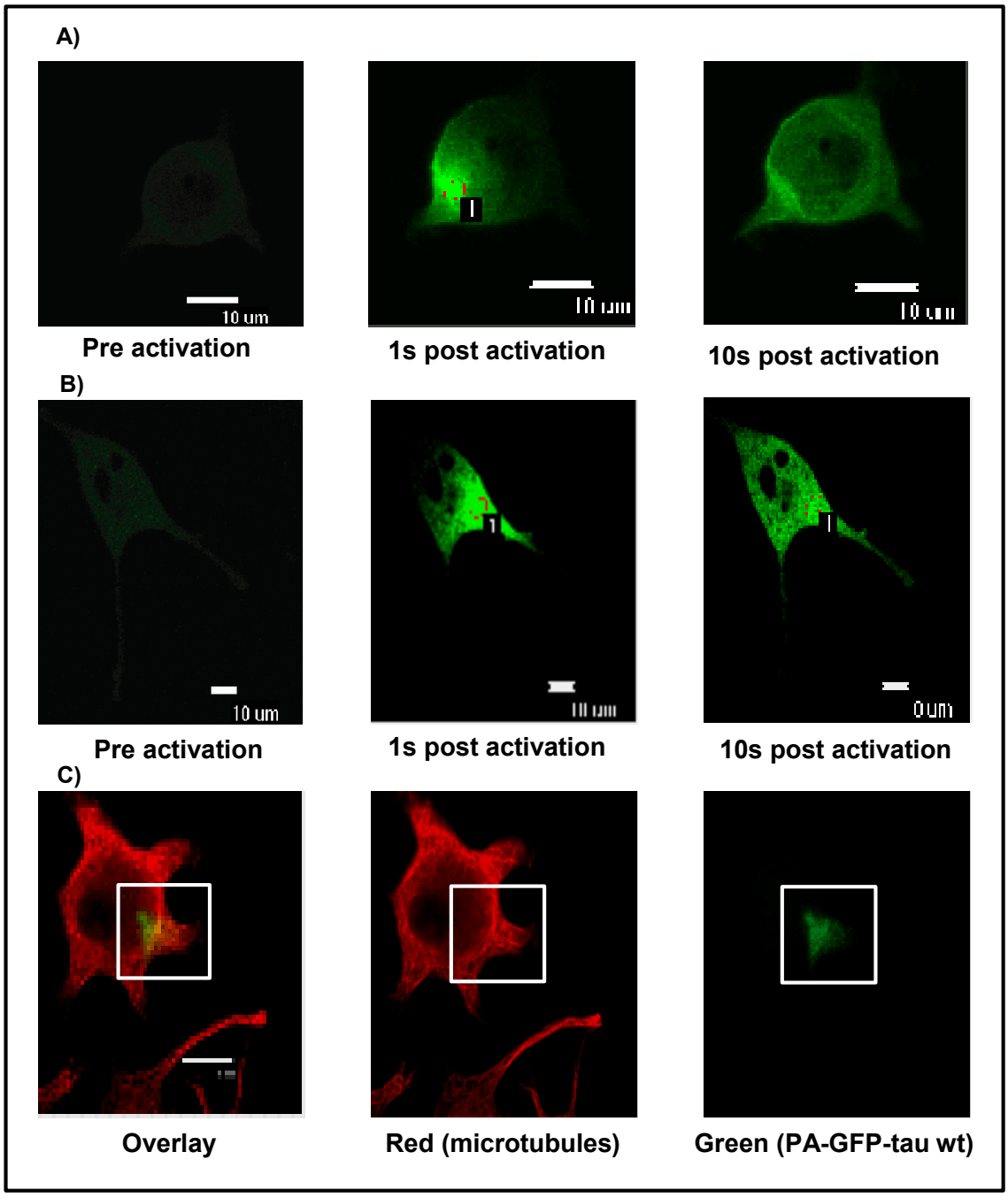

Fig. 3.7 Stable lines expressing PAGFP-tau proteins in living (A, B) and fixed (C) cells. Images after photoactivation of PA-GFP-tau wt expressing cells (A) and PA-GFP-tau delta expressing cells (B) are shown. Note the filamentous pattern of the fluorescent signal in (A). In (C), photoactivation was performed on NP40 fixed-extracted PA-GFP-tau wt expressing cells stained against microtubules (DM1A) and Cy3 (secondary antibody). Note co-localization of the signal for DM1A-Cy3 in red and activated PA-GFP-tau wt in green.

3.1.3 Adjustment of the microscope set-up to perform PA experiments

A photoactivation (PA) experiment involves a number of steps (**section 2.2.5**, **fig. 3.7 A, B**). First, a positive cell expressing a photoactivatable molecule has to be identified and imaged (pre activation step). Next comes the photoactivation of the cell with a near U.V. laser (activation step), and then, the activated cell has to be imaged (post activation step).

To localize positive cells which is difficult due to the low initial pre activation fluorescence, Patterson *et al* recommended irradiation with low levels of near-UV laser light, cotransfection with a second fluorescent protein (mRFP), or to produce a stable line to increase the probability of photoactivating a positive cell (Patterson and Lippincott-Schwartz 2004). Other studies reported the possibility of identifying positive structures by increasing the gain to detect the native weak green fluorescence of PA-GFP (Schimerer and Hill 2005; Stark and Kulesa 2005; Twig, Graf et al. 2006).

In the set-up used in this work, positive cells were localized by scanning the fields with high gains for detecting the low luminescence excited by the 488 nm excitation beam (gains ranging from 170 to 200) before activation. This gain had to be decreased (gains ranging from 85-110) after selecting the region to be activated to allow a high post activation-pre activation ratio (about 60), and low background noise levels.

To help the visualization of positive structures, the use of media without a coloured indicator (DMEM without phenol red) was used.

Imaging of the pre activated cell, activation and image acquisition post activation required the adjustment of different settings. These included:

(1) the optics,
(2) the energy to activate and image the specimens, and
(3) the temporal resolution to acquire the images.

The different variables had to be tested alone or in combination since variation in one could affect the others. In parallel, the microscope software and technical parts were subjected to constant updates performed in collaboration with Nikon representatives Robert Stad, Kees van der Oord and Marteen Balzer which required new adjustments of previous settings. The final parameters used are summarized in the methods **section 2.2.5**). In this section, the selection of these parameters is explained.

The optics

Objectives

The objective numerical aperture (NA) is what mostly influences photobleaching or photoactivation experiments. In addition to their lower resolution, low NA objectives bleach or photoactivate less efficiently and collect less light than high NA objectives. High NA objectives produce a much narrower focus spot, both in axial and lateral direction than low NA objectives. Thus, the objective selection has to consider the thickness of the specimen to analyse. To most efficiently bleach or photoactivate and image molecules in thin cellular extensions, the use of 63x/1.4 oil immersion objectives is generally recommended (Goldman and Spector 2005).

Therefore, a 60x/1.4 oil immersion objective was tested in PA experiments of PC12 cells. Its axial resolving power was compared to a 40x/1.0 oil immersion objective. The aim was to check whether some of the photoactivated molecules were detected with the 40x objective but not with the 60x/1.4 objective due to the lower axial resolution (z-axis) of the latter. If by measuring the fluorescence intensity using the different objectives, the intensity decay (intensity in time) should be different; this could hint that the resolving power of the objectives might not be the same.

To avoid differences due to cell morphology, the PA experiments were performed on the same cells changing the objectives after the signal was undetectable. The order of the objectives used was also exchanged in each PA experiment. The intensity decay curves showed that the behaviour was practically the same in both cases, and the difference was estimated determining the half time of decay ($t_{1/2}$), i.e., the time at which the intensity reaches a 50% of the start value (**section 1.6**). There was practically no difference in the $t_{1/2}$ determined with either objective; some cells showed an increase or decrease not larger than 5-20 %. Therefore, in the system used, the processes could be resolved equally with both objectives tested. In addition, the decay curves obtained were less irregular for the 60x/1.4 objective as for the 40x/1.0 objective, due to the higher NA of the former, thus, this was the objective chosen for the experiments.

To test on the objective refractive index properties and autofluorescence, a 60x water immersion objective (provided by Nikon as testing supply) was tested in PA experiments. No significant improvement could be detected with the water immersion objective (not shown). In addition, the use of the oil immersion objective made it easier to compare experiments in living conditions to fixed specimens (no media). Finally, for

further improvements, a 60x oil immersion VC objective which is corrected not only in the visible range but also in the near UV range was selected.

Pinhole

There are different pinhole settings that can be used in a cLSM. Closing the pinhole reduces out-of-focus blur and this is one of the main features of the cLSM (**section 2.2.5**). However, in photobleaching or PA experiments, the drawback of using smaller pinholes is that this reduces the signal gathered and the quantification of fluorescence intensities becomes less accurate. Activation does not depend on the pinhole size, but the pinhole is important for the detection of the signal from the excited spot. Thus, the different pinhole size options were tested during image acquisition.

PA experiments on fixed specimens showed that the decrease of the fluorescence signal with an open pinhole (150 µm diameter) and the small pinhole (30 µm diameter) was in the same range, of 18.4 % ± 2.6 for O, and 21,4 % ± 2.5 for S after 50 s; and 23.5% ± 3.4 and 27.5 % ± 1.7 (3 cells in each condition). Thus, both pinholes led to similar detection volumes. Nonetheless, and open pinhole was selected to ensure the highest amount of light collected.

Resolution, magnification and scanner zoom factor

With the cLSM, it is possible to acquire images in only a fraction of an imaged field by using a zoom option from the software. The confocal scanner zoom reduces the scan angle that in turn reduces the scan area and the separation of the detection spots. This allows to image with high-magnification and to zoom into a sub cellular compartment. However, undesired bleaching during imaging increases with the zoom factor. In addition, temporal and spatial resolution are connected: to image a larger number of pixels, more time is required, and fewer images in a time interval can be obtained. Since PA experiments aimed to study fast processes, the temporal resolution was given priority, i.e., less pixels were imaged to increase the frequency of image acquisition after photoactivation (see *Temporal resolution*).

The energy

Laser energy for photoactivation (405 nm laser)

Possible sources for photoactivation are laser lines at 364 nm, 405 nm, 413 nm, or

an excitation filter with a band pass for the optimal wavelength excitation from a mercury lamp (Patterson and Lippincott-Schwartz 2004). To perform the photoactivation event as rapidly as possible it is recommendable to use the maximum available power.

The cLSM available at the laboratory, is equipped with a 405 nm laser, with a back aperture energy (total energy that comes out of the fibre) of 2 mW.The energy used for PA was adjusted to photoactivate a small spot that showed a high fluorescence increase without leading to photobleaching of the region. To obtain a small spot of photoactivation, the field of view was reduced so that only a portion of the desired cell would be illuminated with the 405 nm laser. The size of the photoactivated region was fixed by programs developed in the EZ-C1 microscope software by Nikon-Amsterdam collaborators in a way that a "0 µm" scanning field was selected in the photoactivation step. This setting leads to a 5 µm diameter spot. This region however can now be modified to obtain different sizes and shapes according to experimental requirement. To test the energy required, PA experiments were carried out first in PA-GFP-transfected NT2 (NTera2) cells, which exhibit a larger surface for PA (**fig. 3.8**).

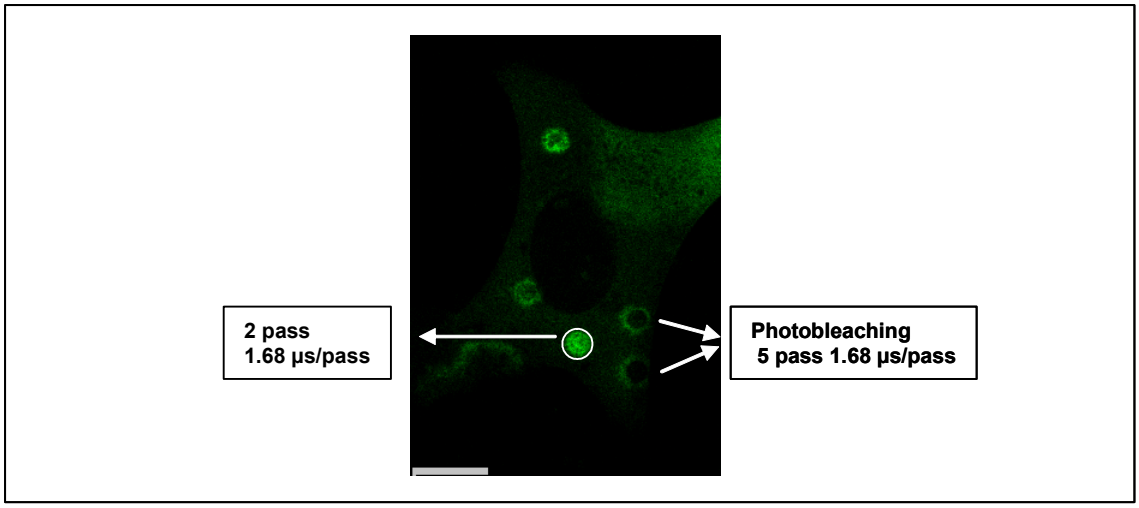

Fig. 3.8 Pixel dwell time adjustment. Different pixel dwell time options were tested on different spots of activation in an NT2 cell transfected with a PA-GFP-tau encoding plasmid and fixed (PFA). In the lower region a proper activation spot was obtained; other tested options yielded a fluorescent rim surrounding the photoactivated spot due to photobleaching at long exposure time (high energy). Scale bar 10 µm.

For the spot size selected, the optimal energy required, as judged later with living PC12 cells from the different stable lines, was of 2 scans of 4.08 µm/s pixel dwell time each.

Laser energy for imaging (488nm laser)

Photoactivated PA-GFP is normally imaged with a 488 nm laser (Patterson and Lippincott-Schwartz 2004). This laser is used during image acquisition to record different images at a fixed time interval after photoactivation.

Fluctuations of laser intensities result in artefact fluorescence variations, thus laser power instabilities were firstly tested. A constant scan of the 488 nm laser for 5 minutes showed a drift of 7.7% in the laser power. This variation is not extreme and no correction for instabilities of laser output was required.

Secondly, the energy used during image acquisition has a major effect on the photobleaching of the samples; this should be kept to a minimum to obtain stable images. This is one of the causes of signal loss after photoactivation performed on living cells together with the dissipation of the fluorescence signal away from the activated spot by diffusion or other mechanisms (of main interest in this work).

In order to decrease photobleaching, different neutral density filters (ND) placed before the 488 nm lasers were tested. PA performed in fixed specimens showed that the highest level of attenuation (3.1% laser transmission) yielded high background noise, and the decay of intensity was very irregular. Because background noise became very high to detect a signal at high transmission levels (25%), the 12.5 % attenuation (ND 8) was selected for the measurements. The decrease of signal reached 81.5 % ± 2.6 after 50 s and a 76.4 % ± 3.4 of the initial levels after 112 s (3 cells used for each case) (**fig. 3.9**).

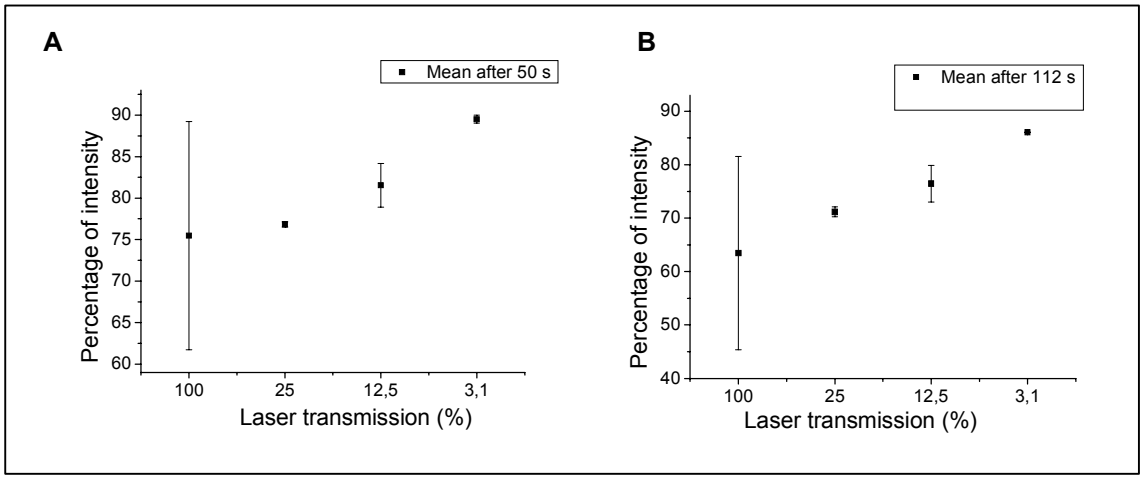

Fig. 3.9 Effect of laser attenuation in PA of fixed specimens. The different levels of laser transmission obtained using different neutral density filters (100%, no ND;, 25% transmission, ND 4; 12.5 % transmission, ND 8; 3.1% transmission, ND 32) are compared. The mean percentage of fluorescence with the standard error of the mean was plotted for every condition (3 cells each) after 50 (A) and 112 seconds (B).

In contrast to PA experiments of fixed samples, those performed in living cells required different energy for photoactivation and the use of media. Nevertheless, the different transmission levels yielded similar results showing that the 12.5% transmission was the optimal condition with a 60-70% of the initial signal detected after more than 112s, higher (20%) than with 25% transmission respectively (6 cells for each case). Therefore, the 12.5% transmission (ND8) for the 488 nm laser was chosen for PA of living and fixed cells.

To determine the total decrease of the signal intensity in living cells including the intensity that dissipates to other cell regions, the decay of intensity with the 12.5% transmission was measured in the whole cell with "IntMotion" program **(fig. 3.10).** The program allowed the selection of the whole cell to quantify the intensity detected in it for every image (frame) (**section 2.2.5**). The percentage of intensity measured after 112 s at the optimized conditions used for the experiments was 90.8 ± 1.9% of the initial intensity (8 cells). No difference was observed between cells expressing different PA-GFP-tau constructs. Therefore, it was assumed that PA of living cells lead to a 10% of signal loss by photobleaching.

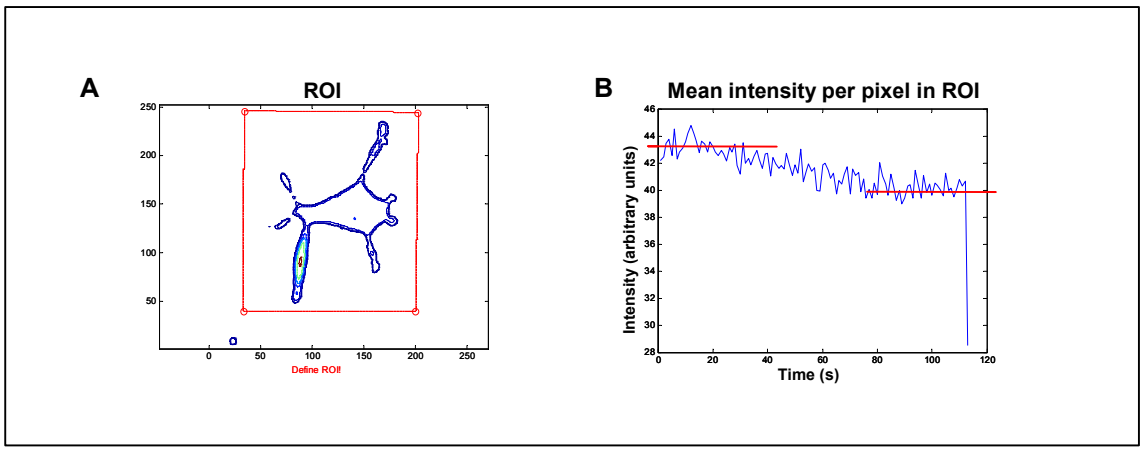

Fig. 3.10 Measurement of signal decay. The intensity decay was measured in the whole cell as shown in (A) (square). (B) shows the decrease of mean fluorescent signal after 112 s. Lines mark initial and final intensity values.This analysis was performed after activating a spot in living cells (lower process in A).

Another parameter to adjust during image acquisition was the detection gain used for post-activation measurements. This should ensure a low initial pre-activation intensity, but a high post-activation signal without reaching saturation levels. Because the fluorescence intensity after photoactivation depended on the expression level of the cells, which varies within the same clonal line and between lines, a range of detection

gains was used. About a 60-fold of activation was obtained.The intensity values measured were always evaluated in relation to the initial pre-activation frame. No images were pixel saturation occurred were included as detected by the saturation indicator tool (**fig. 2.1, section 2.2.5**).

Temporal resolution

To monitor dynamic processes, the scan speed should be set as fast as possible. Strategies used to decrease image noise such as image averaging, should be avoided to allow high temporal resolution. In fact, the image should allow to measure fluorescence intensities rather than acquiring high resolution images. Therefore, the numbers of pixels detected in an image were decreased in order to increase the temporal resolution.

Dynamic approaches aim at determining diffusion properties or transport rate of proteins.To estimate whether the system might be able to detect the proteins diffusing, an initial simple calculation was performed considering the following:

1- Diffusion equation (Berg 1993):

$$\frac{\langle x^2 \rangle}{t} = 2.D$$

$\langle x^2 \rangle$: root square mean displacement
t: time
D: diffusion constant

2- Reports describe diffusion coefficients for a GFP protein in water of 87$\mu m^2/s$ and of 25$\mu m^2/s$ in the cytoplasm (Lippincott-Schwartz *et al.* 2001).

According to 1 and 2, in 1 s, the mean square root displacement expected in the cytoplasm would be of:

$$\langle x^2 \rangle = 7.07\ \mu m$$

Therefore, in a second, the signal would be expected to spread up to a distance of about one spot (5 µm) from the initial activated region.

In addition to diffusion, transport mechanisms could be present during the analysis. Tau proteins were interpreted in the past as being components of the so called “slow axonal transport”, and also recently of the “fast axonal transport”. PA experiment should be able to detect these mechanisms. According to the highest (31.4 mm/d, (Utton *et al.* 2005) and lowest (0.2 mm/d, (Mercken *et al.* 1995) reported values for fast and slow axonal transport respectively, the distance expected for the protein to be

transported would be between 36 µm and 0.23 µm in 100 s. The movement, if present, should be visualized as a shift of the intensity peak in an anterograde or retrograde direction.

Initially, the resolution was set at 512x512 pixels, and the interval between images was 3s. The experiments gave no evidence arguing for slow axonal transport mechanisms. The fluorescence signal dissipated from the site of activation before 3 minutes. Thus, slow axonal transport mechanisms were absent in the cell model analysed or the PA approach could not detect it. Other time intervals were tested, but based on the estimations described previously, the time interval was reduced to 1 s which should be able to detect fast axonal transport if present. For this scan speed, the initial resolution was reduced to 256x256 pixels. A further decrease of resolution to achieve a lower time interval would make it technically difficult to determine the region to be photoactivated.

Controls

Spatial shifts

The movement of the system is one of the aspects which should be controlled. These movements may arise from movements of the cells or the stage where the cells are mounted on.

To decrease cell movement, these were plated on glass-bottom culture dishes coated to improve cell attachment to the surface. Laminin and collagen coatings were tested after the initial treatment with poly-L-lysine coating (**section 2.2.3**). With laminin, fewer cells remained after incubation (less than 60%).The location of the cells was traced over time and analysed. Collagen yielded the best results decreasing cell movements completely (not shown).

To analyse tau mobility in cell processes, cells were differentiated with NGF. Processes obtained after more than 21 days of NGF treatment resulted very mobile and therefore not appropriate for the experiments. Cells incubated for less than 3 days presented few and short processes. From day 3 onwards, processes developed and at day 6, a large number of cells with immobile processes (10 to 100 µm long) could be readily imaged.

Images obtained after PA of cells seeded onto PLL and collagen coated culture dishes and differentiated for 6 days were then used to test the drift of the microscope-

stage. The shift in the centre of gravity of photoactivated cells was analysed with "IntMotion" program (**section 2.2.5**). The results showed that the centre of gravity for all frames measured (total of 20 minutes) was found within 2 pixels from the initial measurement. Therefore, the measurements performed at the conditions described in the work did not require any further adjustment or correction for stage drift.

Fluorophore stability

The photoactivated PA-GFP molecule should show similar excitation properties as eGFP (Patterson and Lippincott-Schwartz 2002).

To determine whether the fluorescent signal of photoactivated PA-GFP remained stable over time, activated cells were measured for long time periods. The signal could still be detected after 30 minutes **(fig. 3.11)**.

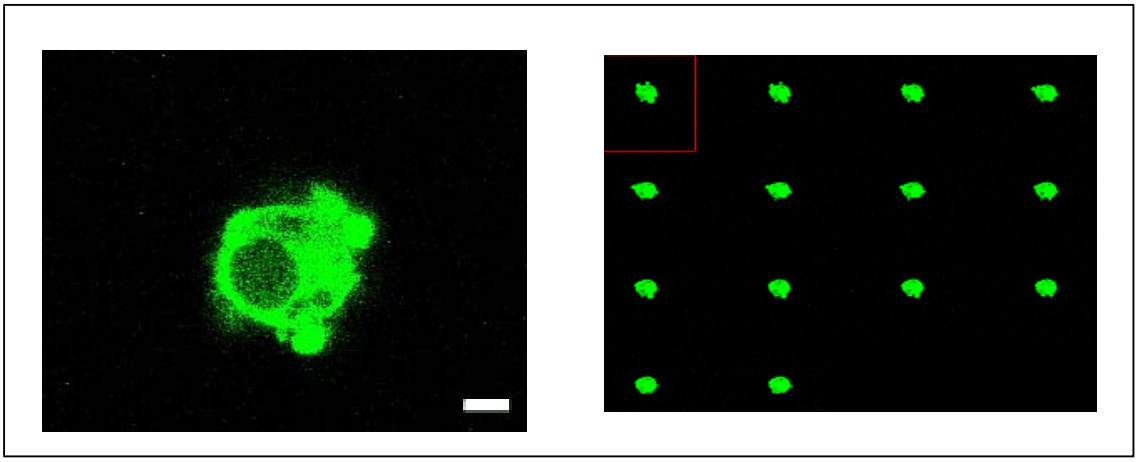

Fig. 3.11 Determination of signal stability. The photoactivated PA-GFP-tau wt expressing cell (left image) was measured for a total time of 30 minutes as shown in a tiled-version of the different frames obtained every 2 minutes (right image). The cell shows typical motions as expected for a healthy cell. Scale bar 5 µm.

Therefore, PA-GFP gives a fluorescent signal after PA that is stable in time.

Cell viability

The viability of photoactivated cells was evaluated in two ways. Cell morphology was checked in time series after photoactivation. Typical motions as the retraction and elongation of processes was visualized**.** When a higher energy for photoactivation was used however, some breakage of processes was observed (**fig. 3.12**). Process integrity and normal motions were taken as a sign for healthy cells. In addition, trypan blue

exclusion experiments were performed after photoactivation. The dye was included in the cell culture dish after photoactivation. At the conditions used, the majority of the cells were able to exclude the dye, a mark of cell integrity.

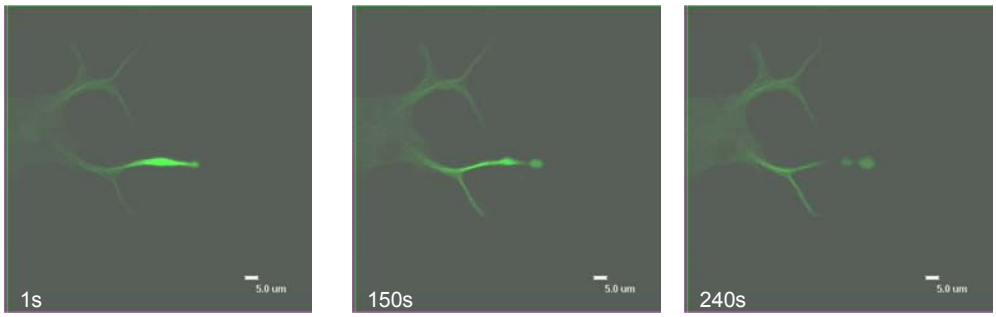

Fig. 3.12 Disruption of a process due to high energy of photoactivation. A region of a process of a differentiated PC12 cell expressing the PA-GFP-tau wt construct was photoactivated with a higher pixel dwell time (20.4 µs/pixel) as the one used for the experiments (8.16 µs/pixel). Pictures were recorded every 3 seconds, and 3 frames are shown. Time after photoactivation is indicated in the pictures.

3.1.4 Analysis of the images obtained

The different post activation frames obtained (time series) were recorded as movies. For further analysis, these ids time series had to be converted to tiff files. Usually 12-bit images (4096 grey values) instead of 8-bit images (256 grey values) increase the effective dynamic range of the measurements. Thus, images were saved as tiff raw format in a 12 bit format.

To quantify the fluorescent signal in time from the movies, different programs were tested.The program Image J was used to trace a line throughout the activated process and find the intensity profile along the line with the maximum placed on the active spot.

The obtained intensity curves were subsequently transferred to Origin program to obtain different parameters, i.e., width and maximum. Unfortunately, the results varied according to the position where the line was traced. Thus, this approach was judged not to be appropriate. It was therefore decided to develop a more complex procedure in collaboration with the Physics department of the University of Osnabrück.

The program “IntMotion” in Matlab software was developed by Dr. Reyher (**section**

2.2.5). As described in more detail in the methods section, the program analyses the full area of the process instead of only the pixels on a line along the process.

The program analyses the 12-bit tiff raw files and performs an initial 2-D filtering (which can be modified according to background noise) to detect the contour of the cell. From this contour, a region of interest (ROI) is selected and is subdivided in subregions where the intensity is quantified.

This process is performed for each individual frame. Finally, the "IntDisTime" graph is plotted for different times and distances through the process (**section 2.2.5**).

"IntMotion" was first tested with fixed samples (**fig. 3.13).** "IntDisTime" plot shows the intensity profile coded in colours in time on the y-axis and the distance along the cell on the x-axis. It is evident from the plot that the intensity obtained by the photoactivation of the spot (marked with a yellow arrowhead) remains at the same place throughout time as expected for a fixed sample. With these fixed cells, it was possible to measure the activated region by using a scale bar.

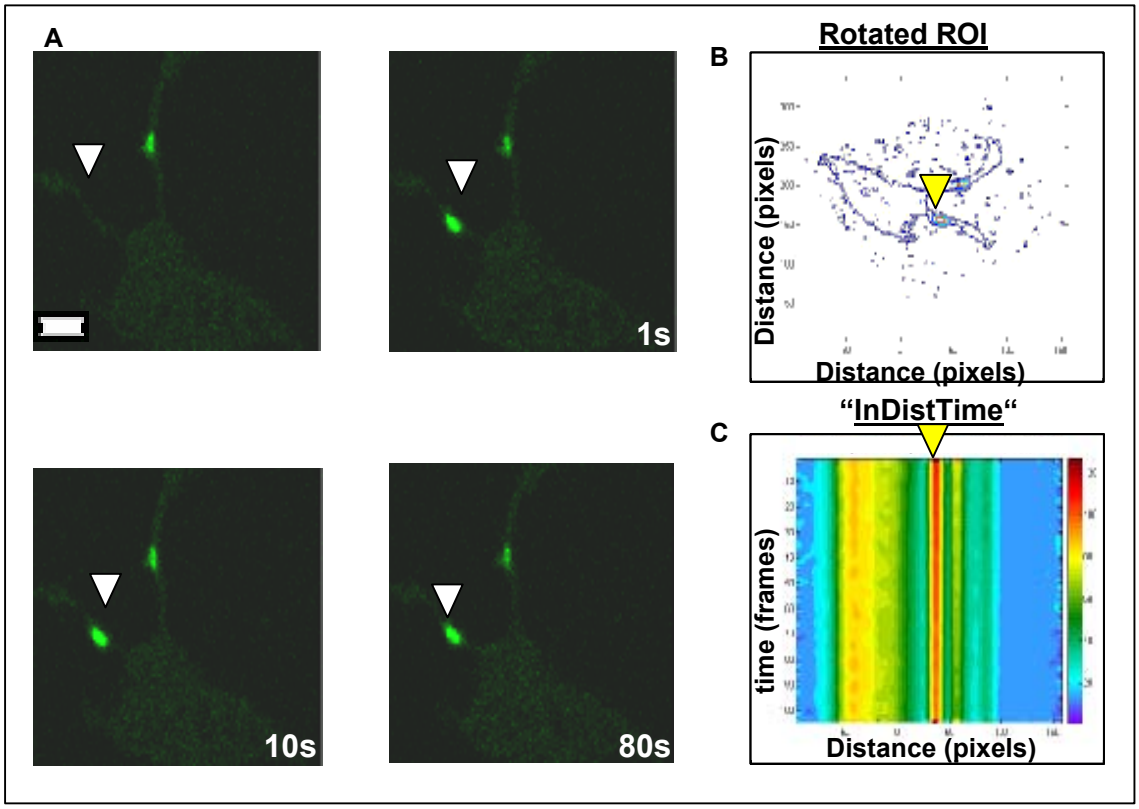

Fig. 3.13 Photoactivation of a fixed sample. After PFA fixation of differentiated-PC12, cells, PA was performed on processes. (A) Different time points after photoactivation are shown. The rotated contour of the cell as recognized by "IntMotion" is shown in (B) and the "IntDisTime" plot with intensity (in colour code) in time (y-axis) and distance (x-axis) in (C). The white and yellow arrowheads mark the activated spot. Scale bar, 10 µm.

The size of the photoactivation spot measured was 5 to7 μm in diameter **(fig.3.13 A).** This is considerably larger than the theoretical value of ≈ 300 nm expected from the resolution limit. The reason for this discrepancy may be residual scanner movement despite the setting of "0 μm scan width" (**section 2.2.5**).

This true spot value was used to extrapolate the measurements in living specimens assuming that the initial fluorescence intensity had been present at a 5 μm region (**section 3.2**).

3.2 Effect of tau structure and cellular interactions on mobility

Tau are microtubule associated proteins (MAPs) that play a role in stabilisation of microtubules (**section 1.3**).

3.2.1 Microtubule interaction

To determine the effect of the microtubule binding region (MBR) on the mobility of tau proteins, a PA-GFP-tau wt and a smaller fragment lacking the MBR (**fig. 3.1**) were analysed by the PA technique in living PC12 cells. This was one of the scenarios used to model tau protein mobility in neurons.

PA experiments were performed in the middle of cell processes which can be modelled as infinite tube-like objects. This was achieved by treating PC12 tau cell lines with nerve growth factor (NGF) which acts as a differentiating agent (**section 2.2.2**).

Photoactivation experiments in the middle of processes of the stable lines showed that the delta-expressing cells exhibited a large region of activation which dissipated earlier (about 10 s) than for wt-expressing cells (**fig. 3.14**).

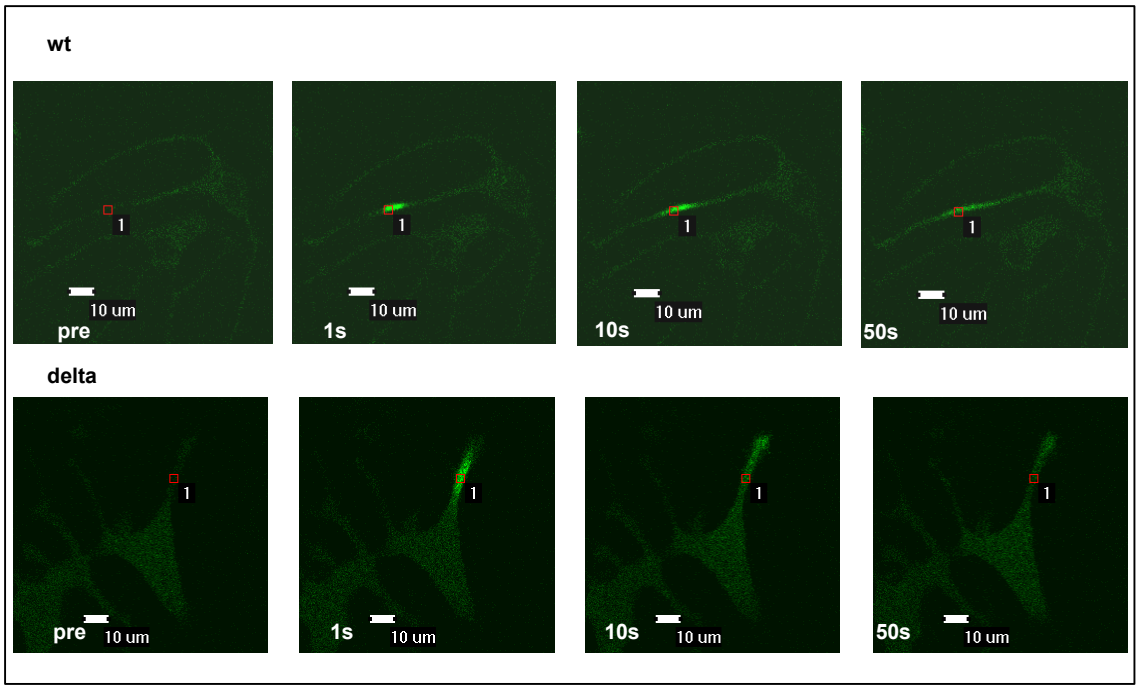

Fig. 3.14 Activation of differentiated PC12 cells. Panels show the dissipation of fluorescence after activation of a region of a process from a cell expressing a PA-GFP-wt tau construct (top panel), and from PA-GFP-delta tau expressing cells (bottom panel). The red circle marks the region where photoactivation was performed. Note the extent of photoactivation at 1s which is larger for the delta- compared to the wt-expressing cells and dissipates already at 10 s.

The "IntMotion" program was used to quantify the differences in mobility. In the "IntDisTime" plots the dissipation of the intensity signal at the site of activation was visualized as the highest red intensities decreased to green at about 15 seconds for wt tau or before 5 seconds for the delta protein (**fig. 3.15 A, B**).In contrast, PA of fixed samples showed a red initial intensity maintained until the end of the 112 s measured (**fig. 3.13).** Therefore, dissipation of the signal could be attributed to the mobility of the proteins away from the activation site and not merely to photobleaching mechanisms.

A simple parameter used for comparison of the different proteins was the fraction of proteins retained at the site of photoactivation at different time points. This "immobile fraction" (IF) is different from the immobile fraction determined by FRAP experiments (Lippincott-Schwartz *et al.* 2001).

To calculate it, the decay of intensity in time at the activated region was related to the initial intensity: $I_t/I_0=f(t)$ (curve in **fig. 3.15**).The activated region was considered to be a 5 µm diameter spot (2.5 µm to each side of the peak of intensity), equal to the size of activation measured in fixed specimens (**fig. 3.13**).

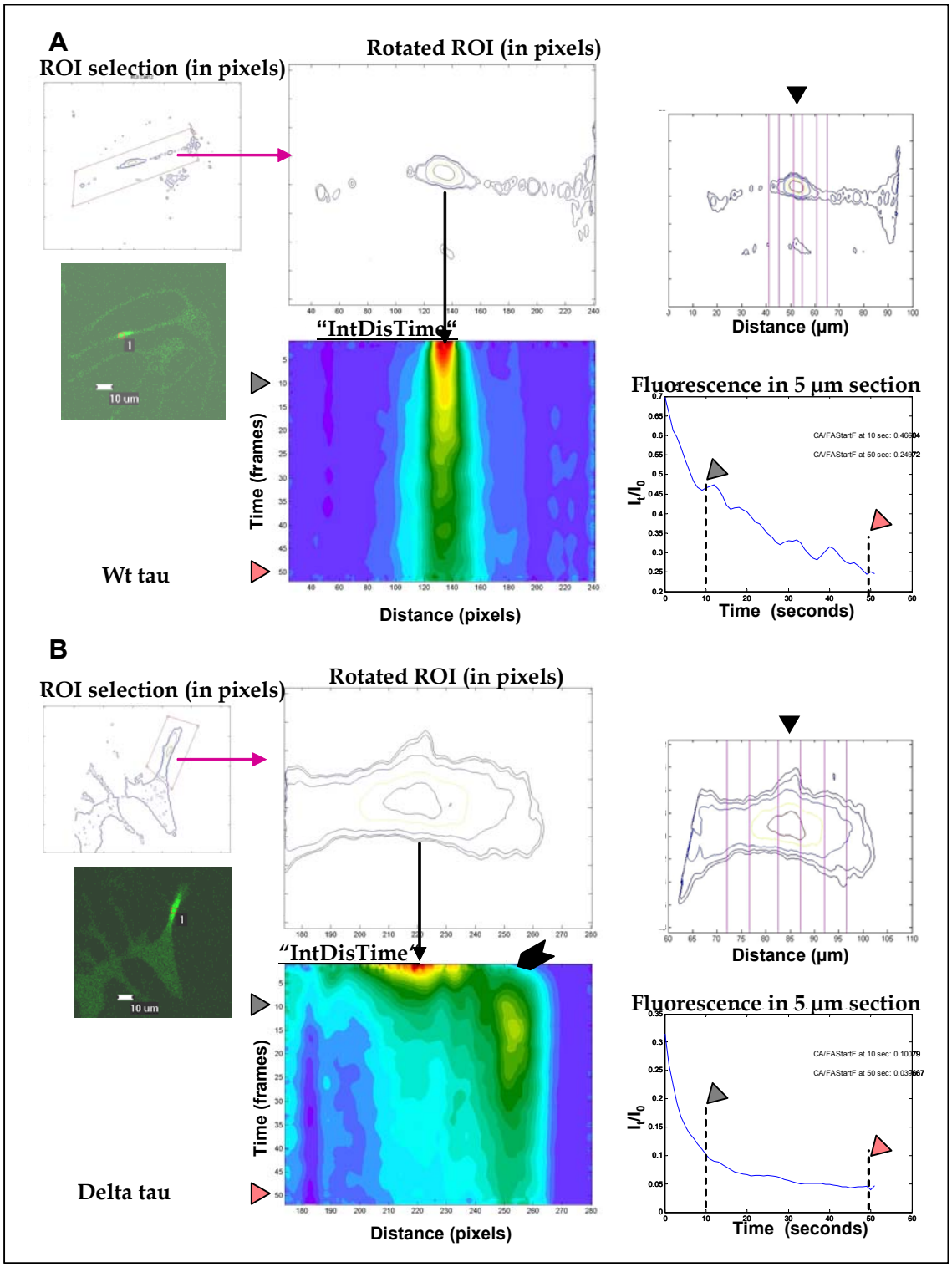

Fig. 3.15 Fluorescence intensity distribution after PA analysed with "IntMotion" program for PA-GFP-wt tau (A) and PA-GFP-delta tau expressing cells (B). A cell contour (left) and the "IntDisTime" plot for selected ROIs (middle panel) with intensity (colours) through distance (x-axis) and time (y-axis) are shown. The decay of intensity divided by the initial total intensity (I_t/I_0) for the activation region (black arrowhead, right top) is analysed by the "IntFlux" program. 10 and 50 s (grey and pink arrow heads) are shown. Note the black thick arrow head showing the accumulation of intensity at the tip in B.

To decide on the time points used for the analysis, the fractions (I_t/I_0) at 5, 10, 20, 50 and 80 seconds were determined from the PA experiments on wt and delta tau expressing cells (**fig. 3.16**).

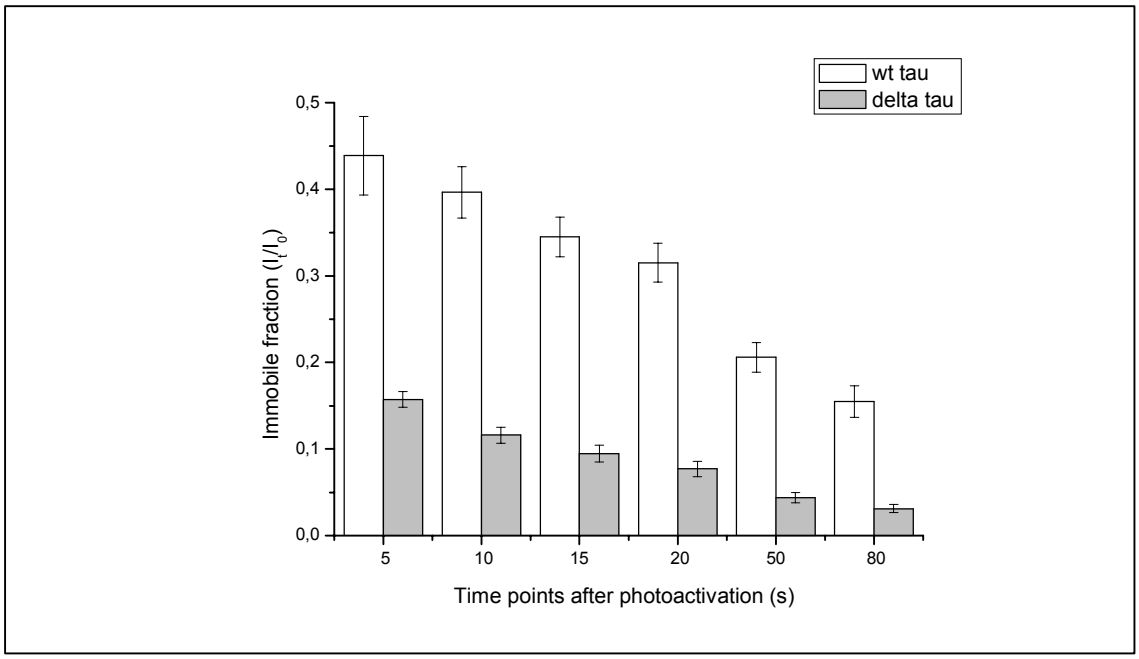

Fig. 3.16 Immobile fraction at different time points (5, 10, 15, 20, 50, 80 seconds) after photoactivation. Means and standard deviation (SD) shown, 8 cells were analysed for each condition.

The mean fraction at times lower than 10 seconds showed a high increase in the standard deviation, for times higher than 50 seconds there was also an increase in the standard deviations for other constructs analysed (not shown in the figure). Therefore 10 and 50 seconds were chosen as the time points for analysis.

As evidenced in the images (**fig. 3.14**), the initial fluorescence region from photoactivated processes in delta tau-expressing cells extended beyond the activated region spot analysed. This suggested that during the delay between the photoactivation event and the acquisition of the first frame, some distribution of the protein had occurred. To extrapolate for this delay, the total intensity measured at the ROI was assumed to be present at the 5 μm region before the first frame was measured (t=-1). With this assumption, the different time points selected (10 and 50 seconds) were divided by the initial intensity measured in the whole ROI instead of the intensity measured at the activation spot. The $I_t/I_{0(total\_area)}$ was compared to the previous $I_t/I_{0(act-area)}$ (**fig. 3.17**).

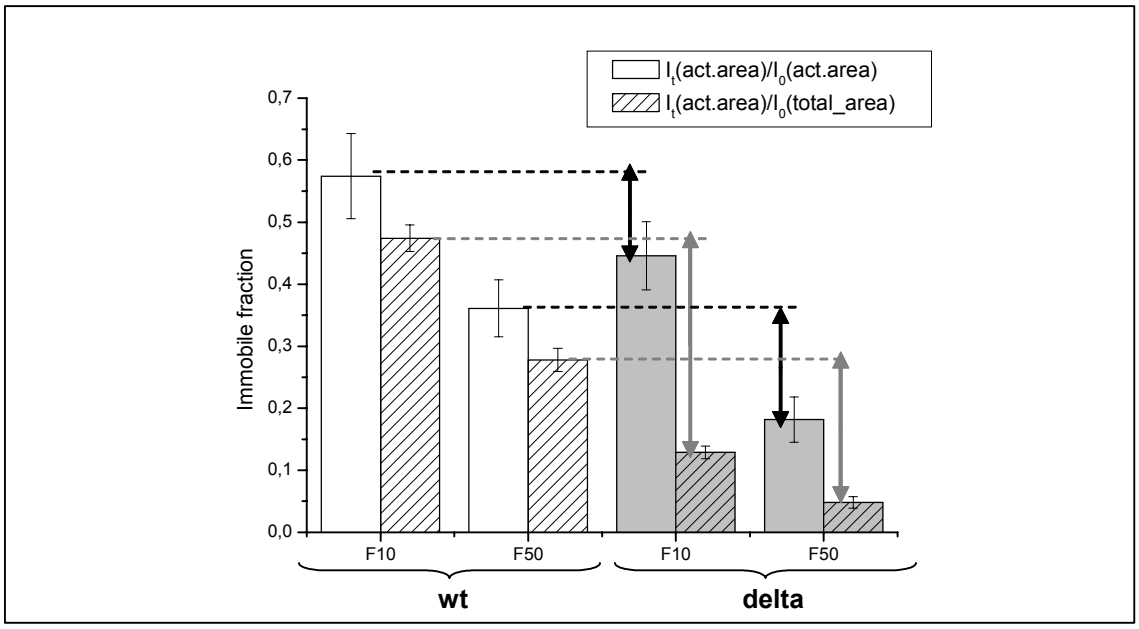

Fig. 3.17 Determination of the immobile fraction under different assumptions. The IF was related to the initial intensity value (I_0) present in the activation area ($I_{0(act.area)}$, blank bars), or the intensity present in the whole total area of the ROI ($I_t/I_{0(tot.area)}$, dashed bars) for wt tau (white bars) or delta tau (grey bars) after 10 and 50 seconds (F10 and F50). Arrows length mark the differences detected between the wt-delta proteins when $I_{0(act.area)}$ is used (black arrow) or when the $I_{0tot.area)}$ is used (grey arrow). Mean and standard error of the mean are plotted, 10-20 cells analysed per condition.

The $I_t/I_{0(tot.area)}$ at both time points (10s and 50s) was reduced (compare dashed bars to blank lines for each time point and construct). In addition, the difference between the constructs was larger (compare difference for each time point between constructs as measured by the arrows length) and yielded the lowest errors (**fig. 3.17**). Therefore, for highest sensitivity, the IFs were calculated as $I_0 = I_{0(tot.area)}$.

With this analysis, a 2.5 fold-difference between the immobile fraction for the wt tau and delta tau after 10 s was determined which increased to a 4 fold difference after 50 s showing that the wt tau construct was less mobile than the delta tau protein (**fig. 3.21, table 9.1**).

A striking feature visualized in the "IntDisTime" plots was the presence of an accumulated intensity towards the tip (black arrow head in **fig. 3.15**); this was the case in many of the cells expressing the delta tau (50%), but not for those expressing the wt (4%). This accumulation occurs before 10 s after photoactivation. To shed more light on this feature, additional experiments were performed on the most distal part of the cells (fig**. 3.18**).

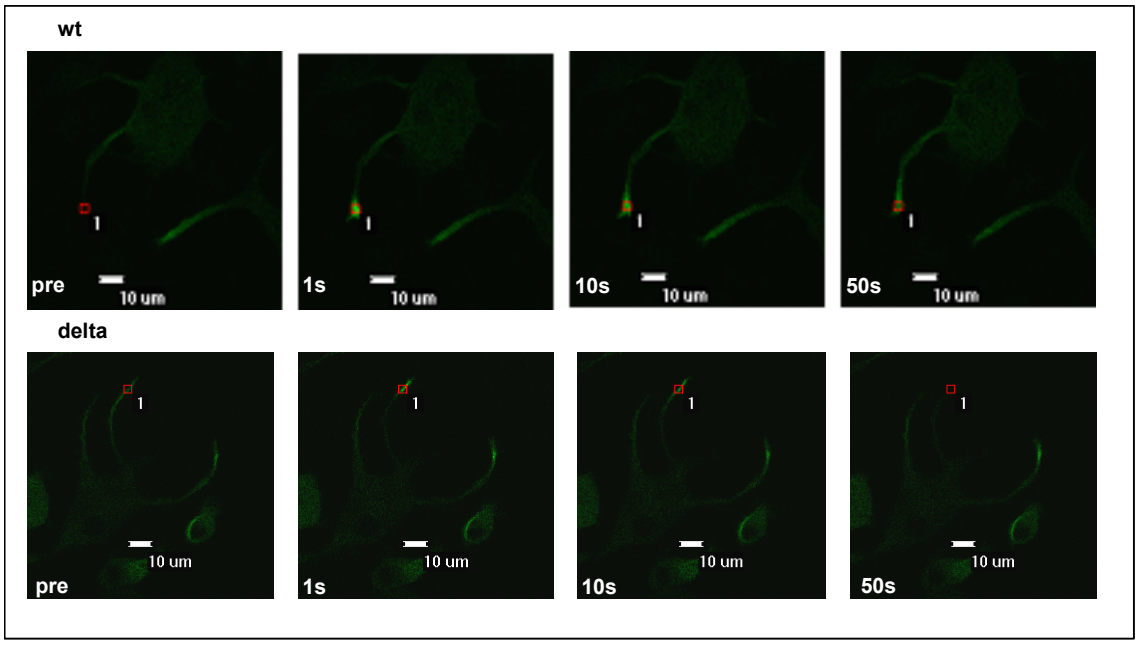

Fig. 3.18 Photoactivation at the tip of processes from PC12 cell lines. Examples of photoactivation experiments performed at the tip are shown for PA-GFP-tau wt proteins (top panel) and PA-GFP-delta tau proteins (bottom panel).

At the tip, as in the middle portion, wt tau showed a lower mobility than the delta proteins in PC12 cells. A 2 to 2.6 –fold higher IF was determined for wt tau- compared to delta tau- cells at 10 and 50 seconds in this compartment (**fig. 3.21**, **table 9.1**).

The IFtip/IFmiddle ratio was higher for delta tau (2 and 2.5 for delta versus 1.4 and 2 for the wt at 10s and 50s respectively, **table 9.1**). In both cases, the data pointed to the fact that proteins at the tip behaved differently, and this was also investigated for other proteins (**sections 3.3, 3.4**).

The PA experiments, as mentioned, were performed on stable lines, were protein expression levels were similar to tau endogenous induced levels. To determine whether expression levels could modify protein distribution and mobility, PC12 cells were transiently transfected (**section 2.2.3**) with the same tau-encoding plasmids.

In transient transfections, the protein expression level is higher (approximately 10 times) than in a stable line, and varies from cell to cell. For the analysis, cells were differentiated two days after transfection (**section 2.2.2**). The processes developed were analysed 6 days after NGF treatment as done with the stable lines.

The analysis showed differences in the IF much higher (up to a 4-fold difference) between the wt and delta IF showing the same tendencies as in stable lines (**fig. 3.21** and **table 9.1**).

Thus, even at higher expression levels and variability, the wt tau- PC12 expressing cells showed a higher IF than the delta tau-expressing cells, and the tip retained the proteins to higher levels.

Next, PA experiments were performed in a different cell model. PC12 cells were used as a neuron-like model because they develop neurite-like processes and are easy to work with. To test whether the results obtained also applied to neurons, the experiments were repeated in mice primary cortical cultures.

Plasmids encoding the PA-GFP-tau wt and PA-GFP-delta tau sequence were transfected in mice primary cortical cultures (**section 2.2.2**). The presence of neurons in the transfected cells was determined by staining with MAP2 antibody, a neuronal marker (**fig. 3.19**).

Cells were analysed one day after transfection. Later time points could not be analysed since the background levels increased and positive transfected cells could no longer be detected. The morphology of the cells was easily recognizable to perform photoactivation experiments with these cells at the middle and the tips of axons.

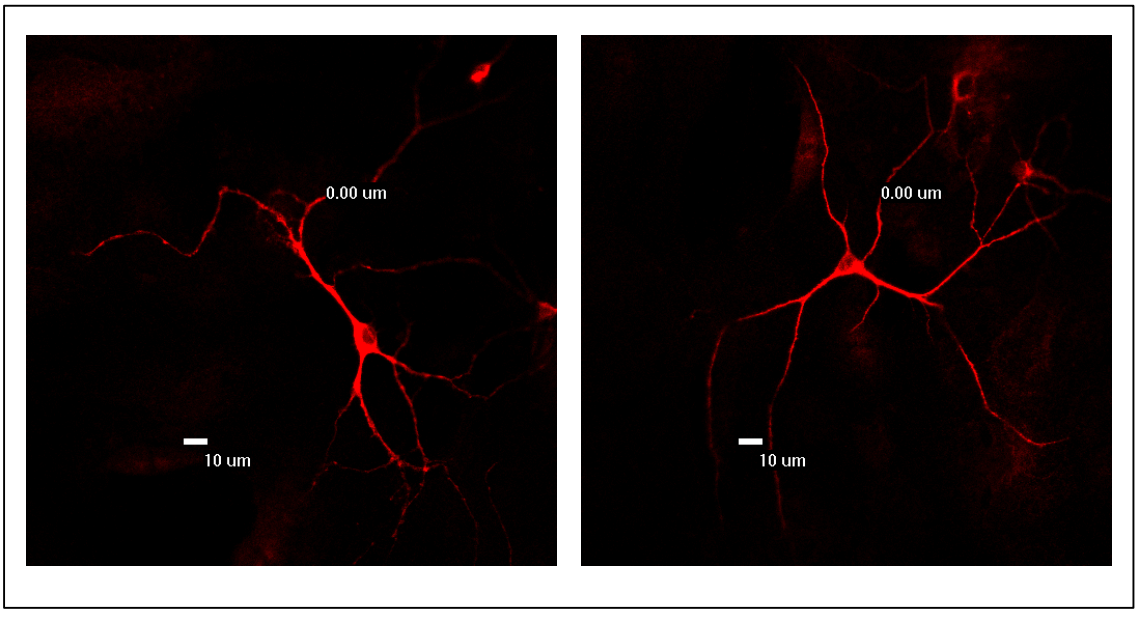

Fig. 3.19 Fixed mice primary cortical culture. Cells from the prepared culture were fixed with paraformaldehyde and stained with an antibody against MAP2 and Cy3-coupled anti-mouse secondary antibody to identify neurons in the culture.

Qualitatively, delta tau-expressing cells also displayed a larger region of photoactivation after 1 s compared to wt tau expressing cells (**fig. 3.20**).

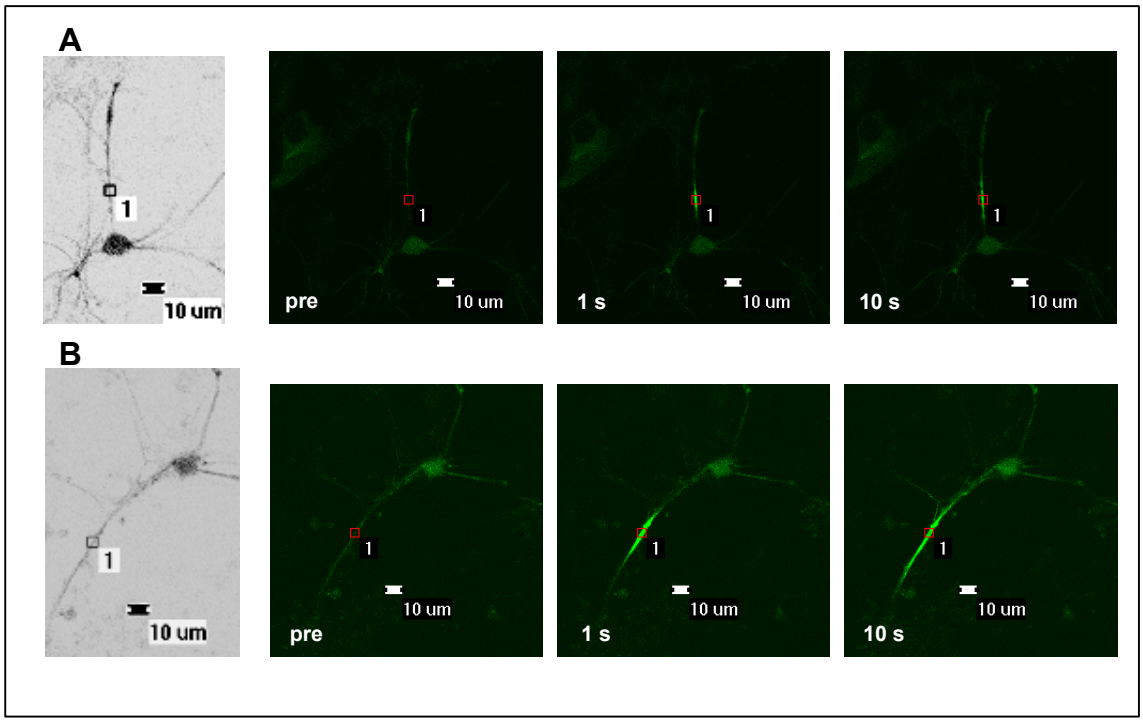

Fig. 3.20 Photoactivation experiments of transfected mice primary cortical cultures. Images of a cell expressing PA-GFP-wt tau (A) and PA-GFP-delta tau (B) after PA. Note the larger activation spot obtained after photoactivation (1 s) for the delta tau expressing cell compared to the wt tau one. The first left image was converted to grey scale and the colour inverted to visualize the contour of the whole cell.

This system however, was not so amenable to work with. The background fluorescence level was high, and the transfection efficiency was low (less than 2%). In some cases, the processes were so long that it was difficult to recognize the beginning and end of a cell to analyse them in isolation.

The results obtained in neuronal axons from primary cortical culture, showed that the wt protein was retained about 2 and 2.5 times as much as the delta protein at the site of activation in the middle or the tip.

At the tip, the fractions for both proteins were also higher than at the middle and a higher IFtip/IFmiddle was observed for delta compared to wt tau expressing cells (**fig. 3.21 and table 9.1**).

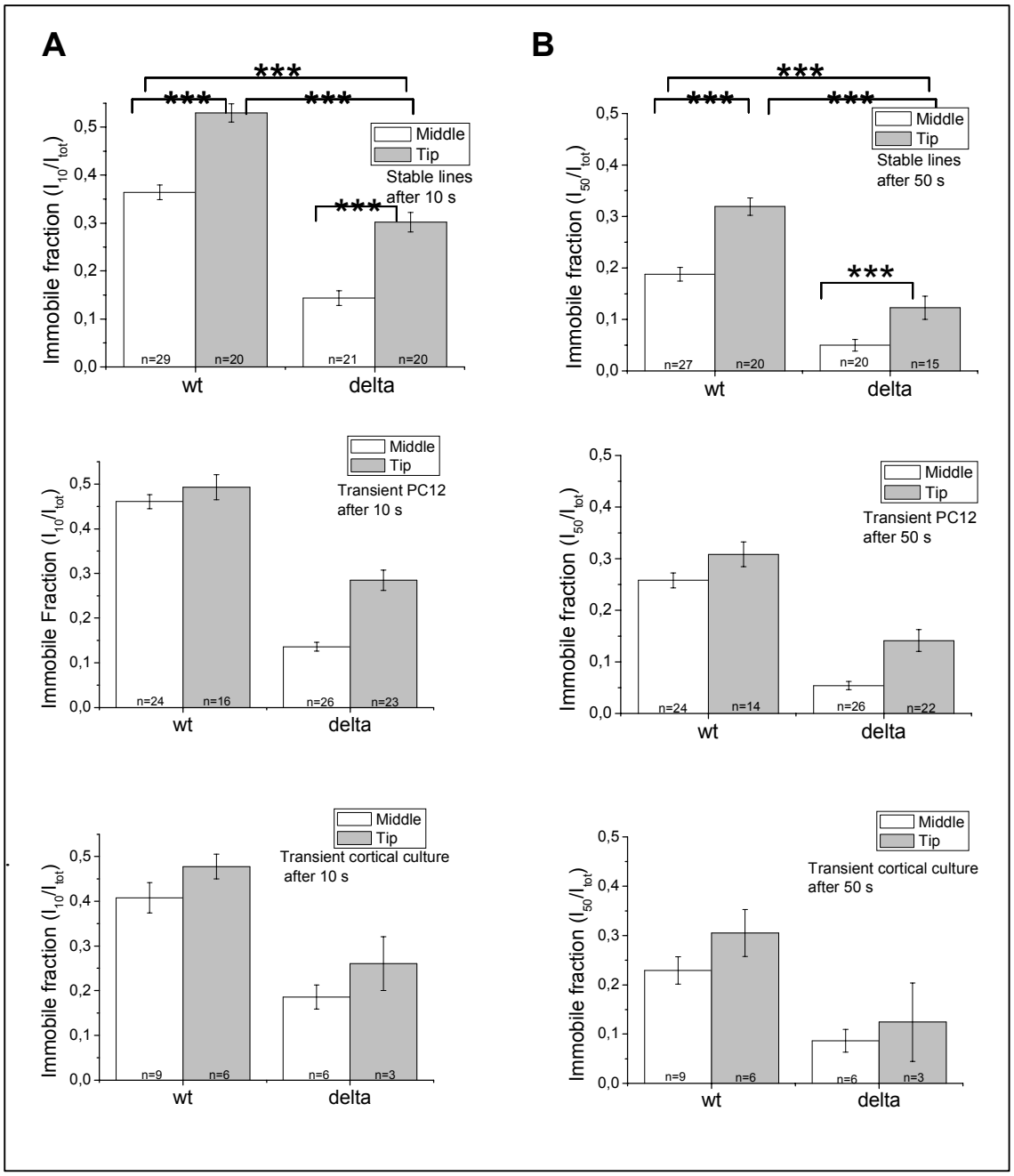

Fig. 3.21 Immobile fractions plotted at 10s (A) and 50 s (B) for wt tau and delta tau expressing cells as analysed in stably transfected PC12 cells (top panel), transiently transfected PC12 cells (middle panel), and transiently tranfected mice primary cortical cultures (bottom panel). Note the higher IF for wt proteins compared to delta proteins. Photoactivation experiments at the middle or tip of processes were performed 6 days after NGF treatment of the PC12 lines and 1 day after primary cortical culture transfection. Cell number (n) is given in the bars. Mean and SE are shown (table 9.1 appendix). Comparisons between groups were based on one-way ANOVA test followed by posthoc Bonferroni tests (* p< 0.05; ** p <0.01; *** p< 0.001).

Thus, the results obtained with PC12 cells could be reproduced in a system where real neurons were used. Regardless of the system analysed -PC12 transient or stable transfections or transiently transfected primary cortical culture-, the analysis demonstrated that tau wt compared to delta proteins were retained to a higher extent at the middle and tip portions of cell processes.

In addition, the most distal portion of the process showed a higher retention of both proteins than the middle part. These features which were evident 10 seconds after photoactivation were maintained also after 50 seconds (**fig. 3.21)**.

To avoid the variability encountered due to the variation in expression levels and the difficulty in working with primary cultures, stable PC12 cell lines were used for further analysis and discussion. Results on transient transfections is given in initial plots and tables (**appendix**).

The difference in the IF described for wt and delta proteins in the different cell models analysed could relate to the difference in size and the regions constituting the proteins. The delta construct is smaller than the wt, and lacks the microtubule binding region (MBR).

To determine whether size contributed to the differences in mobility, an unrelated control was analysed. For that, firstly, a control made up of only one PA-GFP molecule, "PA-GFPx1" (~27 kDa), and then a molecule made up of two PA-GFP molecules, "PA-GFPx2" (~54 kDa) were tested in PA experiments.

Both proteins were detected at high levels in the nucleus, but only a low signal could be detected in the processes making it difficult to perform photoactivation experiments at this portion (**fig. 3.22, D**). This result was in agreement with a study from Chen *et al* who reported that photoactivation of a tandem construct made up of two PA-GFPs crossed the nuclear pore (Chen, Macdonald et al. 2006).

Indeed, the size of the molecules, below the 60 kDa limit to cross the nuclear pore complex (Kubitscheck, Wedekind et al. 1996) could determine the protein enrichment in this region.

Consequently, a construct made up of three PA-GFP molecules arranged in tandem was generated (**fig. 3.1** and **3.4**). This "PA-GFPx3" protein with an estimated molecular weight of 82.8 kDa was excluded from the nucleus (**fig. 3.22, A, B, C**).

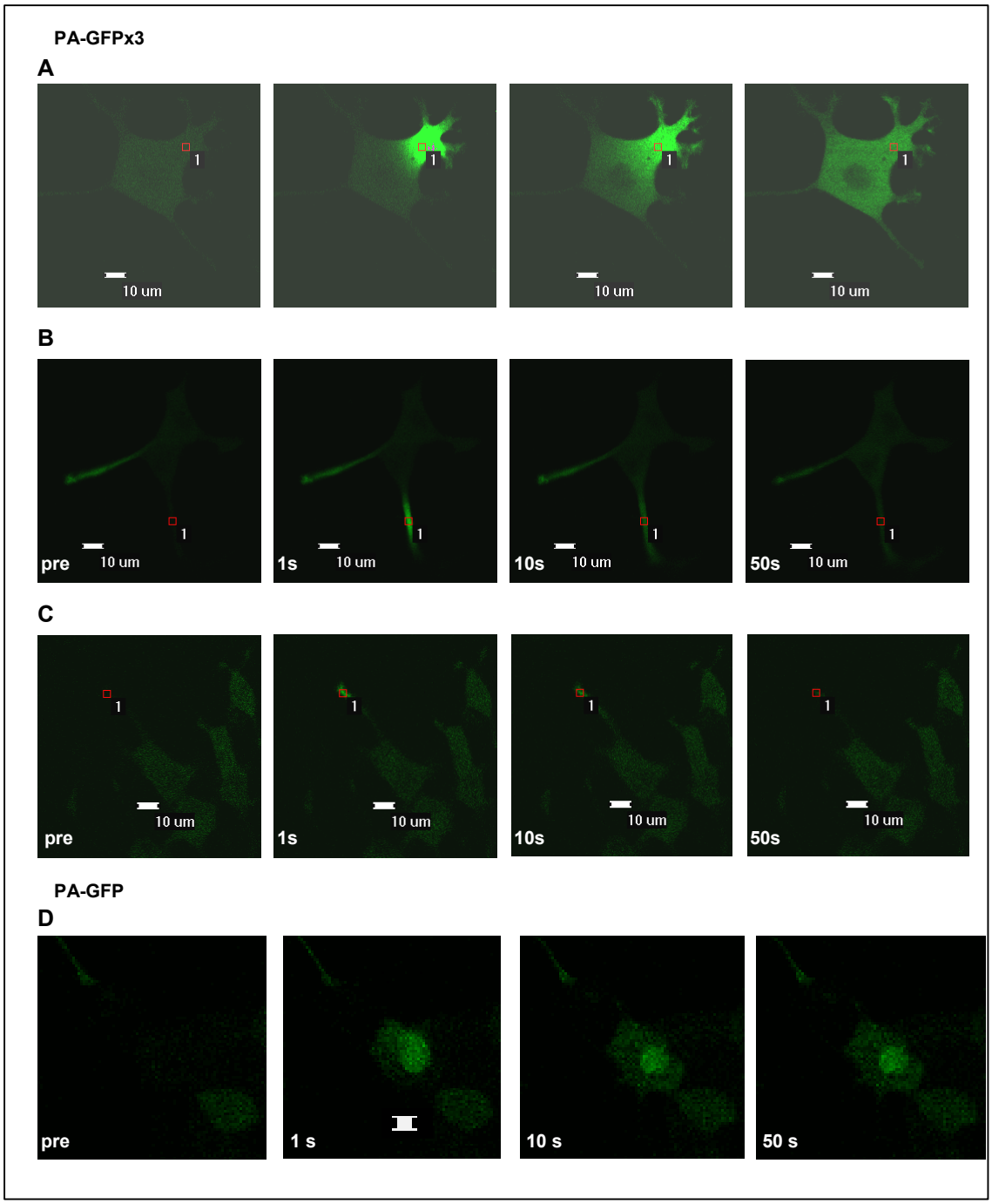

Fig. 3.22 Photoactivation experiments of PA-GFP control proteins. PA-GFPx3 expressing cells were photoactivated at the cell body to show the exclusion of the construct from the nucleus (A), and at the middle of cell processes (B), and at the tip (C) of processes. PA-GFPx1 expressing cells were photoactivated, but the protein was mainly detected at the cell body and retained in the nucleus (D). Scale bar 10 µm.

A stable line with PA-GFPx3 was prepared, and lysates were checked. The protein showed the same band mobility in SDS PAGE blots as the PA-GFP-wt tau protein (**fig. 3.6**). The analysis of a photoactivated cell stably expressing PA-GFPx3 is shown in **fig 3.23.**

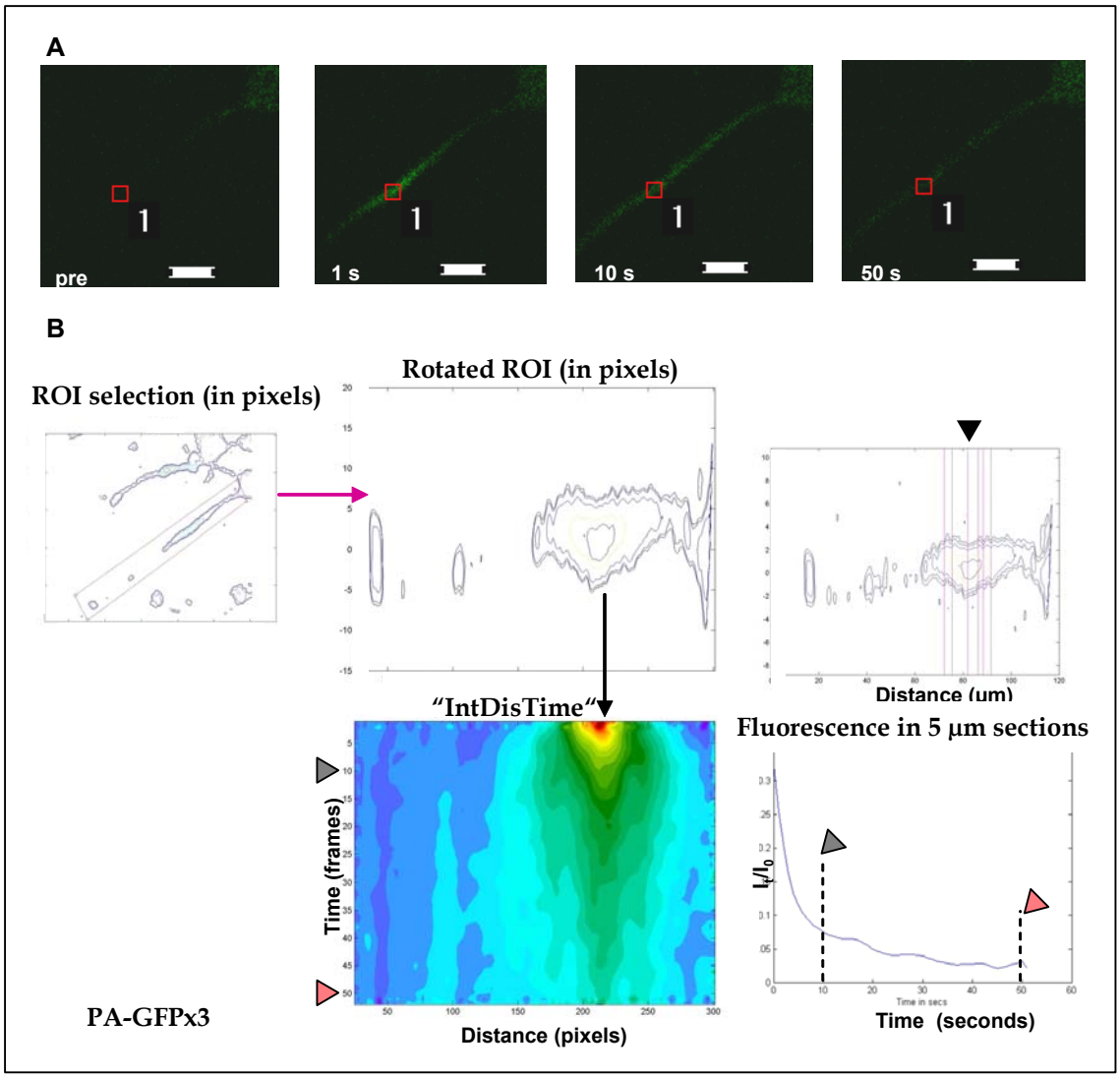

Fig. 3.23 Photoactivation experiment of PA-GFPx3-expressing cell. In (A), images after photoactivation of a cell stably expressing the PA-GFPx3 protein are shown. In (B), the analysis of the images performed with "IntMotion" program is depicted. The "IntDisTime" plot (middle) shows the intensity decay in colours throughout distance on the x-axis and time on the y-axis. The right panel in (B) shows the selected regions on the process (top) to obtain the I_t/I_0 curve (bottom). The same time points marked on the "IntDisTime", 10 seconds (grey arrow head) and 50 seconds (pink arrowhead), are also marked on the curve showing the decay of intensity for the photoactivated central region (marked with a black arrowhead).

The IF for cells expressing the PA-GFPx3 and the delta tau proteins did not differ (**fig. 3.24**). Both constructs showed a higher IF compared to wt tau after 10s or 50s. This was the case whether the middle of the process or the tip was analysed (**fig. 3.24**).

The difference in IF between cells expressing delta and PA-GFPx3 constructs and the wt tau suggested that the presence of the MBR was the major factor determining

higher protein retention at the tip and the middle portion of a process.

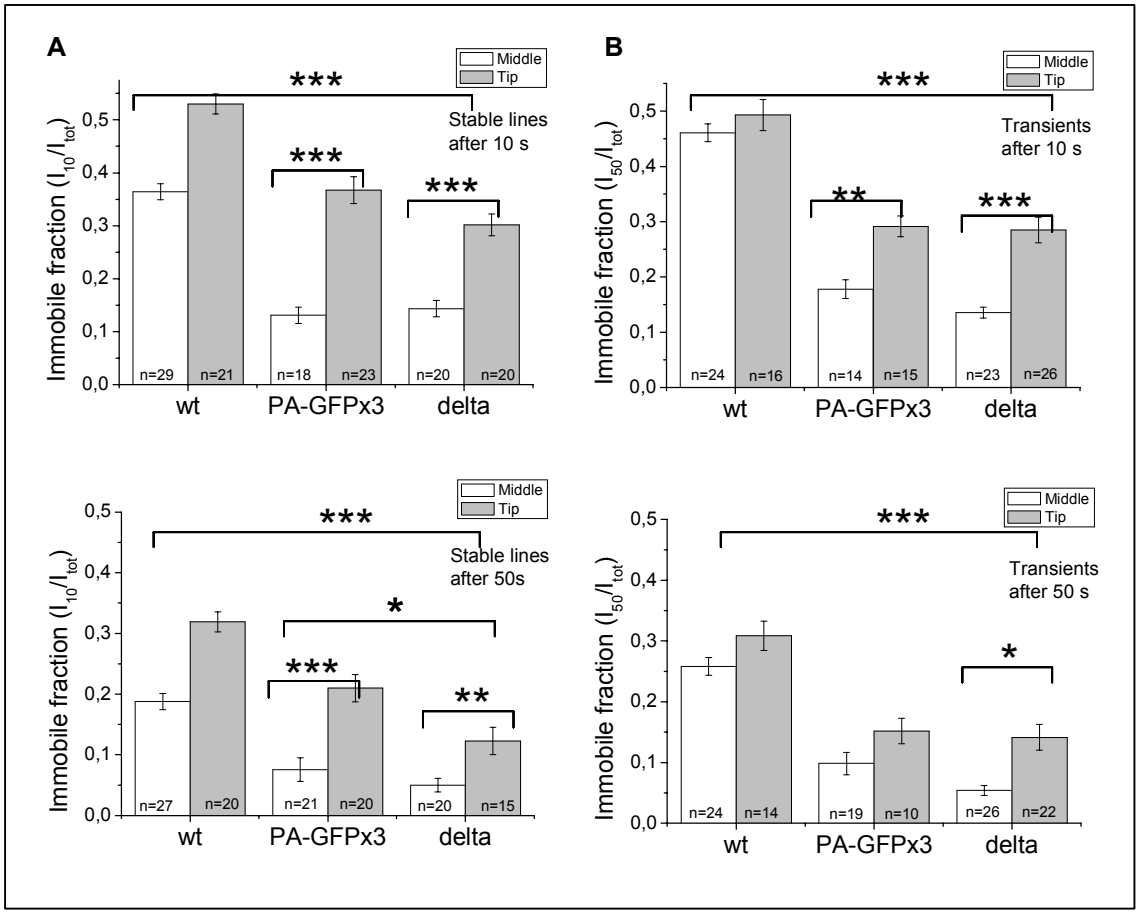

Fig. 3.24 Analysis of photoactivation experiments performed at the middle and tip of the process from cells expressing PA-GFP-wt tau, PA-GFP-delta tau and PA-GFPx3. Wt proteins show a significant higher IF compared to PA-GFPx3 and delta proteins. Stable lines (A) and transient transfections (B) after 10 (top) and 50 (bottom) seconds. Mean and SE are shown (table 9.1 appendix). Cell number (n) is given in the bars. Comparisons between groups were based on one-way ANOVA test followed by posthoc Bonferroni tests (* p< 0.05; ** p <0.01; *** p< 0.001).

To confirm that the microtubule was the main partner affecting the mobility of the proteins, PA experiments were performed after disrupting this component. Stable cell lines were incubated with the microtubule depolymerising drug colchicine. Under the condition used (**section 2.1.3**), processes showed a punctuate appearance **(fig. 3.25 B**). In addition, **fig. 3.25 A** shows the effect of colchicine throughout time as recorded for a stable line expressing the eGFP-tau wt protein. In the eGFP-wt tau line, the fluorescence intensity increased towards the cell body (reaching saturation at late time points), and the processes and cell body shrink throughout time.

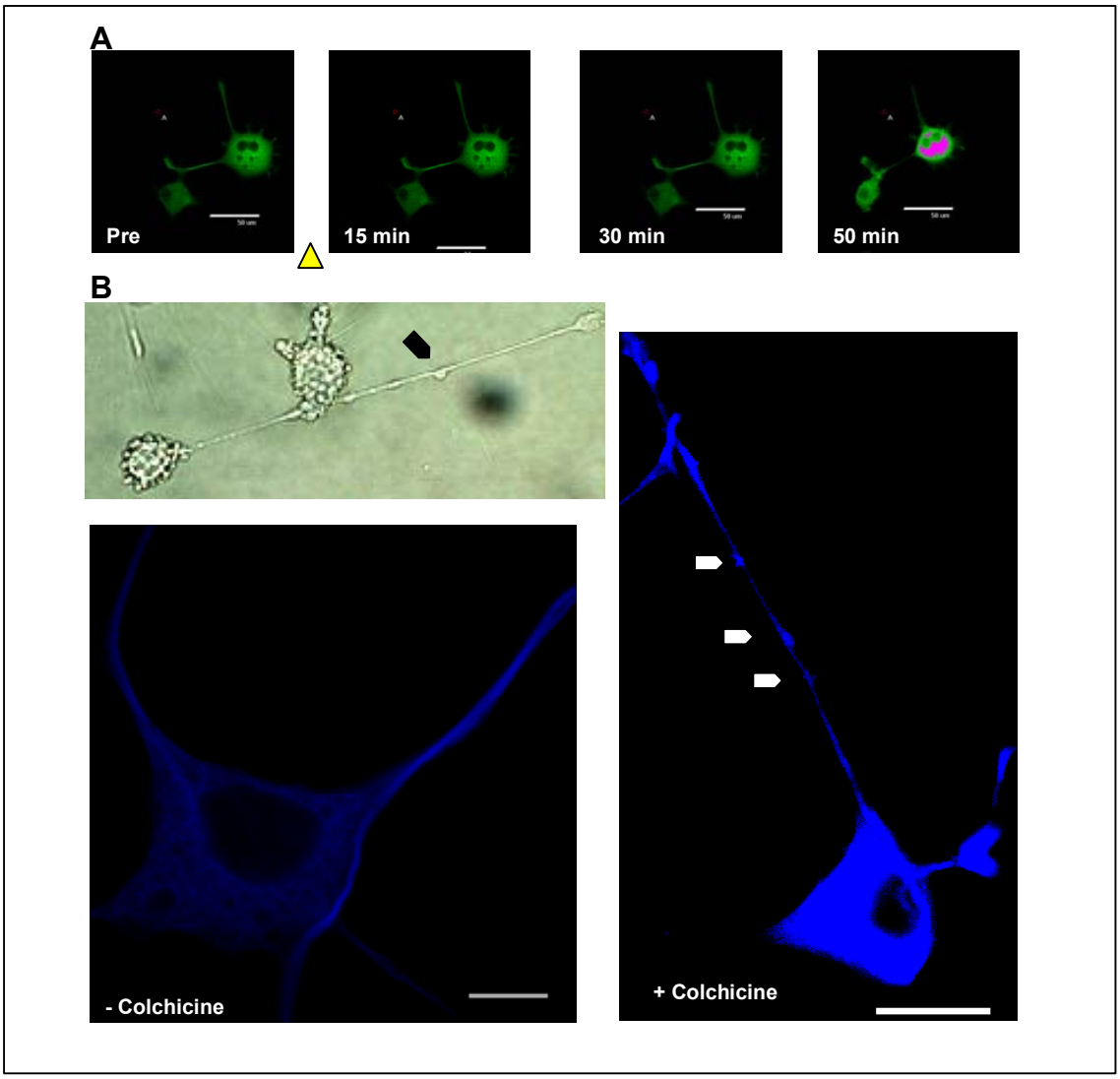

Fig. 3.25 Effect of colchicine on PC12 cells. Pictures showing the effects of colchicine on cells expressing eGFP-tau wt (A) and PA-GFP-tau wt cells (B). In (A), the pictures were taken at the time points indicated keeping the detection gain constant during image acquisition. In (B), a bright field microscope image (above) and fluorescent micrograph of cells fixed and stained with an antibody against microtubules (DM1A) and AMCA anti-mouse secondary antibody (below) are shown after treatment with colchicine at 2 µM for half an hour (Kempf *et al.* 1996) (right) or untreated (left). Yellow arrowhead indicates colchicine addition, white arrowheads points at typical punctuate structures of a process after colchicine treatment. White scale bar, 10 µm.

The IF for photoactivated PA-GFP-tau wt expressing cells after colchicine treatment decreased to about 20% of untreated cell values (**fig. 3.26 and table 9.1**). This was not the case when the delta tau or PA-GFPx3 construct were measured after colchicine incubation which showed no difference to untreated cells (**fig. 3.26**).

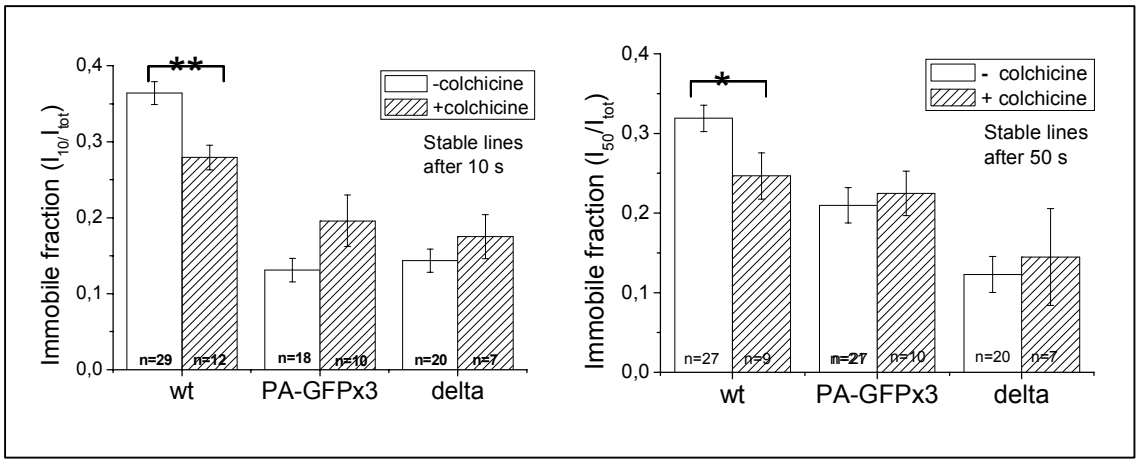

Fig. 3.26 Photoactivation experiments on cells treated with colchicine. Stable lines expressing PA-GFP-tau wt, PA-GFPx3 or PA-GFP- tau delta were incubated with colchicine (dashed bars), and PA experiments were performed and compared to untreated cells. Note the decrease in IF only for the wt protein. IF Mean and SE are shown (table 9.1 appendix). Cell number (n) is given in the bars. Comparisons were performed using two sample paired t-tests (* p< 0.05; ** p <0.01; *** p< 0.001).

Therefore, once the microtubules were disrupted, the mobility of only the MBR-containing protein increased. To investigate whether the microtubules were also responsible for retaining the proteins at the tips, the same experiments were performed on this compartment for the wild type tau protein (**fig. 3.27**).

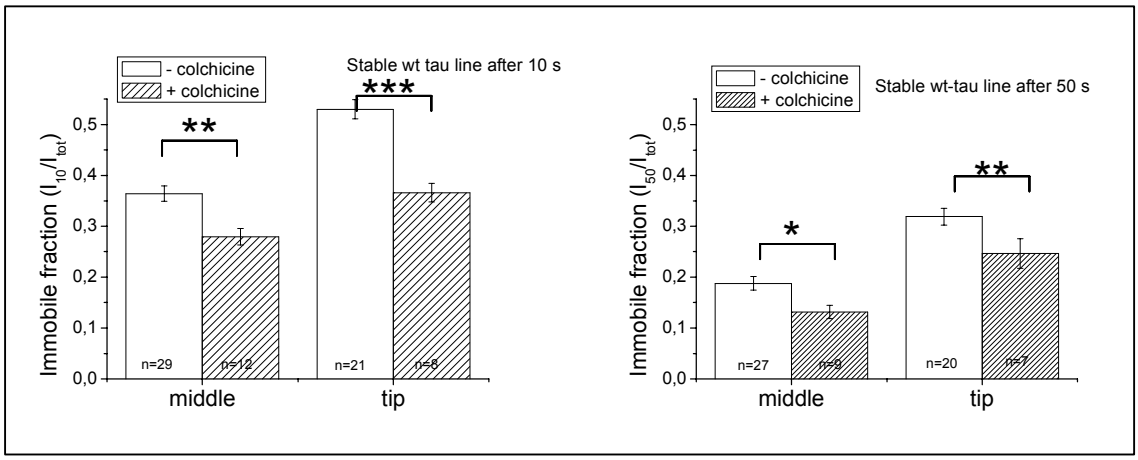

Fig. 3.27 Effect of colchicines in different process regions. Experiments were performed in PA-GFP-wt tau expressing cells incubated with colchicine at the middle and tip of processes.IF are decreased after the treatment.IF Mean and SE are shown (table 9.1 appendix). Cell numbers (n) are given in the bars. Comparisons were performed using two sample paired t-tests (* p< 0.05 p <0.01*** p< 0.001).**

The IF determined after photoactivation of cells expressing PA-GFP-tau wt at the tip of processes showed similar results, i.e., a lower IF in microtubule-disrupted PA-GFP-tau wt cells. Thus, microtubule presence seemed to be required for the retention of wt-tau proteins in middle and tip of cell processes.

To test further this interaction, taxol, a drug that stabilises microtubules and is normally used in *in vitro* studies to purify these filaments (Sontag, Nunbhakdi-Craig et al. 1999) was used in PA experiments. Interestingly, Samsonov *et al* reported that cells treated with taxol exhibited detachment of tau proteins from microtubules (Samsonov *et al.* 2004). Experiments were performed after addition of taxol to stable lines (**fig. 3.28**).

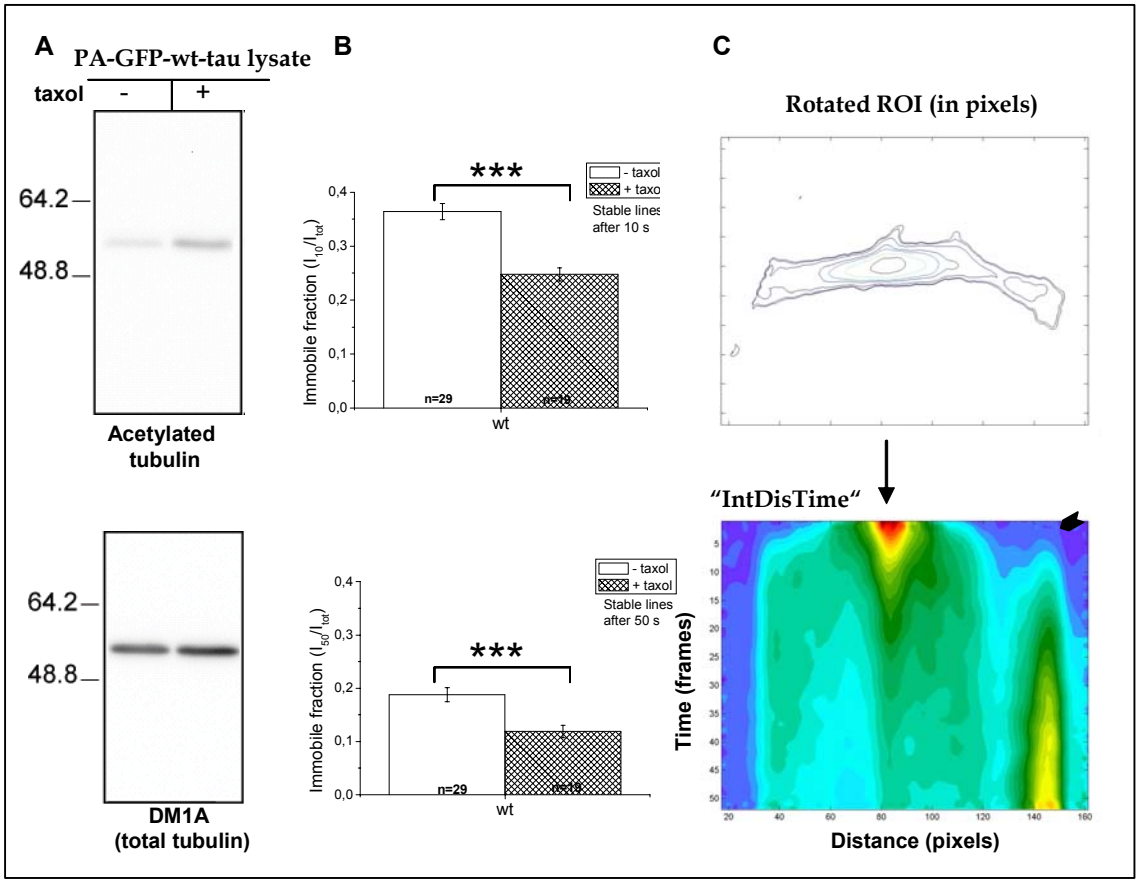

Fig. 3.28 Effects of taxol in wt-tau expressing cells. (A) Blots of lysates of PA-GFP-wt tau expressing cells treated with taxol and compared to untreated cells after staining against acetylated tubulin (marker for tubulin stability, above) and total tubulin (DM1A, below) (Anne Hillje, masterwork). (B) Quantification of PA experiments in taxol-treated (dashed) bar or untreated (blank bar) PA-GFP-tau wt cells. (C) Representative "IntDisTime" plot for a taxol-treated wt cell showing the accumulation of intensity towards the tip (black arrowhead).Taxol induces tau detachment (high IF) while microtubule stability is increased (high acetylated tubulin signal). Mean and SE are shown in B (table 9.1, appendix). Cell number (n) is given in the bars. Comparisons were performed with two sample paired t-test (* p< 0.05; ** p <0.01; *** p< 0.001).

Microtubule stability was monitored by western blots of cell lysates (**section 2.2.4**) to quantify the amount of acetylated tubulin. Indeed, the signal detected demonstrated that the microtubules increased their stability **(fig. 3.28, A, Anne Hillje, master work**).

PA experiments of PA-GFP-tau wt expressing cells at these conditions, showed that, consistent with a detachment of tau from microtubules, a decrease in IF (~65%) compared to the IF of untreated cells could be determined (**fig. 3.28 B, table 9.1, appendix**).

Interestingly, an accumulation of fluorescence intensity towards the tip (**fig. 3.28 C)** in 82% of the cells was also visualized. This accumulation was similar to that detected in PA of untreated delta tau-expressing cells. This issue was further investigated by the "flux analysis" (see **3.2.3**).

The data on PA experiments of wt tau cells under colchicine and taxol treatment confirmed the involvement of tau-microtubule interaction in protein retention at the processes of living cells. In addition, new evidence for the effect of taxol as a drug that detaches tau from microtubule was given.

3.2.2 Actin filaments and tau mobility

The cytoskeleton is the main determinant of neuron morphology; it is composed of microtubules, microfilaments and intermediate filaments (**section 1.1**).

The presence of microtubules and actin filaments can be visualized by staining with antibodies against these structures**.** Actin filaments are prominent at the tips and cell periphery, where microtubule amount decreases (**fig. 3.29 A).**

To determine the relevance of this structure on tau mobility in cells, PA experiments were performed after treating the lines with Cytochalasin B, an actin depolymerising agent. To test the effect of this drug, PA-GFP-tau wt expressing cells were incubated with the drug, fixed and stained to label the actin filaments. Actin structures were absent from the periphery or tips of processes in cytochalasin-treated cells (right panel in **fig 3.29 B**).

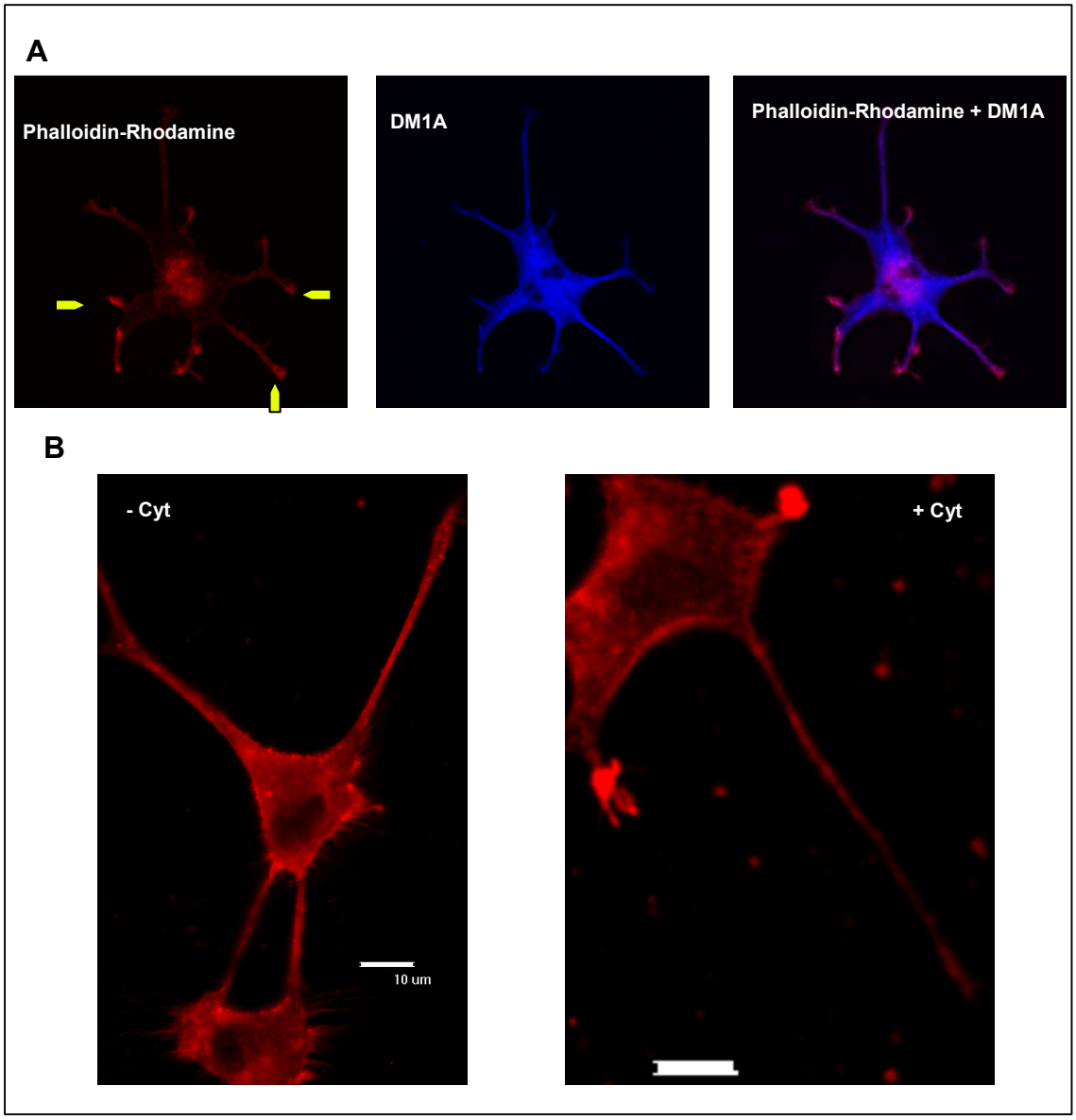

Fig. 3.29 Effect of cytochalasin treatment on the distribution of microtubules and actin filaments in PC12 cells In (A) PC12 cells expressing PA-GFP-wt tau proteins were fixed and stained using DM1A antibody against tubulin and AMCA anti-mouse secondary antibody (in blue, middle picture); and Phalloidin-rhodamine to detect actin, (in red, picture to the right). An overlay showing both features is shown on the left. In (B), cells were incubated with cytochalasin B at 20 µM for 30 minutes (Léger *et al.* 1994) to disrupt actin filaments (left) or with ethanol used as vehicle solution (right) and subsequently treated with Phalloidin-rhodamine. Scale bar, 10 µm

The IF of photoactivated PA-GFP-tau wt expressing cells treated with cytochalasin showed a decrease to 81% or 70% at 10 and 50s compared to untreated cells. In the case

of cells expressing the delta protein, the treatment showed no difference in the IF for treated or untreated cells (**fig. 3.30, table 9.1**).

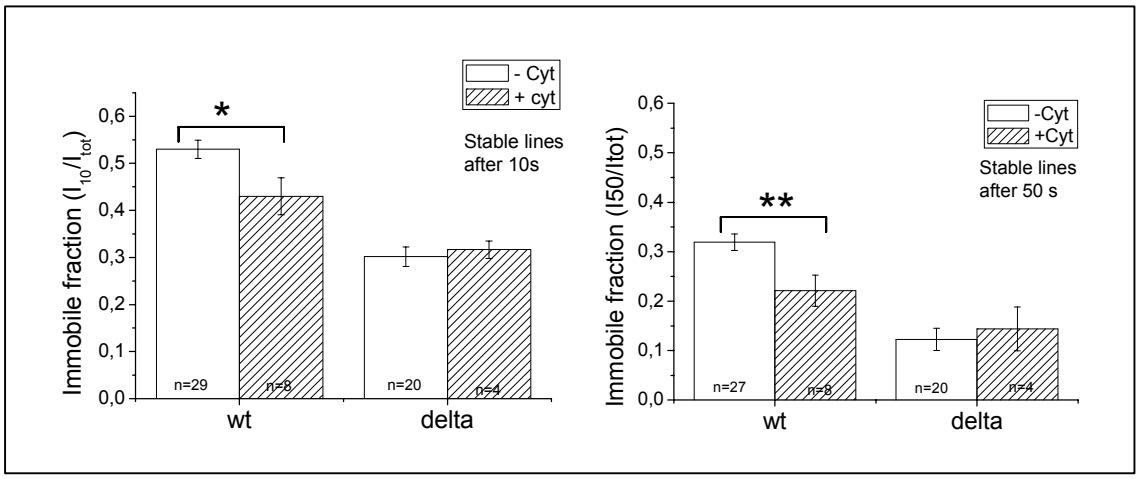

Fig. 3.30 Effect of cytochalasin treatment in cells photoactived at the tip of processes. PA-GFP-tau wt and PA-GFP-delta tau expressing cells were incubated with cytochalasin for 30 min determining a higher retention of wt proteins to the tip. The IF is plotted for 10 and 50s after photoactivation. Cell number (n) is given in the bars. Mean and SE are shown (table 9.1, appendix). Comparisons were performed by two sample paired t-test (* p< 0.05; ** p <0.01; *** p< 0.001).

Hence, actin filaments seemed to contribute to the retention of wt tau proteins at the tip of the cells.

3.2.3 Flux Analysis

To analyse further the mechanisms by which proteins moved, and whether a direction was favoured, the flux of photoactivated proteins was determined.

For this analysis, the fluorescent signal present 10 µm away from the photoactivated spot towards the soma ("proximal flux") or tip ("distal flux") 10 seconds after photoactivation was calculated. A scheme of this analysis is shown in **fig. 3.31 A.**

For this purpose, the fluorescence intensity decay 10 µm away to the right (I_R=f (t)) or left (I_L=f (t)) of the central (I_C=f (t) activation spot ("Fluorescencey in 5 µm sections" plots (section **2.2.5**and **fig. 3.31 B**).

The left or right region might correspond to the proximal or distal region and has to be determined by visual inspection of the process. The 10 s time point was analysed to determine the distribution as quick as possible before further accumulation might be

recorded or lost (**fig. 3.31 B**). In addition, to relate these fractions to the intensity present at the activation spot, I_L and I_R are divided by I_C.

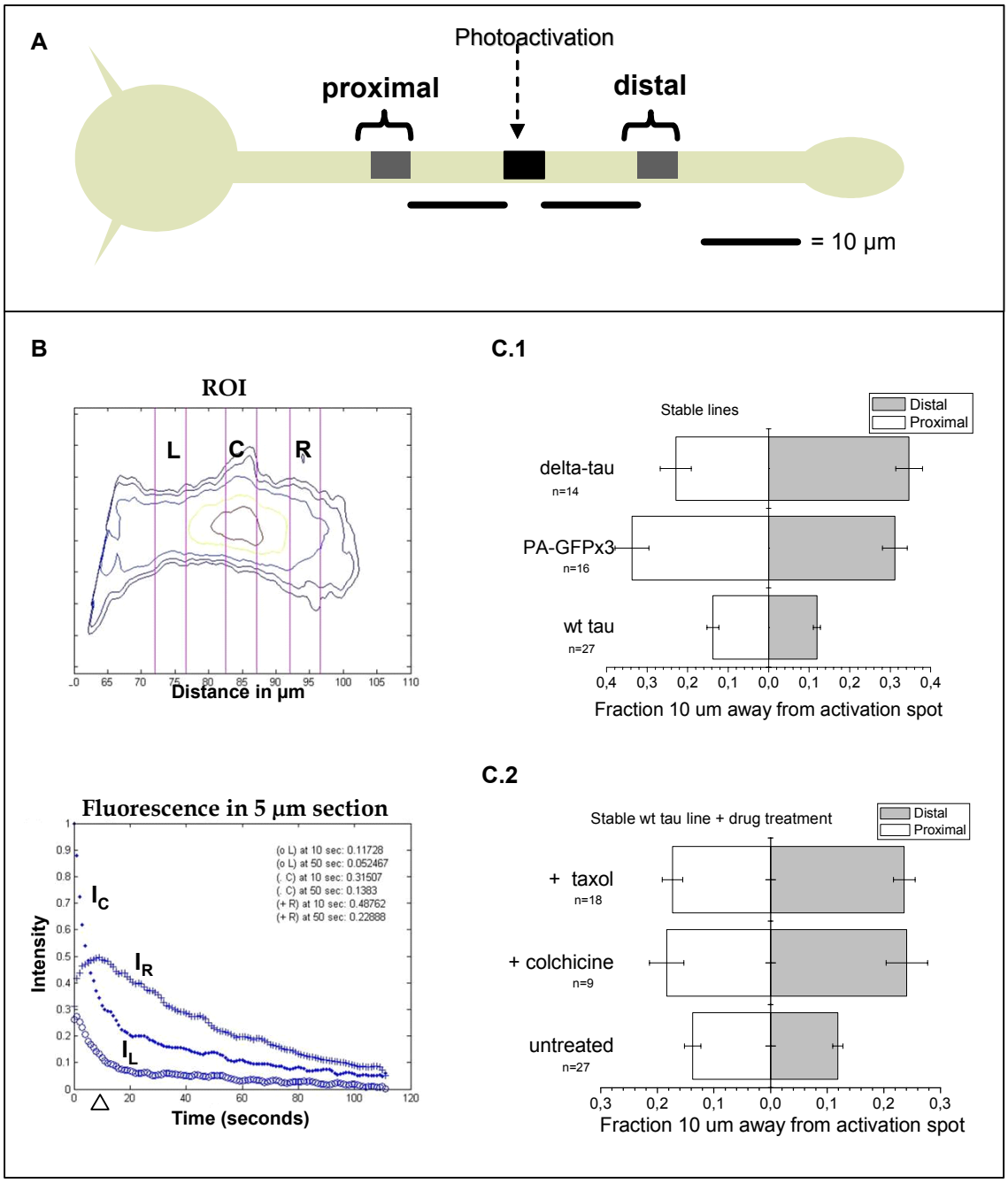

Fig. 3.31 Flux analysis. The scheme in A shows the 5 µm long sections analysed within a process.These regions lie 10 µm away from the activation spot (black box), towards the soma (grey box to the left), "proximal", and towards the tip (grey box to the right), "distal". In B a process of a delta-tau expressing cell is used as an example showing the central (C), left (L), and right (R) sections (above) where the intensity decay in time is analysed (below) at 10 s (arrow head). In this example, R corresponds to distal and L to proximal. In C, the fractions for different stable lines (C.1), and after drug treatments for

the wt tau expressing line (C.2) are shown; n: cell number.

For the stable lines, the wt tau expressing cells showed the lowest fractions (proximal and distal) compared to the delta and PA-GFPx3 expressing cells (**fig. 3.31 C.1; table 9.2**) as expected for the protein showing the lowest mobility. The distal fraction found in delta tau cells was three times higher than in wt-tau expressing cells, whereas the PA-GFPx3 cells showed 2.6 times higher values than wt tau cells. The proximal fraction detected for the PA-GFPx3 was the highest, 2.4 times that of wt tau cells, and 1.5 times that of delta tau cells. Drug treatment, disruption of microtubules or detachment of tau from microtubules on the wt tau line determined an increase in both fractions (**fig. 3.31 C.2**).

To compare the fractions within the processes, a distal/proximal ratio was calculated for the individual cells. This distal/proximal ratio for wt-tau cells approximated to 1, showing no favourable flux in either direction, the PA-GFPx3 showed 1.2 times more proteins moving to the distal than the proximal region, and the delta-tau protein showed a very prominent (more than twofold) distal enrichment (**fig. 3.32 A**).

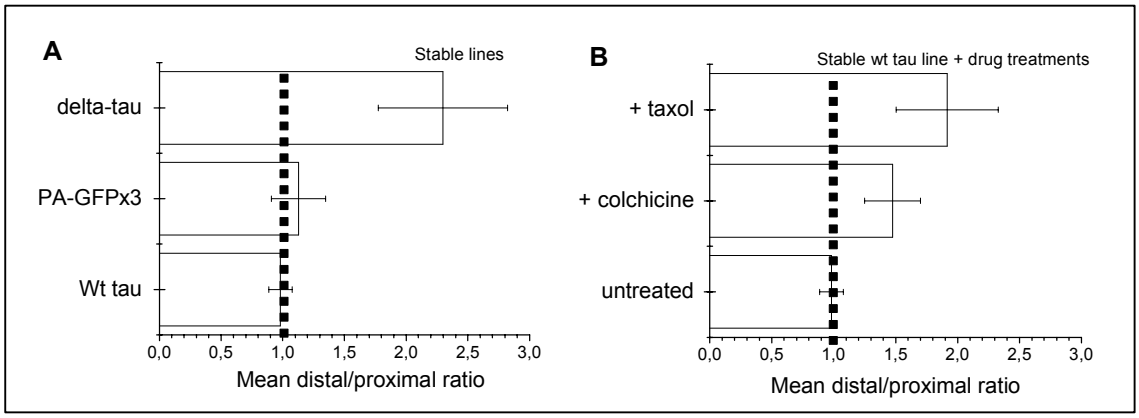

Fig. 3.32 Distal/proximal ratio in stable lines. The fluorescent fractions 10 µm away from the activation spot were analysed by dividing the intensity towards the tip (distal) by that present towards the cell body (proximal) for each individual cell after 10 seconds for the stable lines expressing delta-tau, triplet, or wt tau (A) and for the wt tau expressing cell under different conditions as described in (B). Discontinued line placed on fraction 1.0 to visualize a preferential distal (to the right), or proximal (to the left) flux. Note the prominent distal flux in the case of delta expressing cells and taxol wt-treated cells.

Colchicine and taxol treatment of wt expressing cells provoked a higher proportion of proteins moving to the distal rather than the proximal region (**fig. 3.32 B**). Colchicine treated cells showed 1.5 times higher distal than proximal protein fractions, whereas the

distal/proximal ratio reached a value of 2 in taxol treated wt tau cells. Thus, the "flux analysis" indicated that a fragment of tau lacking the MBR showed a predominant flux towards the tip. Neither the PA-GFPx3 nor the PA-GFP-tau wt revealed this flux.

In the case of wt tau expressing cells however such a flux was present once the interaction with microtubules was abolished.

This data was interpreted considering the structure of tau. The smaller fragment of tau and full tau proteins share the amino terminal fraction region. This projection domain has been suggested to give tau proteins a role as a mediator of microtubule-plasma membrane interactions (Brandt *et al.* 1995). In agreement, high resolution images showed an enrichment of the proteins including the amino-terminus region (wt and delta tau proteins) to the peripheral region of the cells after PA, but not for the PA-GFPx3 expressing cells (**fig. 3.33**).

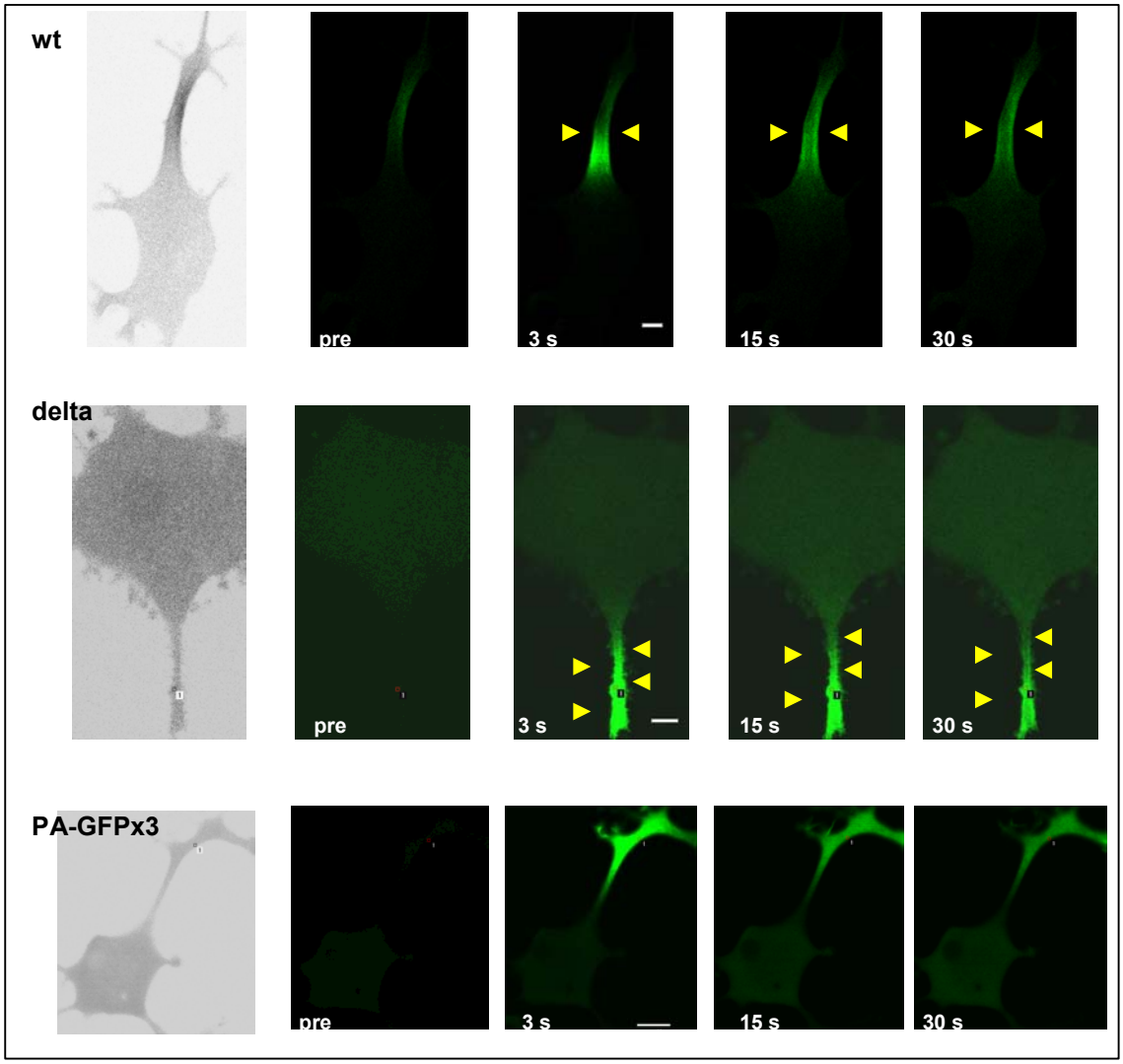

Fig. 3.33 Peripheral enrichment in cells evidenced by high resolution images. PA was performed at a 1024x1024 pixel resolution (every 3 s) to show the enrichment of wt (top) and delta-tau (middle) to the periphery of the cell (yellow arrow head). The signal remains

at this region (15s, 30s) for both, but not for the PA-GFPx3 (bottom) lacking the plasma membrane interaction domain. First picture, converted to grey scale and colours inverted to see cell contour. White bar, 10 µm.

The periphery of the cell is a region where the proteins are able to interact with the actin cortex underneath the plasma membrane.

The flux towards the distal region in delta tau expressing cells indicated that the presence of a plasma membrane interacting region might determine the distribution of delta tau proteins to the tip. In the case of the wt tau proteins, this flux was absent at normal conditions, but could be detected once the microtubule interaction was disrupted either by detaching tau from microtubules (taxol treatment) or by disrupting microtubules (colchicine treatment).

A weak association of wt tau proteins to the plasma membrane might require the disruption of the stronger tau-microtubule interaction to trigger distal flux localizing tau to the tip.

3.2.4 Kinetic modelling

To determine different parameters like diffusion coefficients, and flow velocities as well as association constants, a model that describes the experimental data has to be developed.

As a first approximation, a free diffusion model combined with photobleaching was tested to simulate the behaviour of the proteins. The model assumed free diffusion of molecules from the activation spot along an infinite tube. No restrictions throughout the tube were considered. The model aimed at solving Fick´s second law of diffusion and fit the experimental data. This procedure is still being performed in a collaborative approach with the Physics department of the University of Osnabrück by Dr. Reyher. The experimental data (the curves showing the intensity decay in time for the activated region) must be fitted with a program to show if the model is capable of describing the experimental data (**fig. 3.34**). If this were the case, the diffusion coefficient could be determined for the different proteins.

A final model should be able to determine the mechanism that underlies protein mobility along the processes measured (e.g., diffusion), and the effect of the interaction with cell components on this mechanism.

The lack of transport features in the plots (“IntDisTime”) obtained so far would suggest the absence of this mechanism.

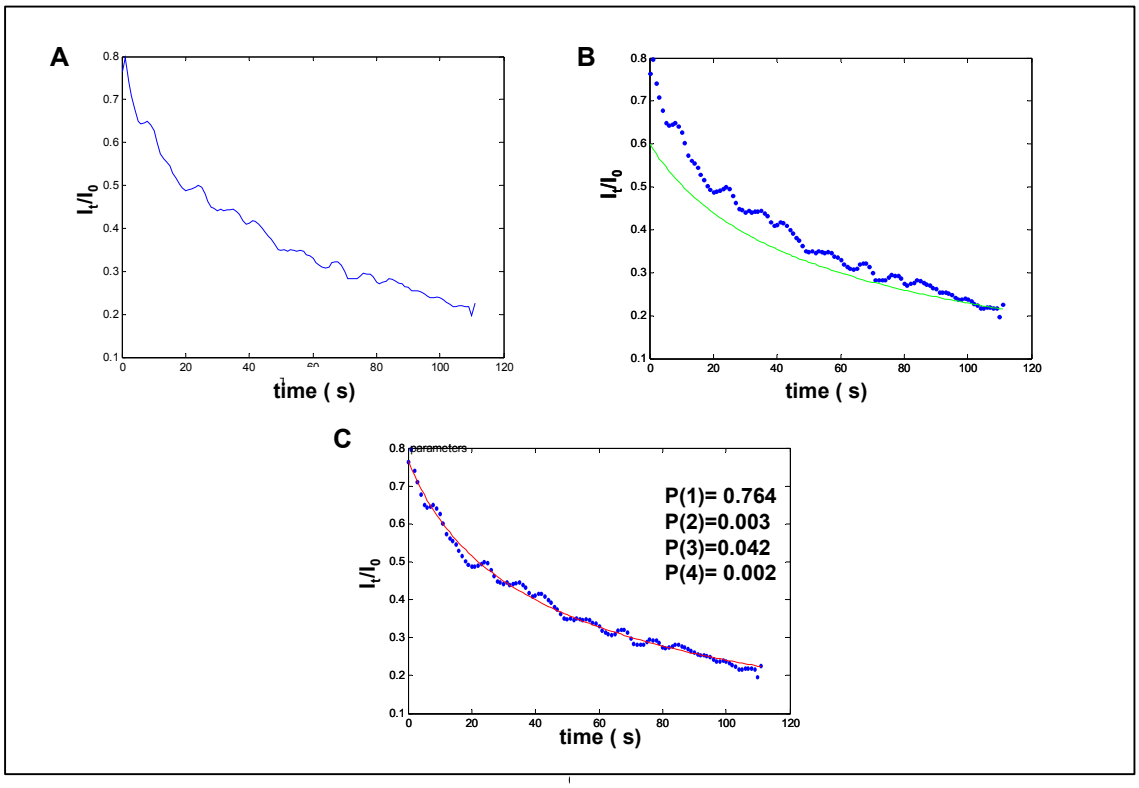

Fig. 3.34 Example of a model used to fit the experimental data. Decay plot obtained from a wt tau cell analysed yielding the fluorescent fraction in time at the region of photoactivation dotted curve in (A) which is used as data from which a simulation is performed as a continous curve (B) and finally this simulation fits the data (continous curve in (C) and the parameters could be obtained. In this case, P(1), start width; P(2), decay constant; P(3), D/2π; P(4), offset. This model is under development.

In addition, to ascertain that no energy-dependent mechanisms were present, experiments were performed after incubation of cells with an ATP-depleting drug, iodo acetic acid (IAA), a glycolitic inhibitor. PC12 cells treated with IAA showed ATP depletion (Toll and Howard 1979).

If energy-dependent mechanisms were present, they should be abolished by this treatment. PA-GFP- tau wt and delta tau transfected cells showed no difference in the immobile fractions measured after PA (**table 9.1**) confirming further the absence of ATP-dependent transport of the proteins.

Taken together, the pulse-escape photoactivation approach could determine different features of tau and tau interactions on its mobility in living cells.

3.3 Mobility of FTDP-17 tau (R406W) in living cells

Several mutations in the *tau* gene have been identified in cases of FTDP-17. One of these mutations, the tau-R406W (mut) leads to tau protein aggregates in the somato-dendritic compartment of neurons in a hyperphosphorylated state (**section 1.3.3**).

Studies on this mutant have shown controversial results regarding its phosphorylation and microtubule binding properties in different cell models (**section 1.3**). In turn, these properties could relate to an abnormal distribution of the protein within the cell.

To analyse the protein dynamics that could account for the misdistribution found in the disease, PA experiments of this mutant protein (mut) were performed in living PC 12 cells.

PA-GFP-tau mut plasmids (**fig. 3.1**) were generated from a flag vector (**section 2.1**) to prepare stable lines expressing the tagged-mutant protein (**fig. 3.6**).

The cells expressing the PA-GFP-tau mut revealed a filamentous distribution pattern (**fig. 3.35)** similar to that previously described for the PA-GFP- tau wt protein indicating that this protein localized to microtubules.

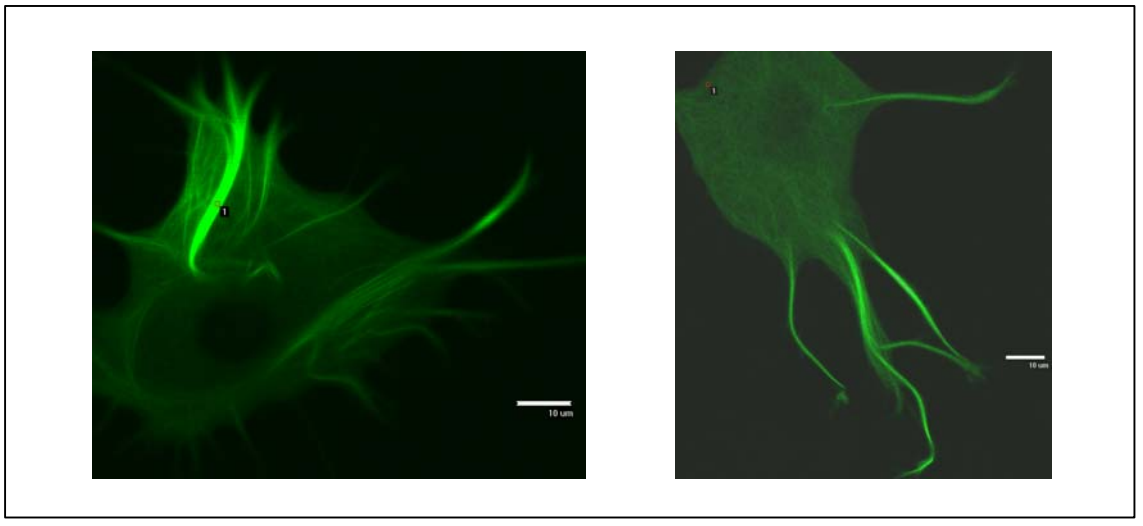

Fig. 3.35 Filamentous pattern of PA-GFP-tau mutant. **6 days NGF-differentiated PA-GFP-tau mut expressing PC12 cells were imaged after PA to show the filamentous pattern distribution of the PA-GFP-tau mut signal. Scale bar, 10 µm.**

The PA-GFP-tau mut proteins exhibited a decreased phosphorylation profile compared to wt expressed proteins in PC12 cells (**fig. 3.36 A,** Anne Hillje, bachelor work, 2006). This reproduced the characteristics found for flag-tau mut and wt proteins in the same cell system (Szofia Séboe-Lemke, unpublished results).

One of the sites displaying a decrease phosphorylation was the PHF-1 site that detects phosphorylated Ser396/Ser404 (**fig. 3.36 B, C**) in accordance to (Pérez *et al.* 2000).

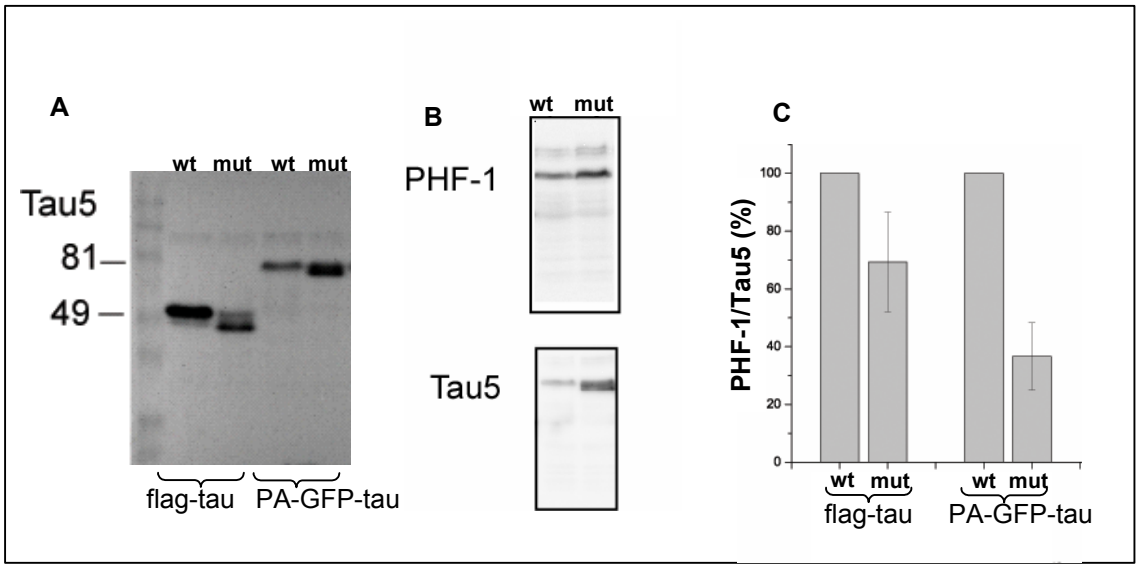

Fig. 3.36 Phosphorylation profile in mut tau expressing cells compared to wt tau cells. In (A), a difference in mobility is shown for WB bands of lysates from cell expressing mut-tau proteins compared to wt-tau proteins either tagged with the flag or PA-GFP epitope. (B) shows the bands of the PA-GFP-tau proteins detected with antibodies against phosphorylated S 396/404 (PHF-1) and total tau (Tau5) to quantify (in C) the amount of phosphorylated tau at the PHF-1 site related to the total tau present. The percentage of the tau wt was set as 100 %. Modified from Anna Hillje bachelor work 2006.

PA experiments in PA-GFP-tau mut expressing cells exhibited no distinguishable differences in "IntDisTime" plots or decay plots compared to experiments on wt protein (**fig 3.37**).

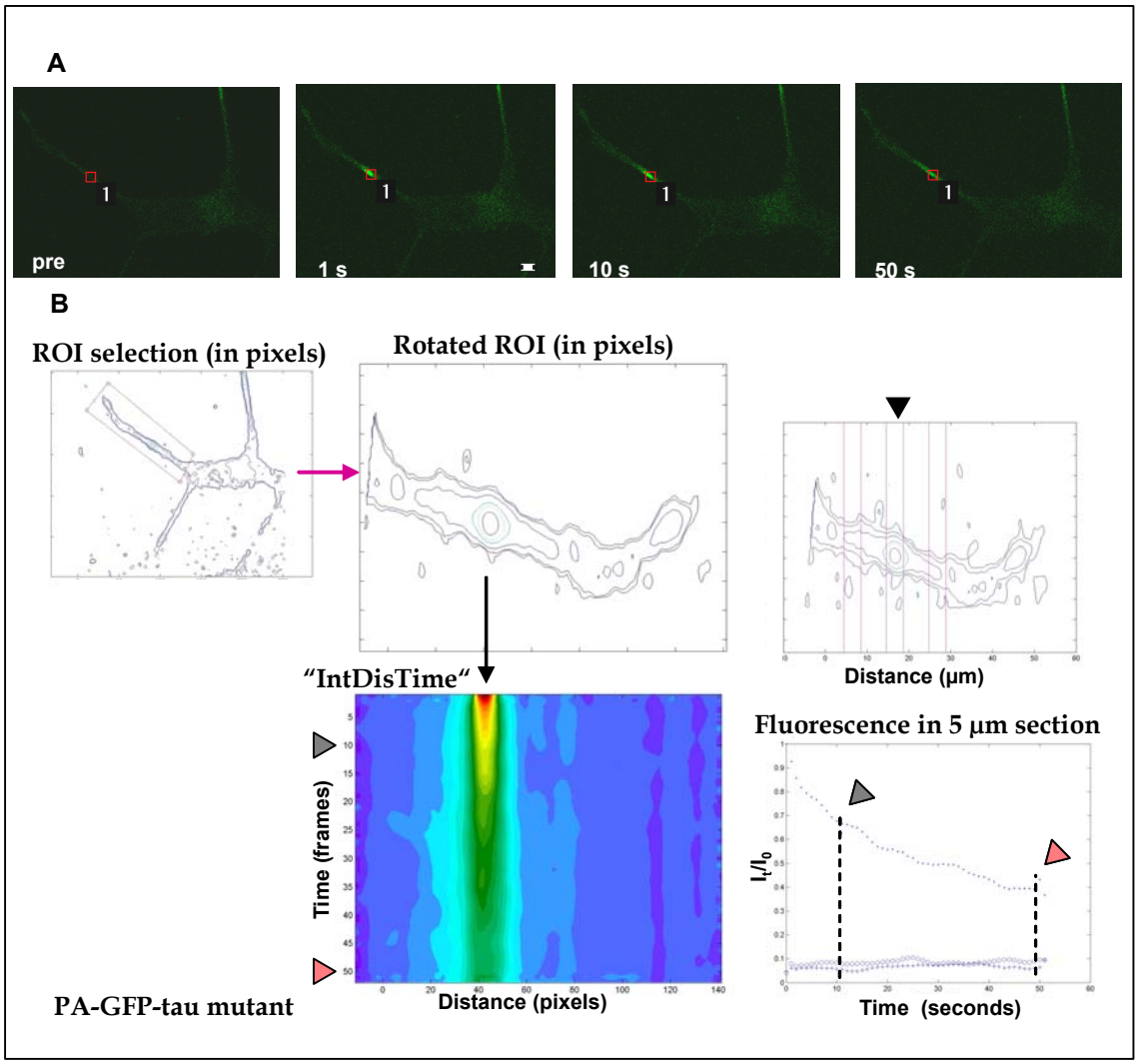

Fig. 3.37 Analysis of a photoactivated cell expressing PA-GFP-tau mut. In (A), frames after PA for a cell stably expressing the PA-GFP-tau mut protein are shown. The cell was analysed with "Intmotion" program (B). The contour of the cell and the process selected (pink box) are shown. In the middle, the "IntDisTime" plot shows the intensity decay (in colours) in time (y-axis) and distance (x-axis). Time points 10 (grey arrow head) and 50 (pink arrowhead) were selected as indicated in the different plots to show the IF marked in the decay curve for the central region (black arrow head, right panel, above).

Accordingly, no main differences in the IF could be found compared to the IF of PA-GFP-tau wt cells at middle portions either at 10 s or 50 s **(fig. 3.38, table 9.1**). A higher (1.3 to 2 times) protein retention at the tip than at middle portions was observed in this case similar to what was previously described for wt tau expressing cells. It is interesting to note however, that the IF at the tip was lower (14%) than the one measured for PA-GFP-tau wt expressing cells at 10 s (see below).

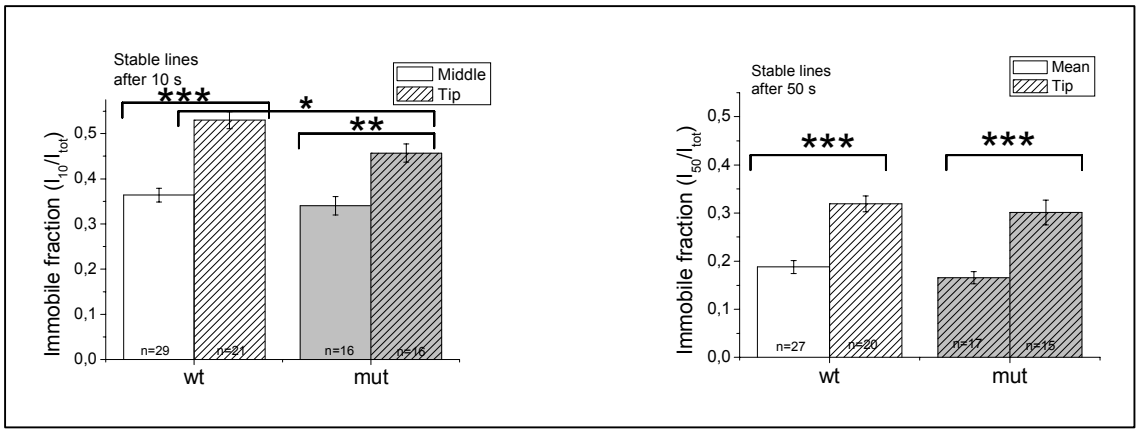

Fig. 3.38 Determination of IF for wt and mut tau expressing cells. Note the significant higher IF at the tip versus the middle for both proteins, but a slight significant higher IF at the tip for wt versus mut at 10s. Mean and SE are shown (table 9.1); cell number (n), given in bars. Comparisons between groups, based on one-way ANOVA test followed by posthoc Bonferroni test (* p< 0.05 ** p <0.01 *** p< 0.001).

To test whether differences in flux were present, the "flux analysis" (**section 3.2**) was performed. The analysis showed no favourable proximal or distal distribution similar to the wt tau analysed cells (**fig. 3.39**).

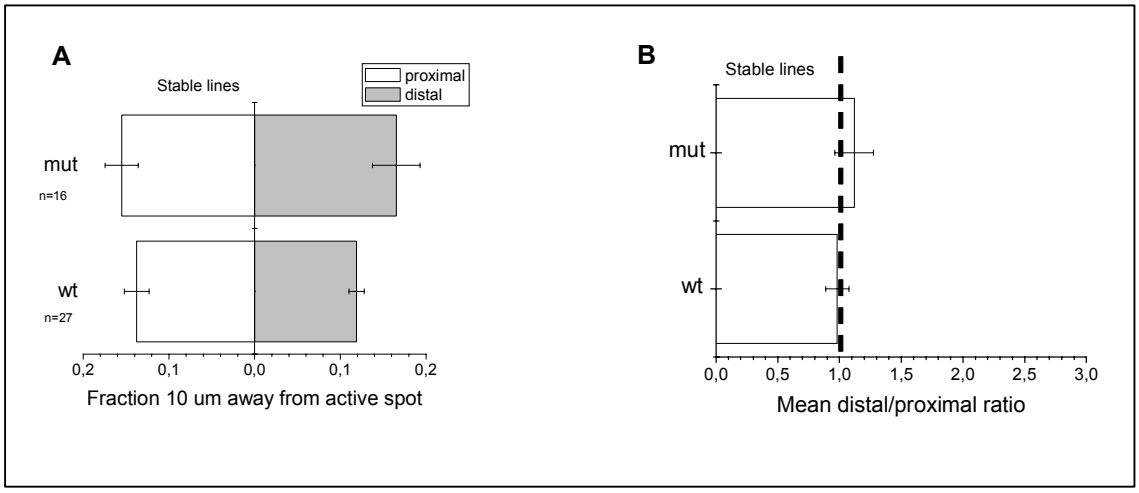

Fig. 3.39 Flux analysis for mut compared to wt. In A) distal and proximal fractions plotted; in B), the distal/proximal ratio. No major differences between constructs.

Thus the data indicated that mut expressing cells showed no main differences in the dynamic aspects analysed by this method so far. This suggested that the presence of the R406W mutation changed the phosphorylation profile of the protein, but its ability to bind to microtubules remained similar to that of wt tau. The curves obtained shall be fitted to determine whether a diffusion model is adequate to describe the experimental data on this protein.

Interestingly, during the analysis, differences in process development after NGF treatment for mut compared to the wt-tau expressing lines could be detected (**fig. 3.40**).

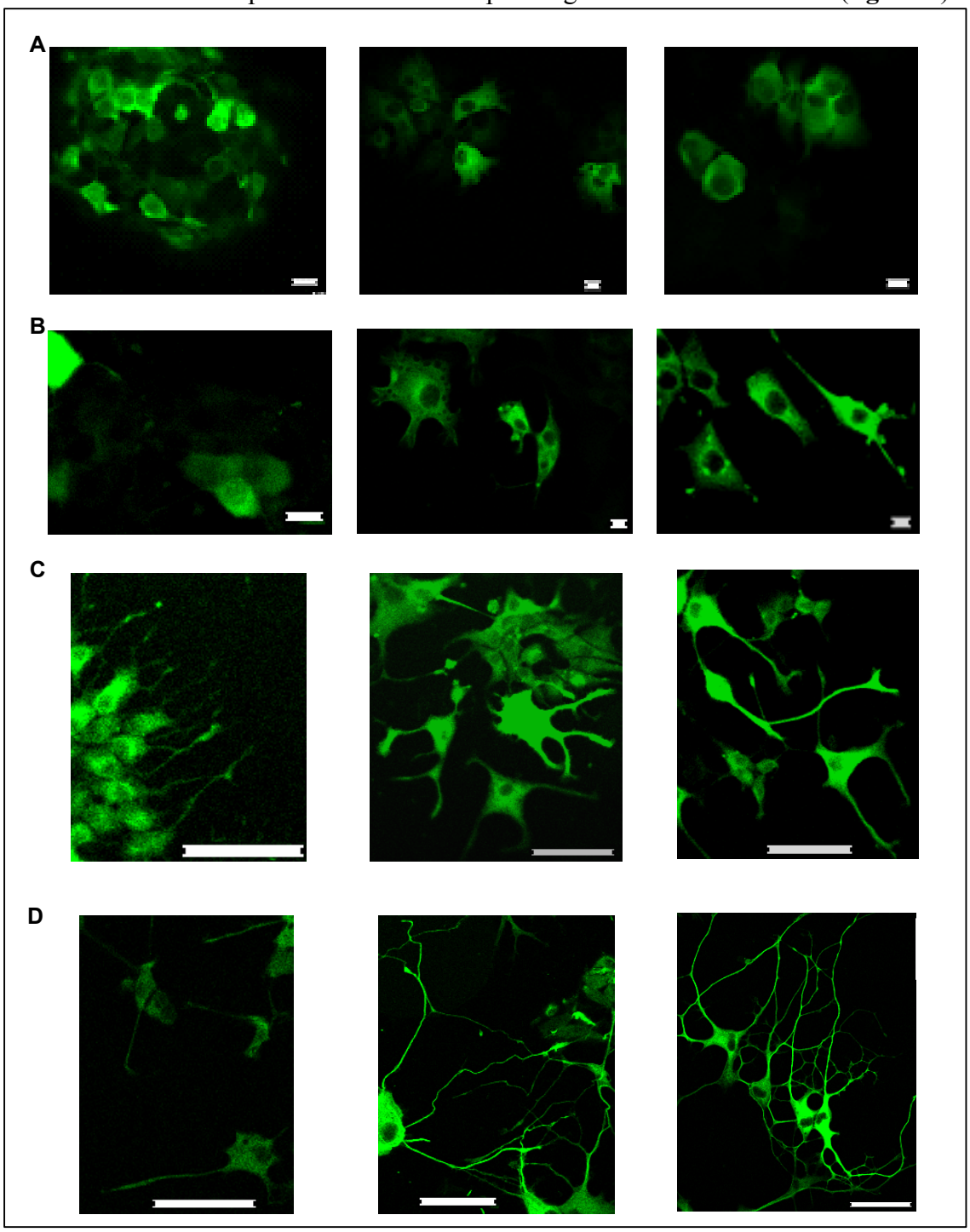

Fig. 3.40 NGF differentiation of stable lines. From left to right, PA-GFP-tau delta, PA-GFP-tau wt, PA-GFP-tau mut after no (A), 3 days (B), 6 days (C) and 10 days (D) of NGF differentiation. Cells were fixed (PFA) and stained against GFP (primary antibody) and Fitc (secondary antibody). Scale bar in A and B, 10 µm long, and C and D 50 µm long.

Mut tau lines developed process earlier than wt tau cells (3 days after NGF treatment) and the processes were longer than those from wt tau after 6 days of NGF

treatment. To obtain more information on process development, time time lapse microscopy of cells expressing eGFP-tau proteins is being performed. For that, process growth for individual cells that are re-located after different NGF time points is being analysed (**Sabine Zessin, master work, 2006, Natalyia Golovyashkina, master work 2007**).

Léger *et al* suggested the requirement of cortical actin disruption together with microtubule assembly for process development in PC12 cells (Léger *et al.* 1994).Therefore, the differences in process formation could relate to differences in association to the plasma membrane. In addition, fractionation analysis performed on flag-tau expressing cells showed that the plasma membrane interaction was absent in mut cells, but not in wt tau expressing cells (Szofia Séboe-Lemke, unpublished results).

To provide more evidence on the absence of plasma membrane interaction in cells expressing mut, high resolution images after photoactivation of regions near the plasma membrane were recorded. Enrichment of the tau mut protein in the plasma membrane could not be detected for the mut expressing cells as opposed (**fig. 3.41**) to wt and the delta expressing cells (**fig. 3.33**).

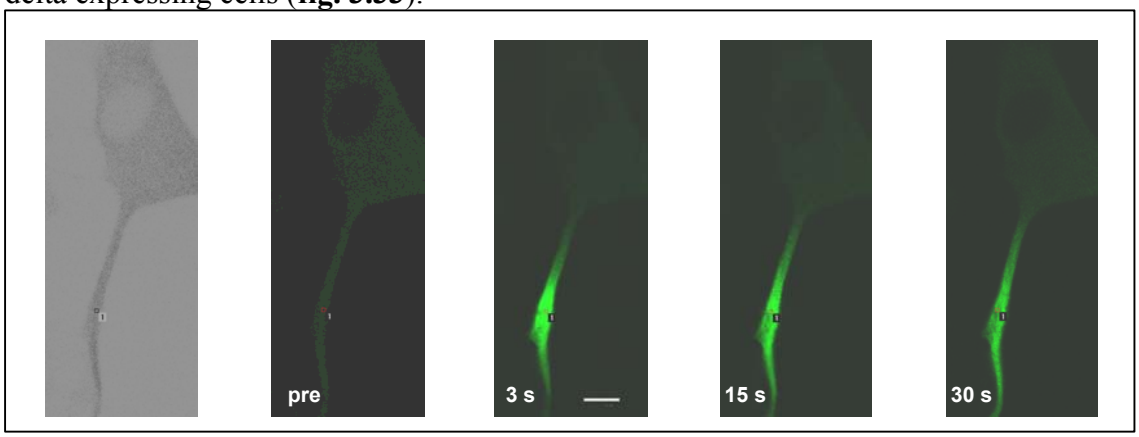

Fig. 3.41 High resolution images for PA-GFP-mut tau. Images taken after photoactivation at a high pixel resolution (1240x 1240) at a 3 s delay.

In addition, as mentioned before, the slight but significant difference (14%) between the IF at 10 s between the wt and lower mut tau value could be interpreted recalling that the tip is enriched in actin filaments that could therefore determine the increased retention of the wt protein interacting with this filament. Furthermore, preliminary data on taxol-treated PA-GFP-tau mut cells did not show an increase in distal flux in contrast to wt tau taxol-treated cells (data not shown).

Taken together the data suggests that the tau (R406W) mutant shows i) a different phosphorylation profile (hypophosphorylation), and a change of conformation due to

this different phosphorylation could have effects determining ii) the absence of interaction with the plasma membrane. Both effects combined could explain the different distribution of these proteins within the cell by a lower plasma membrane-associated flux.

3.4 Effect of AD like tau phosphorylation on mobility

AD is another disease in which the tau protein is involved. This tauopathy is characterised by hyperphosphorylation of tau proteins that become aggregated in the somato-dendritic compartment.

To test the effect of phosphorylation on protein dynamics, a construct mimicking the hyperphosphorylated state of tau in the disease, was analysed in living cells by the PA approach. The "PseudoHyperPhosphorylated" (PHP) tau was created by Eidenmüller *et al* by mutation of 10 S and T residues which are major phosphorylated sites found in AD to E to simulate the negative charge of the phosphate group (Eidenmüller *et al.* 2000). In vivo, PHP tau showed an increased toxicity in NT2N cells expressing this construct as compared to cells expressing the wt-tau construct (Fath *et al.* 2002). Moreover, in mouse hippocampal slices (Shahani *et al.* 2006) and in mouse primary cortical cultures (Leschik *et al.* 2007) the expression of the construct showed neurotoxic effects with the appearance of a ballooned phenotype associated to cell death.

To obtain quantitative data on the effect of disease-like phosphorylation, the PA approach was tested for PHP tau proteins. A fusion protein was prepared (**fig. 3.1**) to generate a cell line (**fig**. **3.6**).The PHP fusion protein in cells showed a filamentous pattern distribution consistent with a microtubule binding protein (**fig. 3.42**).

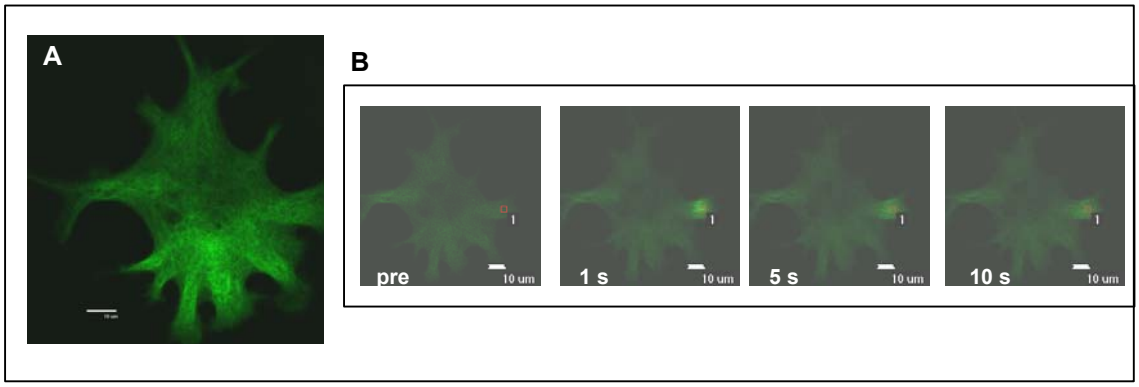

Fig.3.42 PA-GFP-PHP expressing cell after PA to show filamentous pattern of tau distribution. (A) shows a high resolution image 10 s after photoactivation at the cell body for a PC12 cell expressing the PHP fusion protein. In (B), a broad region of a process of cell A was photoactivated to show the indicated frames after photoactivation.

The analysis of the times series obtained after PA (**fig. 3.43**), revealed that PA-GFP-tau PHP expressing cells showed an IF reduced (20%) compared to PA-GFP-wt tau values after 10 s and 50 s (**fig. 3.44, table 9.1**).

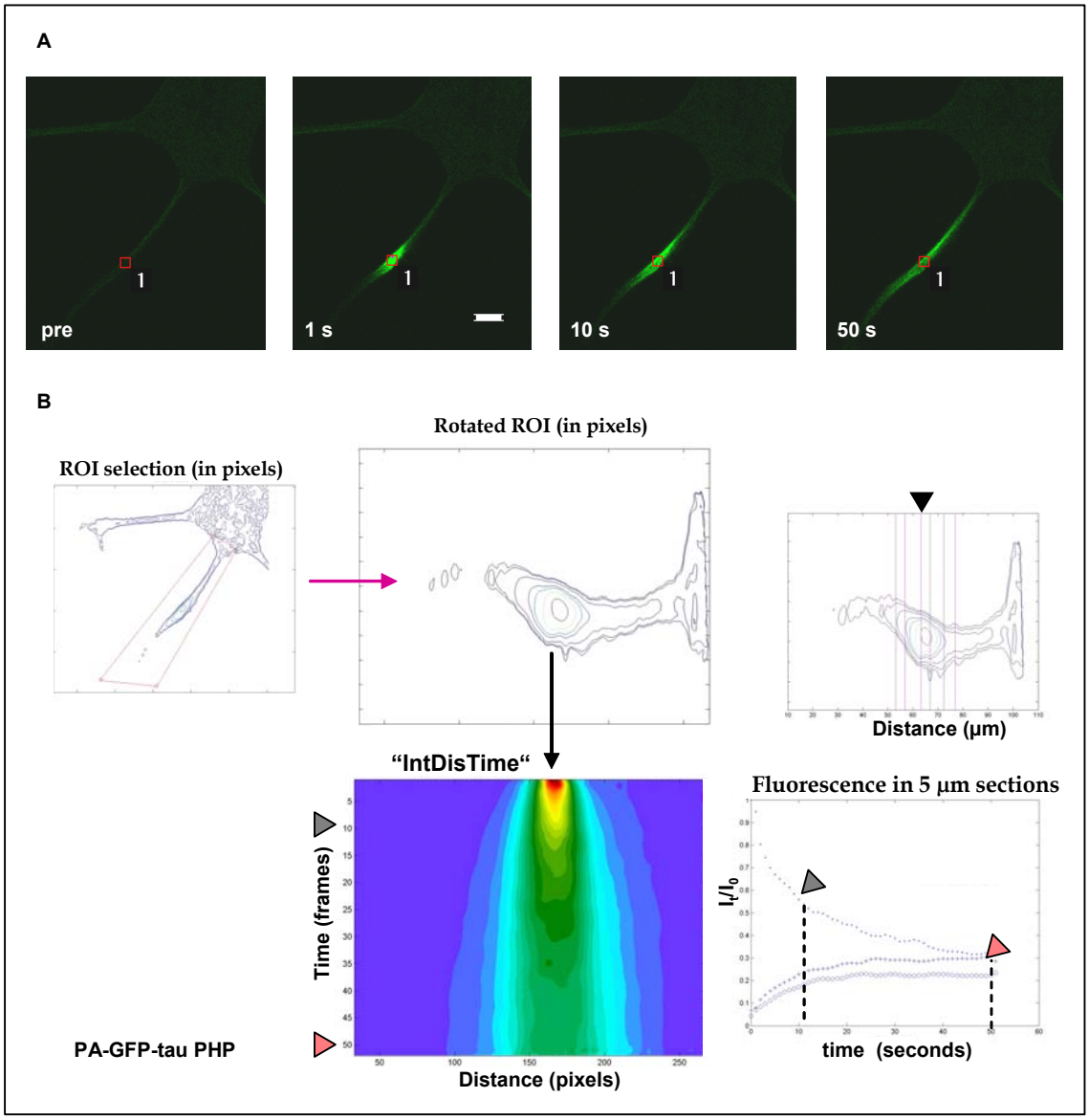

Fig. 3.43 Photoactivation experiments on a stable line expressing PA-GFP-tau PHP. In (A), individual images at different time points after PA for a cell stably expressing the PA-GFP-tau- PHP protein are shown. The cell was analysed with "IntMotion" program as shown in (B) yielding the contour of the cell with the photoactivated process selected for analysis. "IntDisTime" plot shows the intensity decay (in colours) in time (y-axis) and distance (x-axis). Time points 10 (grey arrow head) and 50 (pink arrowhead) marked to determine the IF present at the site of photoactivation (black arrow head) at these values on the decay curve.

At the tip, whereas the retention of PA-GFP-tau wt proteins increased in a 45% and 70% compared to the IF at the middle, PHP showed a lower increase (28%) at 10 and 50s.

To test whether the results were directly related to differences in phosphorylation as mimicked by the phosphorylation-like state of the PHP tau protein, the wild type protein was incubated with an inhibitor of phosphatases (okadaic acid, OA). OA increases the level of tau phosphorylation in PC12 cells (Maas *et al.* 2000).

Cells subjected to drug-dependent phosphorylation, increased their mobility as shown by a 30% and 50% reduction in IF values after 10 s and 50s (**fig. 3.50**). As a control, PHP-tau expressing cells were also subjected to okadaic acid (OA) treatment and showed a slight (10 to 15%) decrease compared to untreated cells which was not statistically significant. No difference could be detected between PHP- or wt- tau expressing cells subjected to OA.

This indicated that the sites mutated in the PHP-tau like the sites phosphorylated by OA are responsible for the increase in tau mobility.

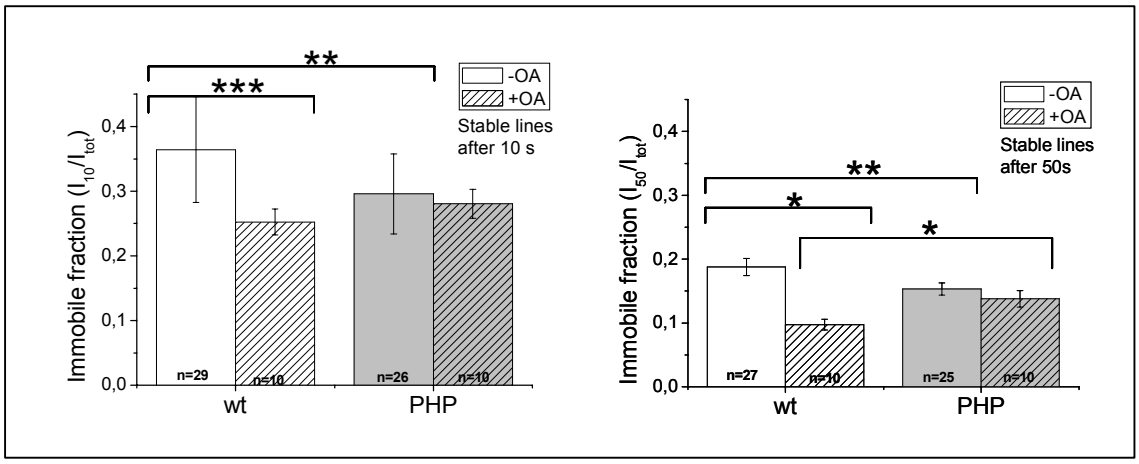

Fig. 3.50. Effect of OA in wt- and PHP-tau expressing cells. Note the decrease of IF after OA of cells for wt proteins similar to the low IF for PHP proteins. Mean and SE are shown (table 9.1, appendix). Cell numbers (n) are given in the bars). Comparisons between groups were based on one-way ANOVA test followed by posthoc Bonferroni tests (* p< 0.05; ** p <0.01; *** p< 0.001).

PHP showed a decrease binding to microtubule in *in-vitro* experiments (Maas *et al.* 2000). The phosphorylations of specific sites on tau wt are known to decrease the affinity of tau for microtubules (Brandt and Leschik 2004). Thus, an increase in free protein through phosphorylation would explain the higher amount of diffusible protein and lower IF in living cells. Interestingly, the lower IF for PHP compared to wt (20%)

was the same at 10 and 50s which was not the case for OA-treated wt tau cells. This could suggest that other phosphorylatable sites on wt could have different effects as detected at later time points of analysis.

To test for a differential distal or proximal protein distribution, the "flux analysis" (**section 3.2.3**) was undertaken.

The analysis revealed a higher fraction of proteins in both directions for PHP-tau cells with or without OA treatment and for OA-treated tau wt expressing cells compared to untreated cells, as expected for the increased mobility observed (**table 9.2, fig. 3.45 A**).

The distal/proximal ratio was calculated (**table 9.3**). No major difference could be detected to the 1.0 position similar to wt-tau expressing cells ananlysed (**fig. 3.51, B**).

Thus, contrary to taxol treatment (**section 3.2.1**), an increase in a tau unbound pool through OA treatment did not lead to a distal flux.

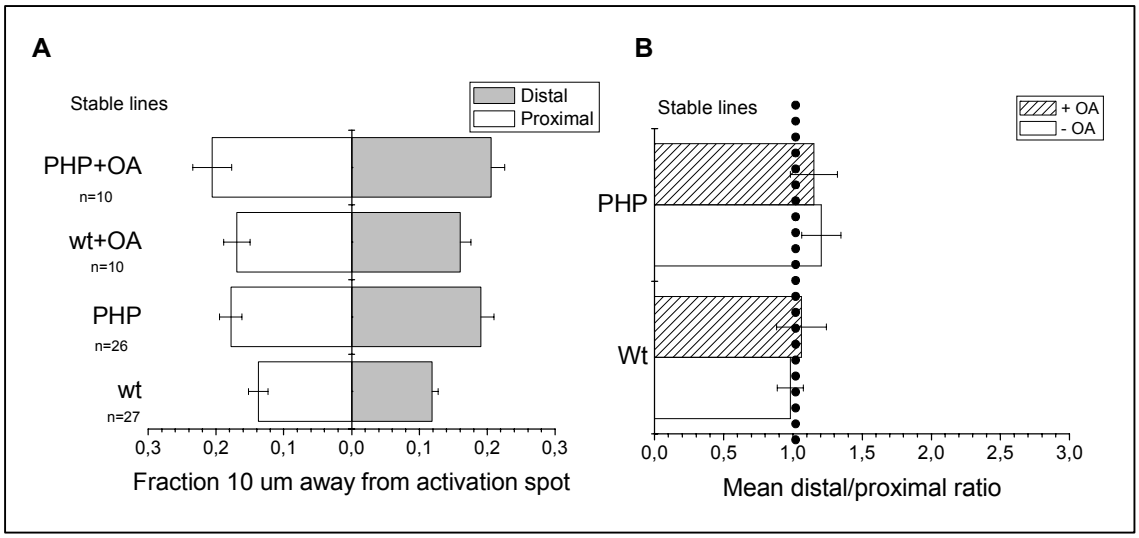

Fig. 3.45 Effect of OA in protein flux for the wt-tau and PHP-tau expressing cells. (A) Protein fraction measured 10 µm away from the activation spot towards tip ("distal") or towards soma ("proximal"). In (B), the ratio fraction tip/fraction soma was calculated for each cell and the mean plotted. The distal and proximal fraction increase in each condition as compared to wt, however, the distal/proximal ratio shows no major differences. Cell number (n) is given in the plot.

Next, another disease-relevant condition was investigated. In AD, tau aggregation is joined by formation of extracellular Aβ aggregates. The relation between Aβ and tau is still under investigation. Nevertheless, incubation of PC12 with Aβ has been reported to increase the phosphorylation of tau (Leschik *et al.* 2007).

Aβ effect on protein dynamics was studied by PA experiments of wt tau expressing cells after incubation with pre-aggregated Aβ. The results (**fig. 3.46**) indicated that the mobility of tau increased (20%) after the treatment. This difference was not present however 50 s after PA.

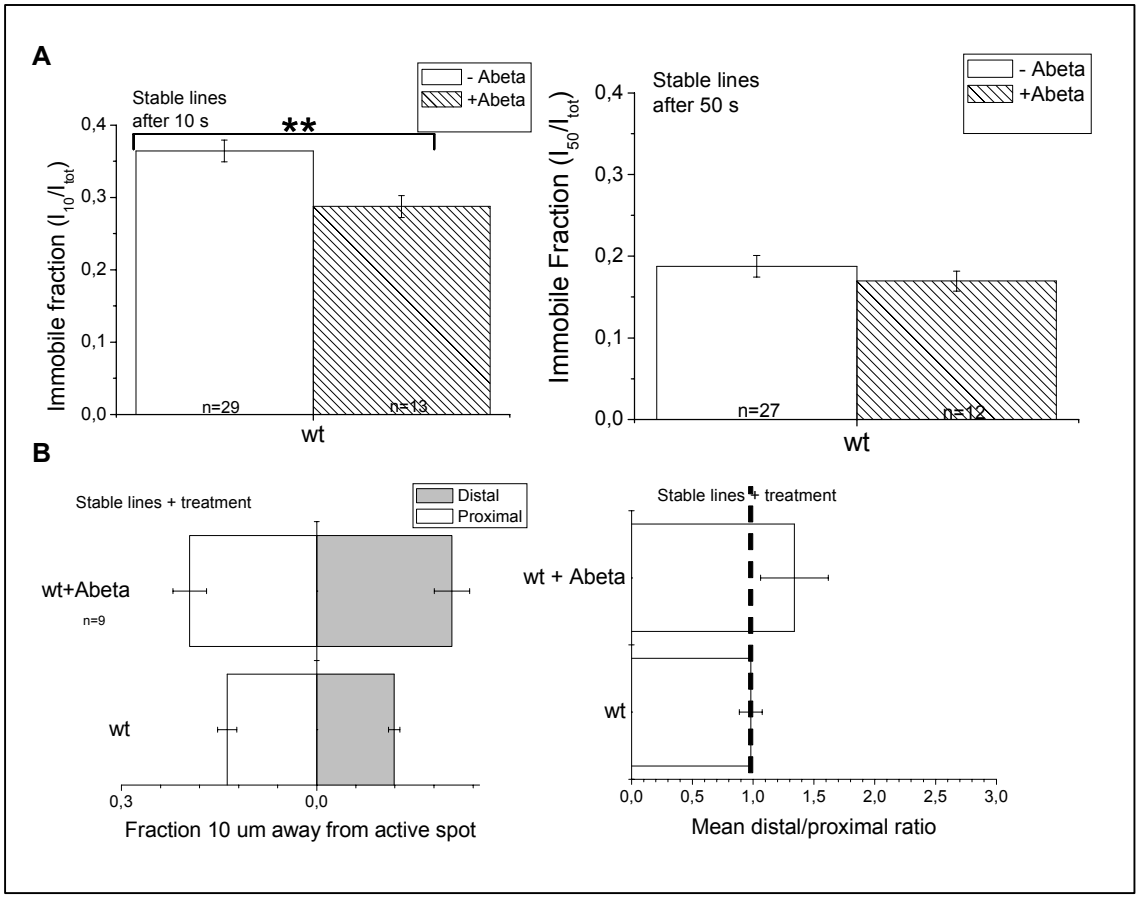

Fig. 3.46 Effects of Aβ on tau mobility. (A) Analysis of the mobile fractions for the wt untreated and Aβ treated cells after 10 s (left) and 50 s (right) Mean and SE are shown (table 9.1, appendix). Comparisons between groups were based on two sample paired t-test (* p< 0.05; ** p<0.01; *** p< 0.001). (B) Flux analysis for the same cells showing the different distal and proximal fraction (left) and its ratio (right). Note the increase of fractions and fraction ratio for Aβ treatment. Cell number (n) is given in the figures.

Therefore, phosphorylation of sites Aβ-related would contribute to increase of tau mobility. The flux analysis in this case, similar to OA-treated cells did not show the effects seen for taxol- wt-treated cells or delta expressing cells.

To quantify the different effects of phosphorylation-related mechanisms, the intensity decay curves will be fitted to a model as explained in **section 3.2.4**. The lower binding to microtubules could translate in a lower diffusion coefficients (D) compared to the D for wt-tau expressing cells. This could provide a tool to determine the

free/bound ratio of tau proteins according to equations derived by Sprague *et al* from protein D values (Sprague, Pego et al. 2004). This shall provide more data on phosphorylation effects.

Regarding the flux analysis, the idea that the plasma membrane association might contribute to the distribution of wt tau proteins towards the tip was reinforced.

Similar to the data on mut expressing cells, fractionation experiments on cells expressing a PHP tau protein revealed a loss of plasma membrane interaction (Maas *et al.* 2000). Accordingly, the IF would not only determine an increase in the levels of unbound protein, but in addition, these free proteins would be less able to interact with the plasma membrane. This would also be the case in the analysed OA-or Aβ- induced phosphorylated wt as well as mut (**section 3.3**) proteins. In all these cases, no preferential flux was observed. Furthermore, PA experiments of taxol-treated PHP or mut tau expressing cells showed no difference in flux analysis as compared to untreated cells (not shown). In contrast, tau delta and wt expressing cells -once microtubule interactions were disrupted-, showed a preferential distal flux (**section 3.2.3**), and both proteins include the amino terminal projection domain reported to provide an association to the plasma membrane (**section 1.3.1**).

4. Discussion

4.1 Pulse-escape fluorescence photoactivation experiments to study tau mobility in living cells

The aim of this work was to study tau protein dynamics in cells and determine quantitative changes in tau´s intracellular interactions at normal and disease-relevant conditions. For this purpose, different tau sequences, wild type and disease- (AD and FTDP-17) related tau sequences were fused to a photoactivatable (PA-GFP) sequence (**fig. 3.1**). The different proteins were chosen to identify the mechanism related to protein distribution found in tauopathies where the normal axonal-enriched tau is localized in aggregates in the somato-dendritic compartment in a hyperphosphorylated form (Weissmann and Brandt 2007).

The technique used for this goal had to allow cells to be analysed in a living environment. Approaches commonly used to analyse protein dynamics in living cells are fluorescence time lapse microscopy, fluorescent recovery after photobleaching (FRAP) and the recently developed photoactivation approach (PA).

Fluorescent time lapse microscopy gives information of protein distribution over time, but it is not well suited to determine parameters such as mobile fractions, diffusion coefficients or protein binding since it does not permit to follow a distinct subpopulation of proteins (Lippincott-Schwartz *et al.* 2003). Nevertheless, this technique can be combined with tracking approaches to determine the trajectories of a set of particles. In this work, though, the proteins analysed were not detected as such structures.

FRAP experiments permit the determination of protein dynamic parameters, however it presented a number of disadvantages for this work. The photobleaching event in FRAP requires high energy, and can thus harm the analysed cells. In addition, the time required for the bleaching event can be detrimental to the kinetic measurement, especially when measuring a fast process. Moreover, an inherent problem of this technique is that newly synthesized molecules cannot be distinguished from other molecules present. To circumvent these problems, the method used in this work was the photoactivation (PA) approach. This method has the advantage of requiring a short time for the PA event (less than 1 s) to photoactivate a subpopulation of proteins. PA allows following movement of structures on a time scale of seconds or minutes. In addition, it has the great advantage of permitting the tracking of labelled structures that remain in the activated region (Trivedi *et al.* 2007). This idea was emphasized in this work, using

the word "immobile fraction" (IF) that quantified the protein fraction retained at the site of PA at different time points (10 and 50 s). The IF gave a simple method to compare protein behaviours in similar environments (cell processes) without the need of further modelling. Thus, cell-component interaction was determined through changes in the protein recorded IFs.

This approach showed that the mobility of a small tau fragment (delta) lacking the microtubule binding region (MBR) in middle and tips of processes was highly increased compared to that of the wt tau protein (**fig. 3.21**, **table 9.1**). To determine whether size or the domains were responsible for the difference, an unrelated control protein similar to the size of wt tau was prepared (**fig 3.4**). The PA-GFPx3 (made up of 3 PA-GFP molecules in tandem) showed a similar IF to delta (**fig. 3.24**) favouring the idea of MBR contribution in protein retention. Indeed, disruption of microtubules (colchicine) and detachment of tau from microtubules (taxol) confirmed the involvement of microtubule interaction on protein retention (**section 3.2.1**). In addition, interaction with actin filaments was shown to strongly affect protein mobility, since disruption of actin filaments (Cytochalasin B) also decreased protein mobility at the actin-enriched tip compartment (**section 3.2.2**).

Moreover, PA permitted to follow directly the selected (photoactivated) population of molecules and give information on the destiny of these molecules such as a compartment accumulation and differential distribution estimated by a "flux analysis" (**section 3.2.3**). In fact, all proteins were found to be highly retained at the tip of the process (see **4.4**).

A flux analysis -as a tool to determine preferential protein distribution in an anterograde or retrograde direction-, revealed that tau proteins were subjected to a distal (anterograde) flux. This flux however, could only be detected once microtubule interactions were disrupted (delta-expressing cells or microtubule-disrupted tau wt cells). This flux was not visualized for disease-related tau proteins that could not interact with the plasma membrane even though microtubule interaction was reduced (PHP or phosphorylated wt, **section 3.4**).Thus, the data indicated that the plasma membrane interaction could contribute to tau normal distribution. These features could not have been assessed by photobleaching techniques where the "label" is lost as bleached regions "recover", preventing tracking of bleached molecules.

In addition, more information shall be obtained from the fluorescence intensity decay curves. For this, further modelling (in progress) is required (**section 3.2.4**). The

elaboration of a model can help reveal the mechanism responsible for protein mobility. Preliminary analysis suggests that tau proteins are subjected to free diffusion mechanisms. This will characterize protein dynamics by determination of D values for the different proteins and conditions analysed and give information such as the free/bound protein ratio (Sprague *et al.* 2004).

Taken together PA of tau molecules demonstrated the possibility of quantifying protein interactions in living cells and relating changes in mobility to disease-related conditions, as a new tool to elucidate disease mechanisms.

4.2 Influence of protein structure on mobility

In this work, factors affecting protein mobility such as protein size and interactions with other molecules, binding to a matrix that might slow or immobilize a protein and hinder free diffusion (Lippincott-Schwartz *et al.* 2001), were analised. However, the effect of protein shape differences has not been considered separately.

According to Einstein equation, diffusion (D) and particle movement are linked:

(1) $$D = \frac{k_B T}{f}$$

D: diffusion constant
kB: Boltzmann constant
T: Absolute temperature in °Kelvin
f: frictional coefficient

In the case of globular proteins undergoing diffusion, the shape of the protein is related to its diffusion coefficient by Stokes law (2) where the frictional coefficient (f_0) takes the hydrodynamic radius of the protein into account.

(2) $$f_0 = 6.\pi.\eta.R$$

η: viscosity index of the media analysed
R: hydrodynamic radius of globular molecule in motion

But, an *effective* frictional coefficient (f) must be calculated when the shape of the protein differs from the spherical assumption. The effective frictional coefficient for non-spherical molecules is in general larger than that of a spherical molecule of the same volume because there is a larger surface in contact with solvent which increases the hydrodynamic drag. f can be calculated by determining the radius of a spherical particle that has a volume equal to the volume of the non-spherical protein and multiplying this by a shape correction factor (F or "Perrin" factor=f/f_0) that determines how far from the spherical assumption the non-spherical shape is.

Therefore, when comparing the mobility of proteins, "shape effects" should also be taken into account in their contribution to mobility if the shapes of the proteins compared should differ. Thus, a correct determination of protein shape is important to estimate its effect on protein mobility. In the case of tau, this might seem quite problematic as it has been described as an "intrinsically disordered protein" (IDP), (Skrabana, Sevcik et al. 2006) lacking defined globular domains. IDPs, in contrast to globular proteins, contain a high proportion of polar and charged amino acids in their sequence, which results in the absence of a well-defined three-dimensional structure.Although the exact structure of the tau protein has not been completely revealed, the shape exhibited by normal tau proteins is far from being globular. Thus, when comparing a free diffusing molecule (PA-GFPx3) with a wild type tau molecule (wt), apart from the evidenced interactions observed i.e., with microtubules, it should not be ignored that the former might be nearer to a globular assumption than the latter.

Initially, tau was described using a prolate ellipsoid model (Cleveland, Hwo et al. 1977) which would yield a correction factor for shape (F) of 2. This correction would determine a D value which would be half of that calculated for a globular protein (equation 1). Therefore, this factor would contribute to lowering wt tau mobility as well.

Additionally, as described throughout this work, tau proteins are subjected to phosphorylation events. Phosphorylated tau showed upward shifts of bands in SDS gels. This mobility shifts were abolished in the presence of urea indicating that they resulted from conformational changes that produced unfolded and SDS-resistant domains in tau proteins (Eidenmüller *et al.* 2000). Circular dichroism studies on tau conformation distinguished specific secondary structure elements suggesting that the normal tau protein might exhibit a "tadpole" shape whereas the hyperphosphorylated tau, at certain conditions would undergo structural changes transforming the C-terminal part of the protein into the molten globule-like state (Uversky, Winter et al. 1998). Eidenmüller *et al* detected conformational changes in the PHP model of AD-like phosphorylation similar to those found in a tau protein subjected to phosphorylation. In this case, a decrease in β-sheet content and an increase in β-turns were detected after phosphorylation as well as in the PHP model (Eidenmüller *et al.* 2000). Thus, phosphorylation of tau proteins changes protein shape. Depending on the degree of asymmetry of the new conformation, this would have an impact on the F which would vary D values.

A study by Salamat-Miller *et al* reported that the shape of proteins as a consequence of their secondary structure affected D values. Using proteins modelling a random coil (RC), an α-helix and a β-sheet structure, they found F values of 1.22, 1.55, 2.38 respectively which were directly related to these changes in shape (Salamat-Miller, Chittchang et al. 2002). In fact, the D value of the RC was double as much that of the β-sheet. Thus, the different conformations exhibited by hyperphosphorylated tau or the PHP-model should affect the D and IF values. In addition, tau wt undergoes phosphorylation to some degree in a cell environment; this degree depends on the cell model analysed. Accordingly, the shape of the protein in each environment would vary and the mobility and D values would change as well.

Phosphorylation and conformational-related effects could also play a role in FTDP-17 R406W tau mutant (mut). In this work, slight changes in mut mobility (only at the tip of processes) and in the flux after drug treatment were observed (**section 3.3**). As discussed, the mut showed a hypophosphorylation profile in agreement with other studies. In fact, Connel *et al* described the same phosphorylation changes of the mutant *in vitro* and *in vivo* and demonstrated related long-range conformational changes (Connell, Gibb et al. 2001). Thus, perhaps, a variation in shape should also be considered in the mild different mobility observed.

In the light of these facts and given the lack of information on the exact protein shape, it would be interesting to establish a model to estimate the effects on mobility. For this, differently-shaped free diffusing proteins could be assayed to determine the IF in a cellular context.

4.3 Diffusion versus transport as a mechanism of protein sorting in neurons.

Several studies on tau mobility were interpreted in a way that tau proteins are transported by the so called slow axonal transport (**section 1.4**). As discussed in section **3.1**, considering the different values obtained for slow or fast axonal transport (**table 4.1**) it should be possible to visualize transport mechanisms if present by the PA approach used in this work. This would have been detected as a shift of the intensity peak in an anterograde or retrograde direction which was not the case. Moreover, experiments aimed at lowering the energy to abolish transport mechanisms (IAA experiments, **table 9.1**), showed no increase in protein retention as would be expected in the case that energy-dependent mechanisms were involved. As a matter of fact, the

analysis of protein transport gained a different perspective recently. As radioactive methods were replaced by fluorescent techniques, protein mobility could be measured more rapidly. The new data indicated that protein mobility was more rapid than previously assumed. Slow transport was reinterpreted in the analysis of different structures, such as neurofilaments, as a mechanism of fast transport made up of pauses and forward and backward movements which explained the previously slow overall rates measured (Trivedi *et al.* 2007) (Wang, Ho et al. 2000). In this line, a report by *Utton et al* reported that this would also apply to tau proteins (Utton *et al.* 2005). In this study, special considerations regarding the fluorescence intensity of tau structures were made arguing that only if particulate structures were visualized could transport be detected. In the present work, no such structures could be detected, neither when the intensity was high, nor when the intensity was fading. In addition, transient transfection were protein expression levels were increased, did also not show these particles. Nevertheless, this type of structure was visualized in PA experiments of other proteins when aggregation could be ascertained (not shown). What type of particles described by *Utton et al* are and the level of expression achieved in their work might be worth considering for further investigation.

Table 4.1 Reported tau values for slow (continous line) or fast (discontinous line) axonal transport

Speed	Method	Reference
0.2-0.4 mm/d (low and high molecular weight tau fractions)	Radiolabeled tau- injected in mice retinal ganglion cells, immunoprecipitated and western blot of segments.	(Mercken *et al.* 1995)
2.3 mm/d	Biotinylated tau microinjected into mature spinal cord neurons in culture	(Hirokawa *et al.* 1996)
1.7 mm/d (1% Triton soluble) **3 mm/d** (1% Triton insoluble)	Radiolabeled tau in motor fibers of rat spinal cord. Detergent separation and western blot	(Tashiro *et al.* 1996)
0.6-0.8 mm/d (hWT) **0.3 mm/d** (R406W)	Radiolabeled tau in ventral roots of transgenic mice	(Zhang *et al.* 2004)
0.927-1.192mm/d different tau isoforms and R406W mutations)	eGFP-tau transfected in cortical neurons and fixed at different time points	(Utton *et al.* 2002)
31.4 mm/d	Time lapse microscopy of eGFP-tau transfected in cortical neurons.	(Utton *et al.* 2005)

In fact, the presence of transport mechanisms might be of great importance for some proteins required at the end of long axons in neurons. However, this might not be the case for tau proteins if diffusion is enough to "push" the proteins along the axon. A requisite for diffusion to take place is the presence of an initial gradient. As previously mentioned (**section 1.7**), a tau gradient might be created by the segregation of tau mRNA towards the proximal axon (Litman *et al.* 1993). In agreement, Konzack *et al*, described a diffusion model responsible for tau movement along short processes (Konzack *et al.* 2007).

All these facts combined could explain the normal distribution of tau proteins with diffusion mechanism playing a role, at least in some short processes, without the need for energy-dependent mechanism. However, a model (in progress) considering the experimental data, should give a hint on the mechanism underlying tau mobility.

4.4 General effect of protein distal accumulation

An interesting finding in this work was the high protein fractions retained at the tip of the process. Regardless of the construct under analysis, this fraction resulted always higher compared to the fraction retained at the middle of the process. The increased distal retention could be evidenced already before 10 s.

Are the proteins trapped in this distal compartment or is it just an effect of diffusion mechanisms which are restricted to one side of the process (tip)? And if the tip acted as a trap, by which mechanism would it play such a role?

Compartments within the cell functioning as a trap have been described in the literature. An example of trapping mechanism was described by Schmierer *et al*. In their study, the kinetics of Smad proteins and their nucleocytoplasmic shuttling was analysed by FRAP and photoactivation techniques (Schimerer and Hill 2005). They reported a selective nuclear trapping of phosphorylated proteins. Proteins shuttled to the nucleus became trapped there by phosphorylation. Phosphorylated proteins showed a decreased nuclear-cytoplasmic export rate compared to the unphosphorylated ones.

In fact, phosphorylation gradients along the axons for tau have been described with tau phosphorylated more concentrated at the proximal axon (**see 4.5**).The mechanism responsible for these gradients has not been established. A similar gradient has not been reported for either kinases or phosphatases, but instead, kinase and phosphatase regulatory proteins or second messengers have been detected in gradients (Mandell and

Banker 1996). In this case, less phosphorylated forms would be retained more at the tip. However, the mobility of wt compared to PHP or mut proteins was lower at the tip (**section 3.4**) arguing against this hypothesis.

Another mechanism explaining the different protein retention would be to consider the tip as a special compartment. In fact, in this part of the process, the cytoskeleton is made up of actin filaments in higher proportion than microtubules (**section 3.2.2**). Microtubules at the tip are mostly excluded as opposed to their distribution along the rest of the process. Then, perhaps the proteins reaching this portion would find a microtubule barrier before being able to get to the middle of the process.

Alternatively, restricted diffusion of the proteins at the distal end might explain this feature. Preliminary data and the high accumulations visualized at the tip would oppose to this last possibility. A simulation model testing the different options described should give an answer or hint to the mechanism underlying this feature.

4.5 Tau proteins mobility and relevance to development and disease

Disease related conditions were modelled and analysed by the PA approach. AD-related Aβ influence, OA-induced phosphorylation of tau, a PHP model of AD-phosphorylation and a FTDP-17 tau mutant were analysed (**section 3.4**). Phosphorylation induced or mimicking conditions determined higher protein mobility compared to wt tau at normal conditions. This was attributed to a lower association to microtubules of the high phosphorylated-like or drug-induced phosphorylated tau protein. In addition, the flux analysis helped determine whether protein distribution was favoured towards the soma or the tip. The analysis revealed that the distal/proximal ratio for the wt, mut, PHP and control were similar whereas the delta showed a high favourable distribution towards the tip. Nevertheless, drug treatment revealed that the disruption of the microtubule interaction for wt tau determined a preferential distribution towards the tip. Similarly, the IF of mut tau showed no difference to that of wt in the middle of the process, but gave a slight difference when the fractions at the tips were compared (**fig. 3.38** after 10s). The data was interpreted to suggest that the weak plasma membrane interaction through the amino terminal projection domain was responsible for the distribution of proteins towards the tip and a higher retention at this compartment. This explained why proteins lacking this interaction failed to show this distribution. But how do all these interactions fit together within a neuron under normal and pathological conditions?

A possible model for these interactions in living normal and disease-like cells is shown in **fig. 4.1**. As previously described, the plasma membrane interaction gives the wt construct the ability to be distributed more favourably to the distal tip only once it becomes detached from the microtubules.

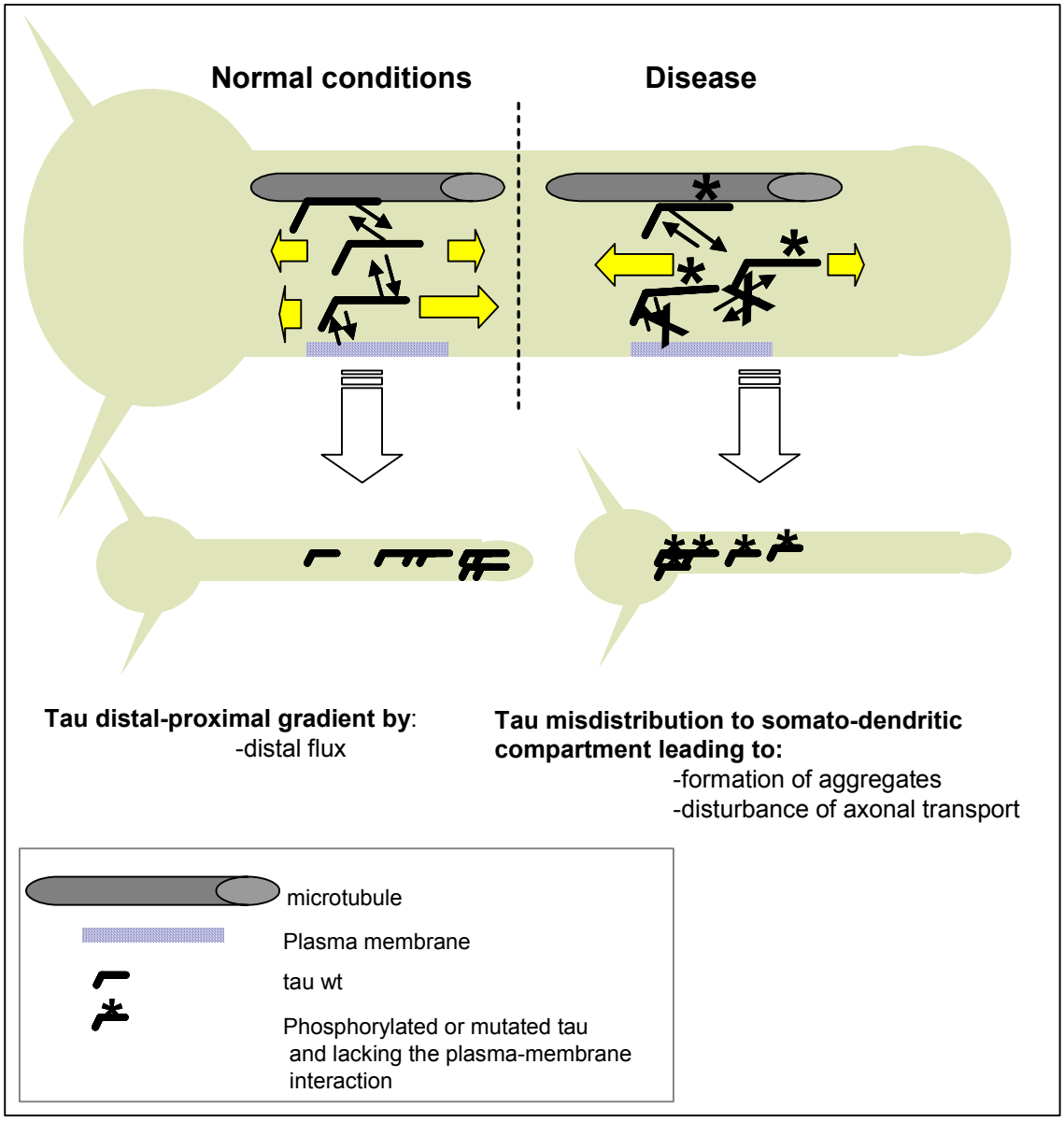

Fig. 4.1: Schematic model of tau distribution at normal and disease-related conditions in neurons. At normal conditions, tau proteins, through interactions with different cell components, are subjected to a net flow towards the distal portion. The interaction of unbound tau with the plasma membrane allowsng its flux would be the key factor underlying the normal distal-proximal gradient for unphosphorylated tau. In disease-related tau proteins, the lack of membrane association either due to the increased phosphorylation or conformational change in mutant proteins determines the loss of distal flux. These determine an abnormal distribution with modified tau forms towards the soma available for aggregation or disturbing the normal axonal transport of other organelles.

In contrast, a phosphorylation gradient of tau has been described with phosphorylated tau being highest at the proximal region (Kempf *et al.* 1996; Maas *et al.* 2000; Mandell and Banker 1996)(Maas *et al.* 2000). This agrees with the higher fraction of mobile PHP protein obtained which shows no distal flux even after taxol treatment (preliminary results).Phoshporylated proteins unable to interact with the plasma membrane would not be preferentially distributed to the tip and instead, a proximal-distal gradient would be the case for phosphorylated tau proteins.

In AD, this result would be achieved through a higher phosphorylation of the protein rendering it less able to bind to microtubules.

Disease-related conditions that cause higher phosphorylation of tau proteins tested showed in all cases a lower IF. The decrease in IF would mean an increase of unbound tau fractions. This can be qualitatively inferred from the images obtained. Wt tau expressing cells would show the lowest free protein amount contributing to low fluorescence background levels in PA-GFP-tau wt -expressing cells (**fig. 3.7, A);** whereas an increase in free tau protein signal in the case of PHP tau cells would increase the background fluorescence level rendering a more diffuse signal where filaments are less clear to visualize (**fig. 3.42**).

The effect of phosphorylation was strongest after OA treatment yielding a decrease of IF of 30% compared to untreated cells. PHP tau expressing cells or Aβ- treated wt tau expressing cells lowered the IF to similar levels (~20%).The differences in these effects could relate to different phosphorylation sites modified in each condition. The inhibition of phosphatases by OA treatment is rather unspecific and yielded the highest mobile protein amounts. In the case of PHP tau, ten specific phosphorylation sites are modified. This case represented a very similar situation to that encountered under Aβ treatment suggesting that Aβ is related to the phosphorylation of these specific sites. In fact, sites which have been mutated in PHP have been found to be related to Aβ dependent phosphorylation (Leschik *et al.* 2007).

Interestingly as discussed for each condition, although the free amount of tau proteins were increased in the tau-disease-related conditions, in none of these cases a preferential flux towards distal regions could be evidenced. In the analysis of taxol-treated wt tau expressing cells however, not only was the mobile fractions increased, but there was also a favoured distal flux. The main difference in these conditions was that the fraction increased in taxol-treated cells is composed of unmodified wt tau proteins, whereas the free fractions increased in disease-related conditions are phosphorylated or

phosphorylated-like tau proteins. These proteins, as previously mentioned, cannot interact with the plasma membrane. This was a hint that the plasma membrane interaction might be the main mechanism involved in the mislocalization of the proteins in pathological conditions.

In the case of FTDP-17, the construct showed no difference in its interaction with microtubules. However, if the amount of protein were increased, a higher amount of protein would be present which would be unable to be distributed predominantly to the distal portion as a result of its lack of plasma-membrane interaction. This could lead to the misdistribution observed in these tauopathies. In turn, other problems would follow such as problems in axonal transport of organelles as could be measured in different tau-disease-like models (Ebneth, Godemann et al. 1998; Künzi, Glatzel et al. 2002).

If tau proteins are favourably distributed to the distal portion of the axon when their free pool fraction is increased (taxol or colchicine incubation) or the microtubule interaction is prevented (delta tau lacking the microtubule binding domain); and the plasma membrane interaction is involved in this mechanism (absent in tau proteins lacking this interaction or in cytochalasin-treated cells), the question that follows is what mechanism determines this? Is there plasma membrane flow that could explain this flux?

Whether the association to some structure in the plasma membrane could then contribute to this flow by some piggy-back mechanism could be an explanation to the flow visualized in the neurites analysed. The tools developed in this work should be able to elucidate this mechanism by studying the dynamics of proteins associated to the plasma membrane.

5. Summary

Tau proteins are members of the microtubule associated proteins (MAPs), and are predominantly expressed in neurons and enriched in the axonal compartment. These proteins are involved in many diseases therefore termed “tauopathies”. In the disease, tau is present in a hyperphosphorylated state that forms aggregates in the somato-dentritic compartment. In order to analyse the distribution of normal and tau proteins present in tauopathies in living cells, a pulse-escape fluorescence photoactivation approach was developed. A wild type “wt”, a R406W mutant “mut”, a hyperphosphorylation model “PHP” (pseudohyperphosphorylated), and a smaller fragment “delta” tau protein, and a control “PA-GFPx3” were fused to the photoactivatable GFP protein. These proteins were expressed in differentiated PC12 cells and mice primary cortical cultures, and analysed in photoactivation experiments.

The data showed that the wt protein was less mobile, both at the shaft or the tip of cell processes, than the delta or control proteins (higher immobile fraction, “IF”). This could be attributed to the microtubule binding domain present only in the wt. Treatment of cells with drugs to disrupt microtubules, or detach tau from the filaments confirmed this interpretation. The mut mobility was comparable to that seen for the wt, suggesting that the interaction with microtubules was unaffected by the mutation. The PHP showed a lower IF compared to the wt, in agreement with previous *in vitro* results showing a lower binding to microtubules. Furthermore, this behaviour could be reproduced by increasing the level of phosphorylation of the wt by drug treatment. Interestingly, for all proteins, the tip showed a higher accumulation of the proteins.

A “flux analysis” was performed to determine the fraction of protein moving towards the distal or proximal portion of the process. Only delta and wt detached from the microtubules showed an increased flux towards the tip. However, when the mut or PHP were analysed, this was not the case. The results suggest that the plasma membrane interaction is involved in the flux of wt tau proteins towards the distal portion; tau proteins that are modified either due to mutations and hyperphosphorylation, lack this interaction and the normal distal localizing mechanism is prevented. These results may explain the mislocalization of the protein seen in the disease, and show the power of live cell imaging to reveal the mechanisms of protein dynamics.

6. Abbreviations

% (v/v) volume percent
% (w/v) weight percent
°C Celsius degree
µ micro
A ámpere
AD: Alzheimer´s disease
Amp^R ampicilline resistance
Apo apochromatic
APP amyloid Precursor Protein
APS ammoniumpersulfat
ATP adenosine-5'-triphosphate
Aβ β-amyloid
bp base pair
BSA bovine serum albumin
BSA bovine serum albumin
C centre
Ca calcium
Cdk5 cyclin-dependent kinase 5
CI centre of intensity
cLSM confocal laser scanning microscope
CMV cytomegalovirus promoter
CNS central nervous system
CO2 carbon dioxide.
Colchi colchicine
C-terminal: carboxy terminal
Cy3 indocarbocyanin
Cyt cytochalasin
d: day
D: diffusion constant
DAPI 4', 6-Diamidino-2-phenylindol
ddH_2O double distilled water.
DMEM Dulbecco's Modified Eagle Medium
DMEM-Ser DMEM-Serum
DMSO Dimethylsulfoxide
DNA Deoxyribonucleic acid
dNTP Deoxyribonucleotide triphosphate
dNTPs Desoxy-Nucleosidtriphosphate
E. coli Escherichia coli
e.g. For example (from latin *exempli gratia*)
ECL enhanced chemoluminescence
EDTA Ethylendiaminotetraessigsäure
EDTA Ethylene diamine tetra-acetic acid
eGFP enhanced Green Fluorescent Protein
EGTA ethylenglycol-bis-(β-aminoethylether)-N,N,N',N'-Tetra acetic acid
ER endoplasmatic reticulum
et al and all others (from latin *et alii*)
EtOH ethanol
f effective frictional coefficient

f_0 frictional coefficient for globular proteins
FCS fetal calf serum
FCS gluorescence correlation spectroscopy
FLIP fluorescence loss in photobleaching
FRAP gluorescence recovery after photobleaching
FTDP-17 Fronto- temporal dementia and Parkinsonism linked to chromosome 17.
g gramm
g µg grame, microgame
G418 geneticin 418
GFP green fluorescent protein
Gly glycin
GPI glycosylphosphatidylinositol
GSK-3 glycogen Synthase Kinase-3
GSK3β glycogen synthase kinase-3
HBSS Hanks Balanced Salt Solution
hr/hrs hour/hours
HRP horse raddish peroxidase
HS horse serum
i.e. that is to say (from latin, *id est*)
I intensity
IAA iodo acetic acid
IF immobile fraction
IFl immunefluorescence
IntMotion Matlab program that analyse intensity
IntDisTime coloured plot depicting intensity in distance and time.
IT intensity tensor
k kilo
K pottasium
k Boltzmann constant
Kan^R kanamycin resistance
kb kilobasepair
kD kilodalton
kDa kilodalton
KFP1 kindling fluorescent protein 1

l Liter
LB Luria Bertani
L left
m Meter
m milli
M Molar
m, min Minute
M, mM, µM Molar, millimolar, micromolar
MAP microtubule associated protein
MBR microtubule binding region
MEM Minimum Essential Medium
Mg Magnesium
mGFP a monomer form of GFP
min Minute
ml, l, µl Milliliter, liter, microliter
mRFP monomer of the red fluorescent protein

mRNA messenger RNA
MSF Mean stationary fraction.
Mut mutant (referring to the R406W mutation in FTDP-17)
MW Molecular weight
Na Natrium
NA numerical aperture
NaCl sodium chloride
NaOH sodium hydroxide
NaOH sodium Hydroxide
ND neutral density (filter)
NB neurobasal
Neo^R neomycin resistance
NFTs neurofibrillary tangles
NGF nerve growth factor
nm Nanometer
NT2/ NT2N human NTera2 neurons
N-terminal aminoterminal
OA okadaic acid
OD Optical density
OD600 Optical density at a 600 nm wavelength
ON overnight
OPTIMEM: reduced Serum Medium powder
p pico
PA photoactivation
PAGE Polyacrylamid Gelelektrophorese
PA-GFP Photoactivatable green fluorescent protein
PA-GFPx3 triplet/tandem, 3 PA-GFP molecules expressed in tandem
PFA paraformaldeheyde
PBS Phosphate buffer solution
PBS Phosphate Buffered Saline
PC12 pheochromocytoma cells
PCR Polymerase chain reaction
PCR polymerase chain reaction
Pen-Strep: Penicillin-Streptomycin
PFA Paraformaldehyd
pH lat. Potentia hydrogenii
pH negative logarithm (log10) of the hydroxonium concentration
PHF-Tau paired helical filament tau
PHP pseudohyperphosphorylated
PHP-Tau pseudohyperphosphoryliertes Tau
PLL Poly-L-Lysin
PMSF Phenylmethylsulfonylfluorid
PP2A Phosphatase 2 A
PVDF Polyvinyliden-Difluorid
R, Arg Arginine
R radius of the molecule in motion
R right
RNA Ribonucleic acid
ROI region of interest
rpm revolutions per minute
RT Room temperature

s seconds
SD standard deviation
SDS sodium dodecylsulfate
SE standard error
T, t time
$t_{1/2}$ half time of recovery
TAE Tris Acetic acid EDTA-Na2-salt
TBE Tris Boric acid EDTA-Na2-salt
TBE TRIS-Borat-EDTA
TBS Tris-buffer solution
TCA Trichloracetic acid
TCEP Tris(2-carboxyethyl)phosphinehydrochlorid
TEMED N,N,N‘,N‘-Tetramethylendiamin
Tfb transformation buffer
TX-100 Triton X-100
Tris 2-Amino-2-(hydroxymethyl)1-1,3-propandiol (Tris/Base)
Tris Tris Hydroxymethylaminoethane
Tween-20 Polyoxyethylensorbitan Monolaurat
UV Ultraviolet radiation
V Volt
Wt wild type
x distance
X g Gravitation constant
η viscosity index of the media

Nucleotides and Amino acids are represented with the single letter code (IUPAC-IUB Commission on Biochemical Nomenclature).

7. Bibliography

Andreadis, A. (2005). "Tau gene alternative splicing: expression patterns, regulation and modulation of function in normal brain and neurodegenerative diseases." Biochimica et Biophysica Acta **1739**.

Baas, P. W. (2000). "Strategies for studying microtubule transport in the neuron." Microscopy research and technique **48**.

Babak, E. A., J. H. McCarty, et al. (1994). "Sense and antisense transfection analysis of tau function: tau influences net microtubule assembly, neurite outgrowth and neuritic stability." Journal of Cell Science **107**.

Berg, H. C. (1993). Random Walks in Biology, Princeton University Press.

Brandt, R. (1996). "The tau proteins in neuronal growth and development." Frontiers in Bioscience **1**.

Brandt, R., M. Hundelt, et al. (2005). "Tau alteration and neuronal degeneration in tauopathies: mechanisms and models." Biochimica et Biophysica Acta.

Brandt, R. and G. Lee (1993). "Functional organization of microtubule-associated protein tau. Identification of regions which affect microtubule growth, nucleation, and bundle formation in vitro." Journal of Biological Chemistry **15**(268).

Brandt, R., J. Léger, et al. (1995). "Interaction of tau with the neural plasma membrane mediated by tau´s amino-terminal projection domain." Journal of Cell Biology **131**(5).

Brandt, R. and J. Leschik (2004). "Functional interaction of tau and their relevance for Alzheimer´s disease." Current Alzheimer Research **1**(4).

Brown, A. (2003). "Axonal transport of membranous and nonmembranous cargoes: a unified perspective." Journal of Cell Biology **160**(6).

Buée, L., T. Bussière, et al. (2000). "Tau protein isoforms, phosphorylation and role in neurodegenerative disorders." Brain Research Reviews **33**.

Busciglio, J., A. Lorenzo, et al. (1995). "ß-Amyloid Fibrils Induce Tau Phosphorylation and Loss of Microtubule Binding." Neuron **14**.

Chen, Y., P. J. Macdonald, et al. (2006). "Probing nucleocytoplasmic transport by two-photon activation of PA-GFP." Microscopy research and technique **69**.

Cleveland, D. W., S.-Y. Hwo, et al. (1977). "Physical and chemical properties of purified tau factor and the role of tau in microtubule assembly." Journal of Molecular Biology **116**.

Connell, J. W., G. M. Gibb, et al. (2001). "Effects of FTDP-17 mutations on the in vitro phosphorylation of tau by glycogen synthase kinase 3beta identified by mass spectrometry demonstrate certain mutations exert long-range conformational changes." FEBS Letters **493**(1).

Dehmelt, L. and S. Halpain (2003). "Actin and microtubules in neurite inititation: are MAPs the missing link?" Neuron.

Drubin, D. G., S. C. Feinstein, et al. (1985). "Nerve growth factor-induced neurite outgrowth in PC12 cells involve the coordinate induction of microtubule assembly and assembly-promoting factors." Journal of Cell Biology **101**.

Ebneth, A., R. Godemann, et al. (1998). "Overexpresion of tau proteins inhibits kinesin-dependent trafficking of vesicles, mitochondria and endoplasmic reticulum: Implications for Alzheimer´s Disease." Journal of Cell Biology **143**(3).

Eidenmüller, J., T. Fath, et al. (2000). "Structural and Functional implications of tau hyperphosphorylation: information from phosphorylation-mimicking mutated tau proteins." Biochemistry **39**.

Fath, T., J. Eidenmüller, et al. (2002). "Tau-mediated cytotoxicity in a pseudohyperphosphorylation model of Alzheimer´s disease." Journal of Neuroscience **22**(22).

Garth, F. H. and J. Yao (2005). "Modeling tauopathy: a range of complementary approaches." Biochimica et Biophysica Acta **1739**.

Goedert, M. and R. Jakes (2005). "Mutations causing neurodegenerative tauopathies." Biochimca et Biophysica Acta: 240-250.

Goldman, R. D. and D. L. Spector (2005). Live Cell Imaging A Laboratory Manual, Cold Spring Harbor Laboratory Press.

Goodwin, J. S. and A. K. Kenworthy (2005). "Photobleaching approaches to investigate diffusional mobility and trafficking of Ras in living cells." Methods **37**.

Gordon-Weeks, P. R. (2004). "Microtubules and growth cone function." Journal of Neurobiology . **58**(1).

Hall, Z. W. (1992). An introduction to molecular neurobiology, Sinauer associates, Inc.

Hirokawa, N., T. Funakoshi, et al. (1996). "Selective stabilization of tau in axons and microtubule-associated protein 2C in cell bodies and dendrites contributes to

polarized localization of cytoskeletal proteins in mature neurons." Journal of Cell Biology **132**(4).

Kandel, E. R., J. H. Schwartz, et al. (2000). Principles of neural science, McGraw-Hill.

Kempf, M., C. Albrecht, et al. (1996). "Tau binds to the distal axon early in development of polarity in a microtubule- and microfilament- dependent manner." Journal of Neuroscience **16**(18).

Kenessey, A. and S. H. Yen (1993). "The extent of phosphorylation of fetal tau is comparable to that of PHF-tau from Alzheimer paired helical filaments." Brain Research Reviews **629**(1).

King, M. E., H.-M. Kan, et al. (2006). "Tau-dependent mictrotubule disassembly initiated by prefibrillar beta-amyloid." Journal of Cell Biology **175**(4).

Konzack, S., E. Thies, et al. (2007). "Swimming against the tide: mobility of the microtubule-associated protein tau in neurons." Journal of Neuroscience **27**(37).

Krishnamurthy, P. K. and G. V. Johnson (2004). "Mutant (R406W) human tau is hyperphosphorylated and does not efficiently bind microtubules in a neuronal cortical cell model." Journal of biology chemistry **279**(9).

Kubitscheck, U., P. Wedekind, et al. (1996). "Single nuclear pores visualized by confocal microscopy and image processing." Biophysical journal **70**.

Künzi, V., M. Glatzel, et al. (2002). "Unhampered prion neuroinvasion despite impaired fast axonal transport in transgenic mice overexpressing four-repeat tau." Journal of Neuroscience **22**(17).

Léger, J. G., R. Brandt, et al. (1994). "Identification of tau protein regions required for process formation in PC12 cells." Journal of Cell Science **107**.

Leschik, J., A. Welzel, et al. (2007). "Inverse and distinct modulation of tau-dependent neurodegeneration by presenilin 1 and amyloid-beta in cultured cortical neurons: evidence that tau phsophorylation is the limiting factor in amyloid-beta-induced cell death." Journal of Neurochemistry **10**.

Lippincott-Schwartz, J., N. Altan-Bonnet, et al. (2003). "Photobleaching and photoactivation: following protein dynamics in living cells." Imaging in cell biology.

Lippincott-Schwartz, J. and G. H. Patterson (2003). "Development and use of fluorescent protein markers in living cells." Science **300**.

Lippincott-Schwartz, J., E. Snapp, et al. (2001). "Studying protein dynamics in living cells." Nature Reviews **2**.

Litman, P., J. Barg, et al. (1993). "Subcellular localization of tau mRNA in differentiating neuronal cell culture: Implications for neuronal polarity." Neuron **10**(4).

Maas, T., J. Eidenmüller, et al. (2000). "Interaction of tau with the neural membrane cortex is regulated by phosphorylation at sites that are modified in paired helical filaments." Journal of biological Chemistry **275**(26).

Mandell, J. W. and G. A. Banker (1996). "A Spatial Gradient of Tau Protein Phosphorylation in Nascent Axons." Journal of Neuroscience **16**(18).

Mercken, M., I. Fischer, et al. (1995). "Three distinct axonal transport rates for tau, tubulin, and other microtubule-associated porteins: evidence for dynamic interactions of tau with microtubules *in vivo*." Journal of Neuroscience **15**(12).

Miyasaka, T., M. Morishima-Kawashima, et al. (2001). "Molecular analysis of mutant and wild-type tau deposited in the brain affected by the FTDP-17 R406W mutation." American Journal of Pathology **158**(2).

Patterson, G. H. and J. Lippincott-Schwartz (2002). "A photoactivatable GFP for selective photolabeling of proteins and cells." Science **297**.

Patterson, G. H. and J. Lippincott-Schwartz (2004). "Selective photolabelling of proteins using photoactivatable GFP." Methods **4**.

Pérez, M., F. Lim, et al. (2000). "The FTDP-17-linked mutation R406W abolishes the interaction of phosphorylated tau with microtubules." Journal of Neurochemistry **74**.

Pisano, C., G. Pratesi, et al. (2003). "Paclitaxel and cisplatin-induced neurotoxicity: a protective role of acetyl-L-carninite." Clinical cancer research **9**.

Popov, S. and M.-m. Poo (1992). "Diffusional transport of macromolecules in developing nerve processes." Journal of Neuroscience **12**(l).

Salamat-Miller, N., M. Chittchang, et al. (2002). "Shape imposed by secondary structure of a polypeptide

affects its free diffusion through liquid-filled pores." International Journal of Pharmaceutics **244**.

Samsonov, A., J.-Z. Yu, et al. (2004). "Tau interaction with microtubules in vivo." Journal of Cell Science **117**(25).

Schimerer, B. and C. S. Hill (2005). "Kinetic analysis of smad Nucleocytoplasmic shuttling reveals a mechanism for transforming growth factor beta-dependent nuclear accumulation of Smads." Molecular and cellular biology(November).

Shahani, N. and R. Brandt (2002). "Functions and malfunctions of the tau proteins." Cellular and molecular life sciences **59**.

Shahani, N., S.Subramaniam, et al. (2006). "Tau aggregation and progressive neuronal degeneration in the absence of changes in spine density and morphology after targeted expression of Alzheimer´s disease-relevant tau construts in organotypic hippocampal slices." Neurobiology of Disease **26**(22).

Skrabana, R., J. Sevcik, et al. (2006). "Intrinsically disordered proteins in the neurodegenerative processes: formation of tau protein paired helical filaments and their analysis." Cellular and molecular neurobiology **26**(7-8).

Sontag, E., V. Nunbhakdi-Craig, et al. (1999). "Molecular interactions among protein phosphatase 2A, tau, and microtubules. Implications for the regulation of tau phosphorylation and the development of tauopathies." Journal of biological chemistry **274**(36).

Sprague, B. L., R. L. Pego, et al. (2004). "Analysis of binding reactions by fluorescence recovery after photobleaching." Biophysical journal **86**.

Stark, D. A. and P. M. Kulesa (2005). "Photoactivatable green fluorescent protein as a single cell marker in living embryos." Developmental dynamics **233**.

Stoothoff, W. H. and G. V. W. Johnson (2005). "Tau phosphorylation: physiological and pathological consequences." Biochimca et Biophysica Acta(1739).

Tashiro, T., X. Sun, et al. (1996). "Differential Axonal Transport of Soluble and Insoluble Tau in the Rat Sciatic Nerve." Journal of Neurochemistry.

Tischler, A. S., L. A. Grene, et al. (1983). "Ultrastructural effects of nerve growth factor on PC12 pheochromocytoma cells in spinner culture." Cell and tissue research **228**.

Toll, L. and B. D. Howard (1979). "Evidence that an ATPase and a protonmotive force function in the transport of acetylcholine into storage vesicle." Journal of Biological Chemistry **255**(5).

Trivedi, N., P. Jung, et al. (2007). "Neurofilaments switch between distinct mobile and stationary states during their transport along axons." Journal of Neuroscience.

Tsien, R. Y. (1998). "The green fluorescent protein." Annual Reviews in Biochemistry **67**.

Twig, G., S. A. Graf, et al. (2006). "Tagging and tracking individual networks within a complex mitochondrial web with photoactivatable GFP." American Journal of Physiology, Cell Physiology **291**.

Utton, M. A., J. Connell, et al. (2002). "The slow axonal transport of the microtubule-associated protein tau and the transport rates of different isoforms and mutants in cultured neurons." Journal of Neuroscience **22**(15).

Utton, M. A., W. J. Noble, et al. (2005). "Molecular motors implicated in the axonal transport of tau and α-synuclein." Journal of Cell Science **118**(20).

Uversky, V. N., S. Winter, et al. (1998). "Hyperphosphorylation induces structural modification of tau-protein." FEBS letters **439**.

Wang, L., C.-l. Ho, et al. (2000). "Rapid movement of axonal neurofilaments interrupted by prolonged pauses." Nature Cell Biology **2**.

Weissmann, C. and R. Brandt (2007). "Mechanisms of neurodegenerative diseases: Insights from live cell imaging." Journal of Neuroscience Research.

Zhang, B., M. Higuchi, et al. (2004). "Retarded axonal transport of R406W mutant tau in transgenic mice with a neurodegenerative tauopathy." Neurobiology of Disease **24**(19).

8. Acknowledgements

There are very many people who supported me and encouraged me during my PhD whom I would like to acknowledge in this section.

First, I would like to thank Prof. Dr. Roland Brandt for giving me the opportunity to work in his lab in such an interesting project; for his supervision, guidance, great ideas, optimism and help in finding my way in a new field and in a new place, and, especially, for always being available for questions and discussions.

Next I want to thank Dr. Reyher for providing me with his programs, and for the time devoted on explanations and exchange of ideas and corrections. My thanks also go to Julia, his wife and my first German teacher.

Very special thanks go to the people from Nikon Amsterdam, Dr. Robert Stad, Dr. Marteen Balzar, and Kees van der Oord for their collaboration and kind help in the setting the microscope system used in this work.

In addition, my thanks go to Prof. Dr. Junge, for his kind and warm support, his advice and his willingness to help. My gratitude also goes to Tobias, and Daniel for programming skills.

I would also like to thank Prof. Dr. Paululat who took part of the evaluation process, Prof. Dr. Steinhoff, the second supervisor to this work and Dr. Schmitz who accepted being part of the committee commission.

Here, I also want to thank my work colleagues. It was very nice being part of the Brandt group, the grill parties, and *winter* Christmas with Glühwein and Feuerzangebowle. All members were very helpful in very different aspects apart from correcting my *Hausaufgabe*!

Very special thanks go to Geli who played a very special role in my life in Osnabrück, who showed me many technical assays and practical tricks at the lab and in life; Moni who was always someone I could count on; and Neelam who was a very important example of a scientist to me. Regina, Rolf, Nataliya, Maggie, Virginia, Diana, Rafa, Pana, Xian, Maria, Anne G, Anne H, Adnan, Dirk, Lakshmi and Prasad shared with me very nice and special moments . I also want to mention Julia and Anna who initially spent a lot of time with me.

I cannot be thankful enough for the opportunity I had here of having two very special “brothers” César and Iván who were with me in most of the way, through good and bad times, side by side scientifically and emotionally. Also Darío who

played an important role not only with helpful corrections, but also with his more mature views and introduced us to his sweet family. You were the people I leaned on most here.

I want to mention the help of my Bielorussian “sister” and great friend Tanja who became a very important person to me and for the best Freundschaft Buch I ever got. Very special thanks go to Hannah who was always there to listen, give kind advice, and prepared the greatest breakfasts that helped me through the last and incredibly tortuous segment of the thesis. Your help was extraordinary.

Among my Russian developed group, I want to thank Marjana for her friendship and support, and especially Andreas who gave me strength when I needed it most and filled my days with flowers, tremendous generosity and mature advice.

Next, I want to thank my people on the other side of the ocean for encouraging me to undertake this enterprise and for giving me support with telephone calls, e-mails and by all possible means.

Firstly, I want to thank all members of my family. My parents Fernando and Aída for trusting me always, and constantly following each step of the way from so far away. You gave me support, advice and love *every* day and made me feel you were close to me. Not to forget the love towards Chemistry and research my mom passed on to me, and my dad for his deep insight into matters. My thanks also go to my two sisters, Paula and Vivi who set an example of passionate hard work and perseverance. They too, through the upbringing of a family, had nevertheless time to devote to their little sister, and thus allowed me not to miss the events in the lives of my beautiful and sweet nephews Sebi, Estefi, Santi and Agus. It was also my nephews, who helped me in a very special way through their drawings, farewell letters and sweet words or sounds. I want to thank both brothers-in-law: Damián, who hinted me for directions to go and was always prepared to offer his help; and Marcelo, for his “Córdoba” humour, statistics and critical advice. I want to thank my dear Omi, who phoned me regularly, and gave me trust. I cannot thank your “pilatos” enough.

My Opa, and my bove -one of the persons whom I always felt believed in me the most-, but unfortunately were not there anymore to see me start this long journey, were of important influence and I am therefore thankful. I also want to thank my cousins, uncles and aunts as well as many other friends of the family

always willing to help and give support. It is amazing to be part of such a big and loving family.

At this point, I want to thank all my friends, and Luciano and his family who encouraged me and prepared many cow-grils in my first PhD years. I cannot thank enough Mariana G, Mariela and Eugenio, Paula, Ceci and Pablo, Caro, Flavia and Jorge, Mariana F, Mariel and Romi for their unconditional friendship, visits, in some cases, and for always making themselves available at any moment that I turned up in my loving Buenos Aires, making sure I left it with typical home-made provisions.

In addition, I want to acknowledge the help of Dr. Ana Franchi and Dr. Mariana F and the people from CEFyBO who allowed me to start doing research and without whom nothing of this would have been possible.

To all these people I want to give my special thanks and let you know that you were a reason for me to go on in this long and winding road.

Finally, I want to thank the DFG for the fellowship I was given and to the University of the beautiful city of Osnabrück that allowed me to work all these years in Germany.

Thanks, Danke, spasiba y Gracias!

9. Appendix

Table 9.1 Protein immobile fractions (IF)

M: middle; T: tip; colchi: colchicine; OA: okadaic acid; IAA: iodoacetic acid; Cyt: Cytochalasin; SEM= standard error of the mean; n: number of cells.

Stable lines

Stationary and mobile protein fractions 10 s after photoactivation

	PA-GFP-protein/ (+treatment)/region	Immobile fraction 10 (I_{10}/I_0) ± SEM	n
Section 3.1	Wt M	**0.364 ±0.015**	29
	Wt T	**0.529 ±0.019**	21
	Delta M	**0.143 ±0.015**	20
	Delta T	**0.301 ±0.020**	20
	PAx3 M	**0.131 ±0.015**	18
	PAx3 T	**0.367 ±0.025**	23
	Wt + colchi M	**0.279 ±0.016**	12
	Wt + colchi T	**0.366 ±0.018**	8
	PA-GFPx3+ colchi M	**0.196 ±0.034**	10
	PA-GFPx3 + colchi T	**0.345 ±0.081**	4
	Delta + colchiM	**0.175 ±0.029**	7
	Delta + colchi T	**0.434 ±0.019**	2
	Wt + taxol M	**0.248 ±0.012**	10
	Wt + cyt T	**0.429 ±0.039**	8
	Delta + cyt T	**0.316 ±0.019**	4
Section 3.2	Mut M	**0.340 ±0.020**	16
	Mut T	**0.457 ±0.020**	16
Section 3.3	PHP M	**0.296 ±0.012**	26
	PHP T	**0.378 ±0.018**	16
	Wt + OA M	**0.252 ±0.020**	19
	PHP + OA M	**0.281 ±0.022**	13
	Wt + Aβ M	**0.287 ±0.015**	10

Stationary and mobile protein fractions 50 s after photoactivation

	PA-GFP-protein (+treatment)/region	Immobile fraction 50 (I_{50}/I_0) ± SEM	n
Section 3.1	Wt M	**0.188 ±0.013**	27
	Wt T	**0.319 ±0.017**	20
	Delta M	**0.045 ±0.011**	20
	Delta T	**0.123 ±0.022**	15
	PA-GFPx3 M	**0.075 ±0.019**	21
	PA-GFPx3 T	**0.209 ±0.022**	20
	Wt + colchi M	**0.132 ±0.013**	9
	Wt + colchi T	**0.247 ±0.029**	7
	PA-GFPx3 + colchi M	**0.093 ±0.029**	10
	PA-GFPx3 + colchi T	**0.145 ±0.061**	3
	Delta + colchiM	**0.067 ±0.021**	7
	Delta + colchi T	**0.225 ±0.028**	2
	Wt + taxol M	**0.119 ±0.012**	19
	Wt + cyt T	**0.221 ±0.031**	8
	Delta + cyt T	**0.144 ±0.044**	4
Section 3.2	Mut M	**0.166 ±0.013**	17
	Mut T	**0.301 ±0.025**	15
Section 3.3	PHP M	**0.153 ±0.010**	25
	PHP T	**0.195 ±0.016**	16
	Wt + OA M	**0.097 ±0.008**	10
	PHP + OA M	**0.138 ±0.013**	10
	Wt + Aβ M	**0.169 ±0.012**	12

Transient transfected cells

Stationary and mobile protein fractions after 10 s photoactivation in transients

	PA-GFP-protein/ (+treatment)/- region	Immobile fraction 10 (I_{10}/I_0) ± SEM	n
Section 3.1	Wt M	**0.461 ±0.016**	24
	Wt M	**0.493 ±0.028**	16
	Delta M	**0.136 ±0.010**	26
	Delta T	**0.285 ±0.023**	23
	PA-GFPx3 M	**0.178 ±0.017**	21
	PA-GFPx3 T	**0.291 ±0.018**	20
	Wt + colchi M	**0.384 ±0.020**	14
	Wt IAA M	**0.469 ±0.022**	12
	Delta IAA M	**0.159 ±0.036**	10
Section 3.2	Mut M	**0.405 ±0.021**	17
	Mut T	**0.422 ±0.027**	11

Stationary and mobile protein fractions after 50 s photoactivation in transients

	PA-GFP-protein (+treatment)/region	Immobile fraction 50 (I_{50}/I_0) ± SEM	n
Section 3.1	Wt M	**0.258 ±0.014**	24
	Wt T	**0.308 ±0.024**	14
	Delta M	**0.054 ±0.008**	26
	Delta T	**0.141 ±0.021**	22
	PAx3 M	**0.098 ±0.018**	19
	PAx3 T	**0.151 ±0.021**	10
	Wt + colchi M	**0.200 ±0.018**	15
	Wt IAA M	**0.252 ±0.020**	13
	Delta IAA M	**0.077 ±0.026**	10
Section 3.2	Mut M	**0.230 ±0.016**	17
	Mut T	**0.255 ±0.040**	11

Primary cortical culture

Stationary and mobile protein fractions after 10 s photoactivation in primary cortical culture

	PA-GFP-protein/ region	Immobile fraction 10 (I_{10}/I_0) ± SEM	n
Section 3.1	Wt M	**0.408 ±0.034**	9
	Wt T	**0.478 ±0.028**	6
	Delta M	**0.186 ±0.027**	6
	Delta T	**0.261 ±0.060**	3

Stationary and mobile protein fractions after 50 s photoactivation in primary cortical culture

	PA-GFPx3-protein /region	Immobile fraction 50 (I_{50}/I_0) ± SEM	n
Section 3.1	Wt M	**0.229 ±0.028**	9
	Wt T	**0.305 ±0.048**	6
	Delta M	**0.087 ±0.023**	6
	Delta T	**0.124 ±0.080**	3

Table 9.2 Proteins proximal-distal flux

(proximal = 10μm to soma; distal= 10 μm to tip; zero reference= activation spot)

Stable lines

	PA-GFP-protein/ region	Mean proximal fraction ± SEM	Mean Distal n fraction ± SEM	
Section 3.1	**Wt**	0.138 ±0.015	0.119 ±0.009	27
	Delta	0.229 ±0.038	0.346 ±0.033	14
	PA-GFPx3	0.337 ±0.042	0.312 ±0.030	16
	Wt +colchi	0.183 ±0.030	0.240 ±0.037	9
	Wt +taxol	0.173 ±0.018	0.237 ±0.018	18
Section 3.2	**Mut**	0.155 ±0,019	0.165 ±0.028	16
Section 3.3	**PHP**	0.178 ±0.016	0.190 ±0.019	26
	Wt + OA	0.169 ±0.019	0.160 ±0.016	10
	PHP + OA	0.205 ±0.028	0.206 ±0.020	10
	Wt +Aβ	0.195 ±0.207	0.207 ±0.027	9

Transients transfected cells

PA-GFP-protein/ region	Mean proximal fraction ± SEM	Mean Distal fraction ±SEM	n
Wt	0.090 ±0.012	0.096 ±0.009	20
Mut	0.116 ±0.020	0.117 ±0.018	17
PA-GFPx3	0.237 ±0.022	0.261 ±0.033	14
Delta	0.242 ±0.025	0.365 ±0.026	24

Primary cortical culture

Table 9.3 Proteins distal/proximal ratio

Stable lines

	PA-GFP-protein (+treatment)	Distal/proximal ratio ± SEM	n
Section 3.1	**Wt**	**1.007 ±0.098**	27
	Delta	**2.300 ±0.523**	14
	PA-GFPx3	**1.128 ±0.218**	16
	Wt + colchi	**1.475 ±0.225**	9
	Wt + taxol	**1.837 ±0.396**	18
Section 3.2	**Mut**	**1.120 ±0.156**	16
Section 3.3	**PHP**	**1.207 ±0.160**	26
	Wt + OA	**1.060 ±0.179**	11
	PHP + OA	**1.150 ±0.171**	10
	Wt + Aβ	**1.340 ±0.780**	9

Erklärung über die Eigenständigkeit der erbrachten wissenschaftlichen Leistung und etwaige frühere Promotionsverfahren

Ich erkläre hiermit, dass ich die vorligende Arbeit ohne unzulässige Hilfe Dritter und ohne Benutzung anderer als der angegebenen Hilfsmittel angefertigt habe. Die aus Quellen direkt oder indirekt übernommene Dateien und Konzepte sind unter Angabe der Quellen gekennzeichnet.

An der inhaltlichen materiellen Erstellung der vorliegenden Arbeit waren keine anderen Personen beteiligt. Insbesondere habe ich hierfür nicht die entgeltliche Hilfe von Vermittlungs- bzw. Beratungsdiensten in Anspruch genommen. Niemand hat von mir unmittelbar oder mittelbar geldwerte Leistungen für Arbeiten erhalten, die im Zusammenhang mit dem Inhalt der vorgelegten Dissertation stehen.

Ich habe bisher an keiner in- oder ausländischen Fakultät weder ein Gesuch um Zulassung zur Promotions eingereicht noch die vorliegende oder eine Andere Arbeit als Dissertation vorgelegt.

....

(Ort, Datum) (Unterschrift)